DEVELOPMENT OF CARBON NANOTUBE BASED HYBRID NANOCOMPOSITES AS SENSING PLATFORM FOR ELECTROCHEMICAL DETECTION OF PHARMACEUTICAL DRUGS OF INTENSIVE CARE MONITORING

THESIS

SUBMITTED IN PARTIAL FULFILMENT OF THE REQUIREMENTS
FOR THE AWARD OF THE DEGREE OF

Doctor of Philosophy

IN

CHEMISTRY

BY

SATYANARAYANA M

(Roll No. 701164)

RESEARCH SUPERVISOR

Dr. K. V. GOBI

Associate Professor

DEPARTMENT OF CHEMISTRY

NATIONAL INSTITUTE OF TECHNOLOGY WARANGAL

WARANGAL – 506 004, TELANGANA, INDIA

May – 2016

DECLARATION

This is to declare that the work presented in the thesis entitled ***"Development of Carbon Nanotube based Hybrid Nanocomposites as Sensing Platform for Electrochemical Detection of Pharmaceutical Drugs of Intensive Care Monitoring"*** is a bonafide work done by me under the supervision of **Dr. K. V. Gobi**, Associate Professor in the Department of Chemistry and was not submitted elsewhere for the award of any degree.

I declare that this written submission represents my ideas in my own words and where others' ideas or words have been included, I have adequately cited and referenced the original sources. I also declare that I have adhered to all principles of academic honesty and integrity and have not misrepresented or fabricated or falsified any idea/data/fact/ source in my submission. I understand that any violation of the above will be a cause for disciplinary action by the Institute and can also evoke penal action from the sources which have thus not been properly cited or from whom proper permission has not been taken when needed.

Date: **(SATYANARAYANA M.)**

Place: **NIT Warangal** Roll Number: **701164**

CERTIFICATE

This is to certify that the work presented in the thesis entitled ***"Development of Carbon Nanotube based Hybrid Nanocomposites as Sensing Platform for Electrochemical Detection of Pharmaceutical Drugs of Intensive Care Monitoring"*** is a bonafide work carried out by **Mr. Satyanarayana M.** under my supervision and was not submitted elsewhere for the award of any degree.

Dr. K. V. GOBI
(Research Supervisor)
Associate Professor

ACKNOWLEDGEMENTS

ACKNOWLEDGEMENTS

During the course of my Doctoral Research work, I have received the assistance and support from the following people:

First and foremost, I am truly indebted and I express my earnest gratitude for my Research Supervisor ***Dr. K. V. Gobi,*** Associate Professor, Department of Chemistry, National Institute of Technology Warangal for his inestimable expertise and astute guidance. His unabated enthusiasm, which stems from his absolute command over the subject, has been a constant source of inspiration for me to work hard and the outcome is expressed in the form of this thesis. I consider myself as very fortunate for being his Doctoral Research Student and it would have been impossible to achieve this goal without his sturdy support and care.

I am grateful to ***The Director***, National Institute of Technology, Warangal for giving me the opportunity to carry out the work and allowing me to submit in the form of thesis. I greatly acknowledge ***Ministry of Human Resource Development, Govt. of India*** for the financial support in the form of Institute fellowship.

I express my gratitude to the Doctoral Scrutiny Committee members: ***Prof. V. Rajeswar Rao***, Chairman and Head, Department of Chemistry, ***Prof. B. V. Appa Rao***, Department of Chemistry and ***Prof. M. K. Mohan***, Department of Metallurgical and Materials Engineering, NIT Warangal for their detailed review, constructive suggestions and excellent advice during the progress of this research work.

My sincere thanks are due to ***former Heads*** of the Department of Chemistry during the period of my research work.

I would like to thank all the faculty members from Chemistry Department namely ***Prof. P. Nageswara Rao, Prof. A. Ramachandraiah***, ***Prof. G.V.P. Chandramouli***, ***Prof. I. Ajit Kumar Reddy, Prof. K. Laxma Reddy, Prof. B. Rajitha, Dr. P. V. Srilakshmi, Dr. Venkatathri Narayanan, Dr. Vishnu Shanker***, ***Dr. D. Kasinath, Dr. B. Srinivas, Dr. K. Hari Prasad*** and the **other faculty members** for their valuable advice and encouragement throughout the research work.

I convey my special thanks from the bottom of my heart to my senior ***Dr. K. Koteshwara Reddy*** and my juniors, ***Mr. K. Yugender Goud, Mr. V. Sunil Kumar***

and ***Ms. S. Manasa*** for their continuous support and encouragement in each and every step of my research work.

With all happiness I acknowledge the cheerful assistance rendered by all my research colleagues *Dr. K. Chaitanya Kumar, Dr. M. Nookaraju, Dr. B. Janardhan, Dr. S. Kanakaraju*, *Dr. B. Santhosh Kumar, Dr. M. Narsimha Reddy, Mr. G. Srinivasa Rao, Mr. K. Vimal Kumar*, *Dr. T. Surendar, Mr. V. Krishnaiah, Dr. T. Ramesh, Mr. A. Ajay Kumar, Mr. Ashutosh Kumar Yadav, Mr. E. Hari Mohan, Mr. Phani Kumar, Mr. M. Sai, Mr. Chirra Suman, Dr. O. Surender Reddy, Dr. Venkatrajam Marka, Mr. V. Jeevan* and my friends *Mr. K. Syam, Mr, Kali Suresh, Mr. G. Naresh* and other co-research scholars for their munificent support.

I am grateful to the lab assistants *Mr. Praveen, Mr. Srinivas* and ***other supporting staff*** of the Department of Chemistry, NIT Warangal for their cooperation.

My heart goes to my beloved ***Family Members*** who with all their patience, prayers and faith in the Almighty, waited all these long years to see me reaching this stage. Their blessings and care always gave me new fervour and gusto to do something more with perfection.

I always remember and cherish the encouragement and inspiration provided by all my friends and well-wishers during the course of my research work.

Date: **SATYANARAYANA M.**

CONTENTS

Table of Contents

SYMBOLS AND ABBREVIATIONS

IUPAC	:	International Union for Pure and Applied Chemistry
cm	:	Centimeter
s	:	Seconds
nm	:	Nanometer
i	:	Current
E	:	Potential
ν	:	Scan Rate
µA	:	Microampere
mV	:	Millivolt
µM	:	Micromolar
nM	:	Nanomolar
M	:	Molarity
F	:	Faraday Constant
k°	:	Heterogeneous Rate Constant
R	:	Gas Constant
T	:	Absolute Temperature
A	:	Geometric surface Area of Electrode
Z′	:	Real Impedance
Z″	:	Imaginary Impedance
R_{CT}	:	Charge Transfer Resistance
Z_W	:	Warburg Impedance
Ω	:	Ohm
Da	:	Dalton
LDL	:	Low-detection-limit
RSD	:	Relative Standard Deviation
INH	:	Isoniazid
5-FU	:	5-fluorouracil
CLP	:	Clopidogrel
DTIC	:	Dacarbazine
B-R Buffer	:	Britton-Rabinson Buffer
MWCNT	:	Multiwall Carbon Nanotubes
GNP	:	Gold Nanoparticles

SNP	:	Silver Nanoparticles
Chit	:	Chitosan
CV	:	Cyclic Voltammetry
CA	:	Chronoamperometry
DPV	:	Differential Pulse Voltammetry
EIS	:	Electrochemical Impedance Spectroscopy
SEM	:	Scanning Electron Microscopy
EDXA	:	Energy Dispersive X-Ray Spectroscopic Analysis

CHAPTER 1

INTRODUCTION

1.1. General introduction

With the drastic increase in industrial development and in public health criteria, the modern trend in health industry is that the science is needed to detect and to quantify various analytes in complex matrixes and sophisticated conditions at sub-micron concentrations. Thus, improved performances in analytical techniques for rapid and reliable monitoring are needed. In order to answer severe norms in worldwide legislation, rapid, sensitive and specific tests need to be developed with the aim to achieve accurate results.

Sensitivity, selectivity, and rapid and cost-effective detection of target molecules are the main drivers for the development of new chemical sensors and biosensors for their use in a wide range of fields from environmental, pharmaceutical, agriculture or food applications, to health care including clinical diagnosis and treatment of diseases amongst others. During the last decade, the incorporation of nanomaterials into chemical sensors and biosensors has boosted the advances in this area leading to relevant enhancements in their performance.

Electrochemical techniques are powerful and versatile analytical tools that offer high sensitivity, accuracy, precision and miniaturization as well as a long linear dynamic range with relatively low-cost instrumentation. Electrochemical measurements are two-dimensional, with the potential being related to qualitative properties and the current related to quantitative properties. Thus, compounds can be selectively detected by electrochemical methods. This selectivity depends on the accessible potential range and the number of compounds that are active in this range.

A study on the state of art of sensors with a special attention to the chemical sensors will be given in this chapter. A brief demonstration of different types of sensors classified by their transduction methods will be followed by the role of nanocomposites as a recognition layer in the chemical sensors with a brief literature report. Then, with a description of the literature reports on the use of chemically modified electrodes (CMEs) in the analyses of pharmaceutical drugs, the objectives and followed by research framework will be presented.

1.2. Chemical sensors – Overview

As per IUPAC, the definition for the chemical sensor is "A chemical sensor is a device that transforms chemical information, ranging from the concentration of a specific sample component to total composition analysis, into an analytically useful signal". The chemical information, mentioned above, may originate from a chemical reaction of the analyte or from a physical property of the system investigated[1].

Chemical sensors contain two basic functional units: a receptor part (Recognition element) and a transducer part (Transduction technique). In the receptor part of a sensor the chemical information is transformed into a form of energy which may be measured by the transducer. The transducer part is a device capable of transforming the energy carrying the chemical information about the sample into a useful analytical signal. The transducer as such does not show selectivity.

Chemical sensors can be classified according to the operating principle of the transducer.

1.2.1. Optical sensors

Optical sensors, represent a group of chemical sensors in which electromagnetic radiation is used to generate the analytical signal in a transduction element. The interaction of this radiation with the sample is evaluated from the change of a particular optical parameter and is related to the characteristics and concentration of the analyte. Optical sensors can be divided based on various optical transduction principles (absorbance, reflectance, luminescence, fluorescence), covering different regions of the spectra (UV, Visible, IR, NIR) and allowing the measurement not only of the intensity of light but also of other related properties, such as lifetime, refractive index, scattering, diffraction and polarization. Optical sensors are often referred to as 'optodes' and the use of optical fibres is a common feature.

The continuous monitoring of an analyte, through optical means, can be categorized into two subcategories, named as direct sensing scheme and reagent mediated sensing scheme. In direct sensing scheme, an intrinsic optical property (such as absorption, fluorescence, etc.) of an analyte is monitored for sensing purposes [2–5]. Based on the employed direct sensing spectroscopic techniques to design and fabricate an optical chemical sensor, the optical chemical sensor divided into various subcategories, namely

- Absorption – based Sensing
- Fluorescence – based Sensing
- Raman and Surface Enhanced Raman Scattering (SERS) – based Sensing

When the analyte does not have an adequate intrinsic optical property which may be monitored directly, a reagent mediated sensing scheme is applied. In the situations when an analyte does not have enough spectroscopic optical response to monitor it directly in the sample, sensing can be accomplished by introducing a suitable indicator into the sensing system whose spectral properties reflect the analyte's concentration [6–8]. Practically all known indicator mediated sensors are based either on absorption or on luminescence measurements.

- Indicator – mediated Colorimetric Sensing
- Indicator – mediated Luminescence Sensing

1.2.2. Mass sensors

Surface Acoustic Wave Sensors

These make use of the piezoelectric effect. Change in the mass on the surface of a vibrating piezoelectric quartz crystal causes a proportional decrease in the vibrational frequency of the crystal. They rely on a change in mass on the surface of an oscillating crystal which shifts the frequency of oscillation [9–11]. The extent of the frequency shift is a function of the amount of material absorbed on the surface. Piezoelectric sensors have received their widest use in gas phase analyses.

Quartz Crystal Microbalance (QCM) based sensors

QCM is an ultrasensitive mass sensor. The piezoelectric AT-cut quartz crystal is sandwiched between a pair of electrodes. The electrodes are connected to an oscillator and an AC voltage is applied over the electrodes. The quartz crystal oscillates at its resonance frequency due to the piezoelectric effect. The cut angle with respect to crystal orientation determines the mode of oscillation [12–15].

Microcantilever sensors

Microelectromechanical systems can be composed of multiple micron-thick cantilevers (visualize miniature diving boards) that respond by bending due to changes in mass [16–19]. Appropriate coatings are applied to the cantilevers to adsorb chemicals of interest.

1.2.3. Thermal sensors

Generation of heat during enzyme/substrate reactions can be used in a calorimetric based biosensor. Danielsson and colleagues did the pioneering work on this technique which is applicable to a wide range of analytes [20–23]. Changes in solution temperature caused by the enzyme/substrate reactions are measured using a thermistor or transistor and compared to a sensor with no enzyme to determine the analyte concentration [24–26]. Utilizing this approach for receptor-ligand reactions has received little interest because there is no temperature change at steady-state and transient measurements are very difficult to make. Calorimetric microsensors have been manufactured for detection of cholesterol in blood serum based on the enzymatically produced heats of oxidation and decomposition [27,28]. Industrial applications are possible for monitoring sugars and amino acids for biotechnology processes [29].

1.2.4. Electrochemical sensors

Electrochemical sensors operate by reacting with the analyte of interest and producing an electrical signal proportional to the analyte concentration [30,31]. There are several types of electrochemical sensors: such as; conductometric, potentiometric, amperometric and voltammetric sensors.

Conductometric sensors or Chemiresistor

This is based on the inflection of resistivity of the selective material whereas resistivity is the reciprocal of conductivity. In a typical chemiresistor, the conductivity of a material can be changed upon contact with chemical species when clamped between two contact electrodes at which the resistivity of the entire device can be measured, and this is commonly used in gas sensing [32–34]. In conductometric sensors, the chemically interactive layer is at the top of an electrode and immersed in the solution of electrolyte and a suitable counter electrode is then provided to complete the electrical circuit. This is typically found in various biosensors, where the selectivity of the response comes from some biological interactions [35–38].

Potentiometric sensors

Potentiometric sensors have found the most widespread practical applicability since early 1930's due to their simplicity, familiarity and cost. They involve the establishment of a local equilibrium at the sensor surface, where either of the electrode or membrane potential is measured, and information about the composition of the sample is obtained

from the potential difference between reference electrode and the indicator electrodes [39–42]. Basically, in potentiometric sensors, the potential difference between the reference electrode and the indicator electrode is measured without polarizing the electrochemical cell, that is, very small current is allowed. The reference electrode is required to provide a constant half-cell potential. The indicator electrode develops a variable potential depending on the activity or concentration of a specific analyte in solution. The change in potential is related to the concentration of the analyte in a logarithmic manner. Potentiometric devices can be categorized into three basic types:

i) Ion-selective electrodes (ISE)

ii) Coated wire electrodes (CWE)

iii) Field effect transistors (FET).

Ion-selective electrode is an indicator electrode capable of selectively measuring the activity of a particular ionic species. In classic configuration, ISE are mainly membrane-based devices, consisting of permselective ion-conducting materials, which separate the sample from the inside of the electrode. One of the electrodes is the working electrode whose potential is determined by its environment while the second electrode is a reference electrode whose potential is fixed by a solution containing the ion of interest at a constant activity. Since the potential of the reference electrode is constant, the value of the potential difference (cell potential) can be related to the concentration of the dissolved ions [43–46]. Under classical CWE design, a conductor is directly coated with an appropriate ion-selective polymer (usually poly(vinyl chloride), poly (vinylbenzyl chloride) or poly(acrylic acid)) to form an electrode system that is sensitive to electrolyte concentration [47–50]. The field effect transistor (FET) is a solid-state device that exhibits high input impedance and low output impedance hence capable of monitoring charge build up on the ion sensing membrane. Polymer matrix (electrode modifiers) of the potentiometric sensors can be altered by the immobilization of biological/biomedical materials leading to the development of potentiometric biosensors [51–54].

Voltammetric / Amperometric Sensor

Voltammetry/amperometry is a method of electrochemical analysis in which the signal of interest is a current that is linearly dependent upon the characteristics and concentration of the analyte. As certain chemical species are oxidized or reduced (redox

reactions) at inert electrodes, electrons are transferred from the analyte to the working electrode or to the analyte from the electrode. The direction of flow of electrons depends upon the properties of the analyte and can be controlled by the electric potential applied to the working electrode [31,55–57]. The basic instrumentation of these sensors requires controlled applied potential equipment, and the electrochemical cell consists of three–electrode cell; namely, working electrode, reference electrode and counter electrode. The working electrode is the electrode at which the reaction of interest occurs, the reference electrode provides a stable potential compared to the working electrode while an inert conducting material (e.g. platinum, graphite) is used as the counter electrode (auxiliary electrode). A supporting electrolyte is required in controlled potential experiments to eliminate electromigration effects, decrease the resistance of the solution and maintain the ionic strength constant [58–60].

A voltammetric sensor can operate in other modes such as linear or cyclic or pulse voltammetric modes. Consequently, the respective current potential response for each mode will be different. Usually, voltammetric sensors examine the concentration effect of the detecting species on the current-potential characteristics of the reduction or oxidation reaction involved, the mass transfer rate of the detecting species in the reaction onto the electrode surface and the kinetics of the faradaic as well as the charge transfer reaction at the electrode surface that are directly affecting the current potential characteristics. This mass transfer can be attributed to; (a) an ionic migration as a result of an electric potential gradient, (b) diffusion under a chemical potential difference or concentration gradient and (c) a bulk transfer by natural or forced convection. In electrochemical cell, the electrode reaction kinetics and the mass transfer processes contribute to the rate of the faradaic process and this provides the basis for the operation of the voltammetric sensor [58–60]. A situation where a voltammetric sensor operates with a small overpotential, the rate of faradaic reaction is also small; as a result, a high-precision instrument for the measurement is needed. An amperometric sensor is usually operated under limiting current or relatively small overpotential conditions. If operated under an imposed fixed electrode potential, then the cell current can be correlated with the bulk concentration of the detecting species (the solute). This operating mode is commonly classified as amperometric in most sensor work, but it also is referred to as the chronoamperometric method, since time is involved.

The analyte molecules interact with the immobilized layer interface (e.g polymers, nanoparticles, enzymes etc.) in a lock and key mechanism to generate an electrical signal through the chosen transducer [61–64]. The generated signal is amplified and monitored with an artificial intelligence such as computer hardware/software to produce measurable analytical signal. The signal can be in the form of current, potential or impedance. Furthermore, it is possible to change the properties of the sensor by changing parameters (e.g. sensing material or temperature) during manufacturing or operation of the sensor in order to improve selectivity and sensitivity. If the signal is in the form of current, the current can be measured at a fixed potential or potential difference across an electrochemical cell is scanned from one pre-set value to another and the cell current is recorded as a function of the applied potential. The rate of flow of electrons is proportional to the analyte concentration. The working electrode can be modified with different materials such as polymers, nanoparticles or composites of polymers and nanoparticles etc., to increase its sensitivity and reduce electrode fouling of reduced or oxidized species [65–67].

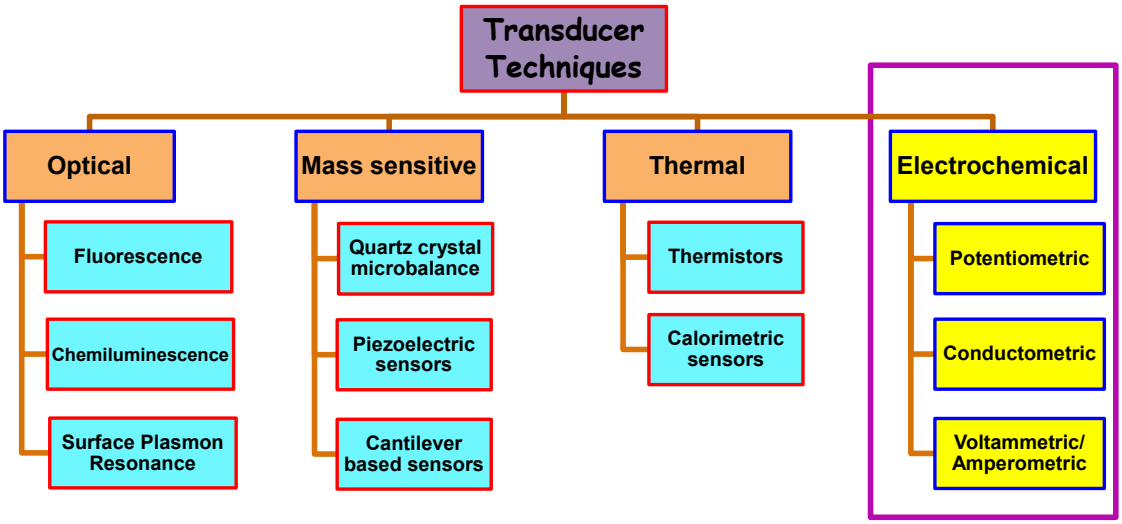

***Figure 1.1**. Various transduction techniques applied in chemical sensor systems.*

1.3. Electrochemical techniques employed in this research

Electrochemistry affords some of the most sensitive and informative analytical techniques in the chemist's tools. Electroanalytical methods such as cyclic voltammetry, stripping voltammetry, differential pulse voltammetry, square wave voltammetry, impedance spectroscopy and chronoamperometry complements other analytical techniques such as chromatography and spectroscopy, and are not only capable of assaying trace concentrations of an electroactive analyte but also supply useful

information concerning its physical and chemical properties. Electrochemical methods of analysis include all methods of analysis that measure current, potential and resistance and relate them to the analyte concentration. Quantities such as oxidation potentials, diffusion coefficients, electron transfer rates, and electron transfer numbers, which are difficult to extract using other techniques, are readily obtained using electroanalytical methods.

Electrochemical methods of detection are based on electrochemical processes that take place on the electrode surface. There are different modes of electrochemical detection. Voltammetric and amperometric assays are based on the measurement of current at the working electrode resulting from the application of a voltage at the electrode-solution interface. In case of voltammetry, the current is measured as a function of changing potential that can be applied in different ways (linear, cyclic, pulse modes). Amperometric measurements are performed by maintaining a constant potential at the working electrode with respect to a reference electrode and measuring the generated current wit time. Impedance spectroscopy involves the use of a small-amplitude perturbing sinusoidal voltage signal to the electrochemical cell and measuring the current response in the form of impedance.

Among the various electroanalytical techniques, cyclic voltammetry and differential pulse voltammetry are two commonly and widely used techniques. Along with them, electrochemical impedance spectroscopy provides critical information related to the electrode–solution interface and electron transfer behaviour between electrode and electroactive species and chronoamperometry provides the diffusion behaviour of the analyte towards the specific electrode system.

In this section, we have provided basic principles and brief information of the most widely used electroanalytical techniques such as cyclic voltammetry, chronoamperometry, electrochemical impedance spectroscopy and differential pulse voltammetry, which are used in our investigations in the development of electrochemical sensor system.

Cyclic voltammetry

This technique works by varying the applied potential of the working electrode at a particular scan rate (ν) in both forward and reverse directions while monitoring the current. The resultant trace of current against potential is termed as a voltammogram.

During cyclic voltammetry measurement, the potential is ramped from an initial potential, E_i, to a more negative or positive potential but, at the end of the linear sweep, the direction of the potential scan is reversed, usually stopping at the initial potential, E_i (or it may commence an additional cycle). The potential is applied between the reference electrode and the working electrode, and the resultant current between the working electrode and the counter electrode (auxiliary electrode) is measured. This data is then plotted as current versus potential as shown in Figure 1.2. The forward scan produces a current peak for any analyte that can be either reduction current or oxidation current depending on the initial scan direction over the range of potential scanned. The current increases as the potential reaches the reduction potential of the analyte, but then decreases as the concentration of the analyte is depleted close to the electrode surface. If the redox couple is reversible, then reversing the applied potential makes it to reach a potential that re-oxidizes the product formed in the first reduction reaction, thus producing a current of reverse polarity from the forward scan. The oxidation peak usually has the same shape as that of the reduction peak. As a result, the information about the redox potential and the electrochemical reaction rates of compounds can be obtained. For instance, if the electron transfer is fast at the electrode surface and the current is limited by the diffusion of species to the electrode surface, then the peak current is proportional to the square root of the scan rate.

Important parameters are usually obtained from cyclic voltammograms for analysis of redox properties of an electroactive sample. These parameters include peak potentials (E_{pc}, E_{pa}) and peak currents (i_{pc}, i_{pa}) of the cathodic and anodic peaks, respectively. Consequently, important information about the sample under investigation can be obtained from the above peak parameters. This includes whether the electrochemical process displayed by the sample is reversible, irreversible or quasi–reversible. It also gives an insight into how fast the electron process is, relative to other processes such as diffusion. For instance, if the electron transfer is fast relative to the diffusion of electroactive species from the bulk solution at the surface of the electrode, the reaction is said to be electrochemically reversible and the peak separation (ΔE_p) is given by equation below;

$$\Delta E_p = \left| E_{pa} - E_{pc} \right| = 2.303\, RT/nF$$

where ΔE_p is the peak separation (V), E_{pa} is the anodic peak potential (V), E_{pc} is the cathodic peak potential (V), n is the number of electrons, F is the Faraday constant (96486 C mol^{-1}), R is the gas constant (8.314 J mol^{-1} K^{-1}) and T is the absolute temperature of the system (K). The number of electrons (n) involved in the electrochemical process can be estimated from the above equation. Thus, for a reversible redox reaction at 25 °C (298 K) with n electrons, ΔE_p should be (0.0592/n) V or about 60 mV for one electron. In practice, this value is difficult to attain because of cell resistance. Irreversibility due to a slow electron transfer rate results in ΔE_p > (0.0592/n) V, possibly, greater than 70 mV for a one-electron reaction.

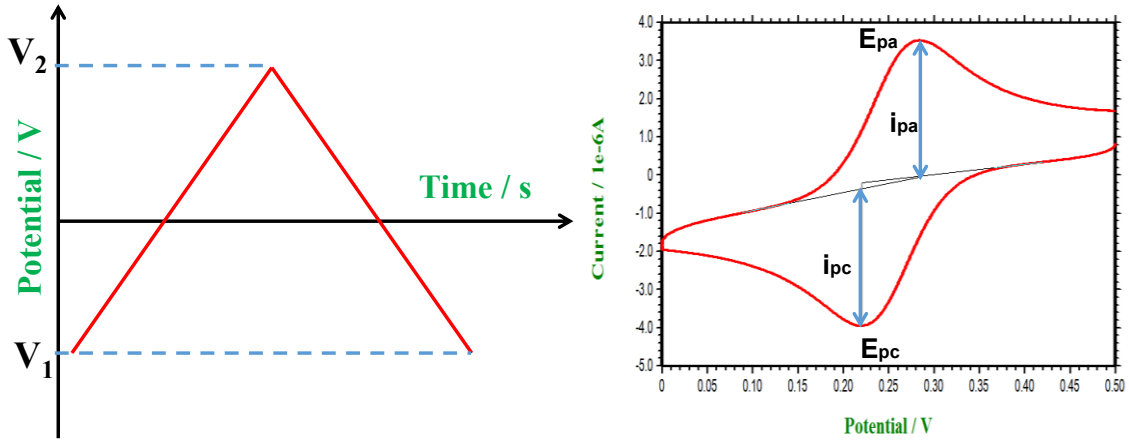

***Figure 1.2**. Profile of applied potential in CV and a typical cyclic voltammograms.*

For reversible reaction, the concentration is related to peak current by the Randles-Sevcik equation (at 25 °C).

$$i_p = 2.69 \times 10^5 n^{1/2} A D^{1/2} v^{1/2} C$$

where i_p is the peak current in amperes, ν is the potential sweep rate in V s^{-1}, A is the electrode surface area (cm^2), n is the number of electrons transferred, D is the diffusion coefficient (cm^2 s^{-1}), and C is the concentration in mol cm^{-3}. Several voltammograms performed at different scan rates can lead to the preparation of linear plots whose slopes could give further information about the redox properties of the sample in question. For instance, when the peak current is plotted against the square root of the scan rate, the slope of the linear plot can be used to estimate the diffusion coefficient according to the Randles- Sevcik equation[68] shown above.

For an irreversible electrode process of the electrochemical reaction of an analyte, the Laviron's equation[69] was used to estimate αn and k° values as follows:

$$Ep = E^{\circ} + \frac{RT}{\alpha nF} ln\left[\frac{RTk^{\circ}}{\alpha nF}\right] + \left[\frac{RT}{\alpha nF}\right] ln(\nu)$$

where α is the electron transfer coefficient, k° is the standard rate constant of the electrode surface reaction, ν is the scan rate, n is the electron transfer numbers and E° is the formal potential. The values of k° and αn can be calculated from the intercept and slope of the linear plot of E_p with respect to ln(ν), if the value of E° is known. The value of E° can be obtained from the intercept of the E_p vs. ν plot by extrapolation to the vertical axis at ν = 0. From the slope of the E_p vs. ln(ν) plot, αn can be calculated. Generally, α can be assumed to be 0.5 for an irreversible electrode process. So the electron transfer number (n) for the electrochemical oxidation of analyte also can be calculated, and the k° value is determined from the intercept of E_p vs. ln(ν).

Chronoamperometry

Chronoamperometry (CA), another commonly used electroanalytical technique, is a useful tool for determining diffusion coefficients and for investigating kinetics and mechanisms. Chronoamperometry experiments are most commonly either single potential step, in which only the current resulting from the forward step as described above is recorded, or double potential step, in which the potential is returned to a final value (E_f) following a time period, usually designated as t, at the step potential (E_s).

The most useful equation in chronoamperometry is the Cottrell equation,[68] which describes the observed current (planar electrode) at any time following a large forward potential step in a reversible redox reaction (or to large overpotential) as a function of $t^{-1/2}$.

$$i = nFAC\pi^{-1/2}D^{1/2}t^{-1/2}$$

where n = stoichiometric number of electrons involved in the reaction;

F = Faraday's constant (96,485 C/equivalent),

A = Electrode area (cm^2),

C = Concentration of electroactive species (mol/cm^3),

and D = Diffusion constant for electroactive species (cm^2/s).

Using this Cottrell equation, the diffusion coefficient can be calculated by simply rearranging the equation, providing the number of electrons obtained from the CV experiment and providing values for the other variables. Another useful parameter to calculate is the "true" area of the electrode. In many cases the geometric area of an electrode is not the same as the electrochemically active area. Geometric area calculations assume a smooth surface, but any surface roughness actually increases the available area of the electrode.

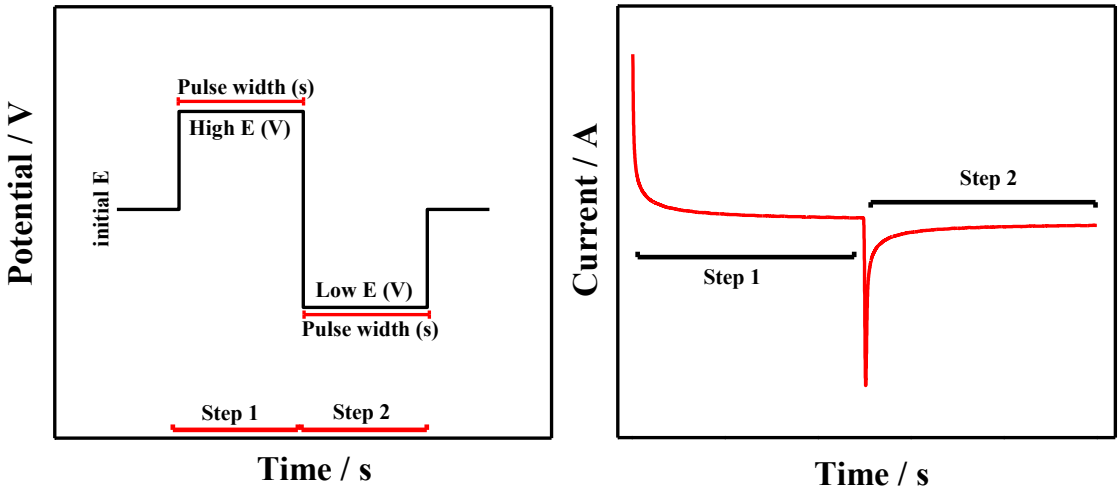

***Figure 1.3**. Profile of applied potential in double - step CA and a typical double - step CA plot.*

Electrochemical Impedance Spectroscopy (EIS)

Electrochemical Impedance Spectroscopy (EIS) or ac impedance methods have seen tremendous increase in popularity in recent years. Initially applied to the determination of the double-layer capacitance[70] but now a days it is applied to the characterization of electrode processes and complex interfaces. EIS studies the system response to the application of a periodic small amplitude ac signal. These measurements are carried out at different ac frequencies and, thus, the name impedance spectroscopy was later adopted. Analysis of the system response contains information about the interface, its structure and reactions taking place there.

Macdonald, in his review[71], outlined the foundation of electrochemical impedance spectroscopy (EIS). Electrochemical impedance spectroscopy is an excellent, non-destructive, accurate and rapid in situ technique for examining processes occurring at

electrode surfaces. Impedance spectroscopy involves the use of a small-amplitude perturbing sinusoidal voltage signal to the electrochemical cell and measuring the current response. The resulting faradic impedance spectrum, known as a Nyquist plot, corresponds to the dependence of the imaginary number on the real number, and contains extensive information about the electrified interface and the electron transfer reaction. Nyquist plots commonly include a semicircle region lying on the X-axis followed by a straight line. The semicircle portion (observed at higher frequencies) relates to the electron-transfer-limited process, while the straight line (characteristic of the low-frequency range) signifies the diffusion-limited process. Such spectra can be used for extracting the electron transfer kinetics and diffusional characteristics. Fast electron transfer processes include only a linear part in the impedance spectrum, while at slow electron transfer processes are characterized by the presence of a large semicircular region. The diameter of the semicircle equals the electron transfer or charge transfer resistance (R_{CT}). The intercepts of the semicircle with the Z' axis correspond to those of solution resistance (R_s). Another representation of EIS data is Bode plot, where the impedance is plotted with log (frequency) values on the X-axis and both the absolute values of the impedance ($|Z| = Z_0$) and the phase-shift on the Y-axis. Unlike the Nyquist Plot, the Bode Plot does show frequency information. Bode plots contain all the necessary information and that is why they are mainly used in the circuit analysis. The Bode magnitude plots may be easily predicted from the circuit impedance.

Impedance is the total complex resistance encountered when a current flows through a circuit made of combinations of resistors, capacitors, or inductors. Electrochemical transformations occurring at the electrode–solution interface can be modelled using components of the electronic equivalent circuitry that correspond to the experimental impedance spectra. A particularly useful model to interfacial phenomena is the Randles electronic equivalent-circuit model. This includes the double-layer capacitance C_{dl}, the ohmic resistance of the electrolyte solution R_s, the charge transfer resistance R_{CT} and the Warburg impedance W resulting from the diffusion of ions from the bulk solution to the electrode surface.

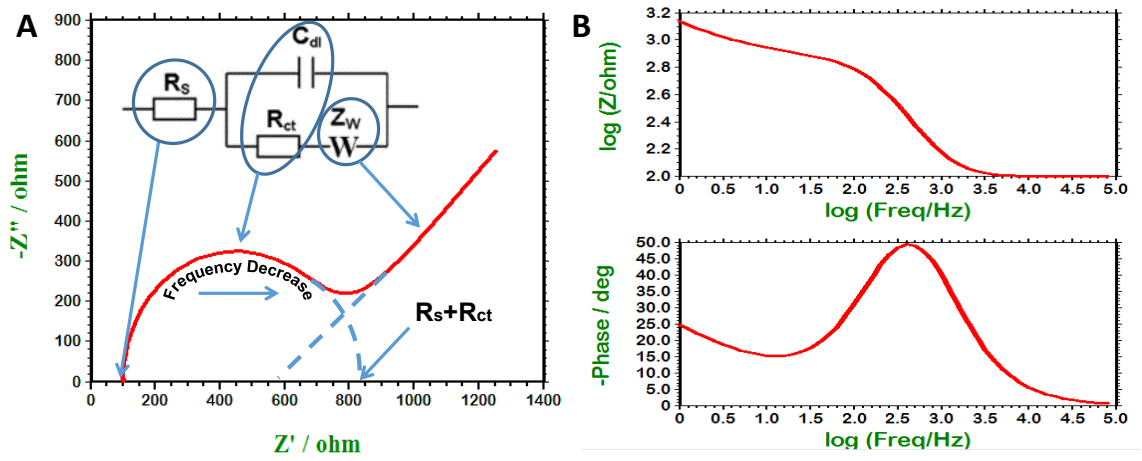

Figure 1.4. *Typical spectra of EIS measurements (A) Nyquist plot (Inset: Randles Equivalent circuit with Warburg) and (B) Bode plot.*

Differential Pulse Voltammetry

Differential pulse voltammetry (DPV) involves the application of a linear potential ramp with fixed magnitude pulses to the working electrode (Figure. 1.1). The current is sampled twice, just before the pulse application and again late in the pulse life, when the charging current has decayed. The first current is subtracted from the second, and this current difference is plotted against the applied potential. The use of the pulse minimizes the effect of charging current which gives more reliable oxidation or reduction current of analyte. The resulting differential pulse voltammograms consists of current peaks that are directly proportional to the concentration of the corresponding analytes. By changing the pulse height and pulse width, the sensitivity and the selectivity of the analysis increases.

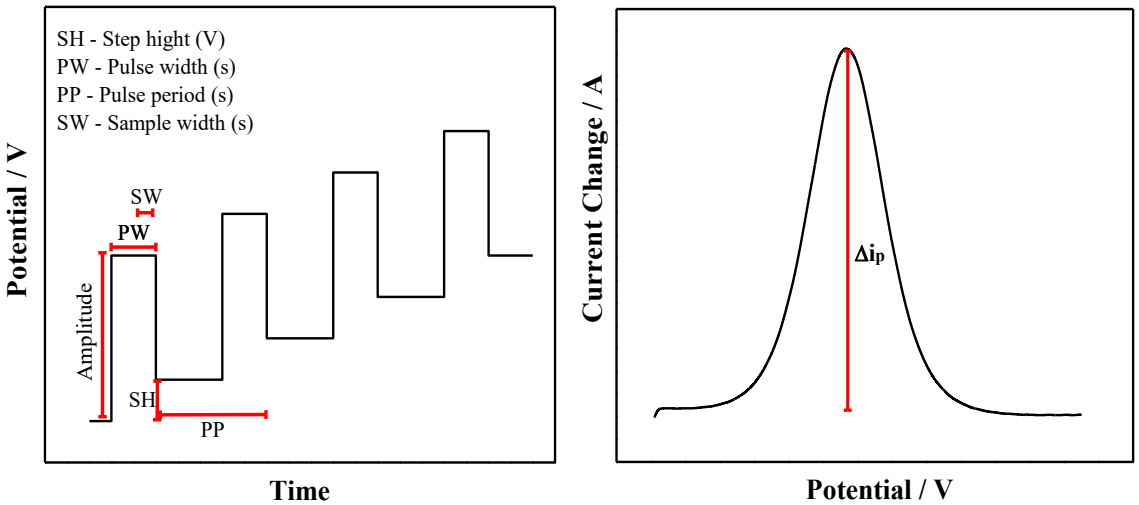

Figure 1.5*. Profile of applied potential in DPV and a typical differential pulse voltammogram.*

1.4. Chemically Modified Electrodes (CMEs)

A chemical sensor involves a sensing layer together with a transducer. The sensing layer represents the main part of the sensor. Many organic, inorganic or hybrid organic-inorganic based materials can be used as active sensing layers, provided that the analytes can diffuse into the sensing matrix and be trapped, thus modifying the physical or/and chemical properties of the material. The active layer can also be doped with specific probe-molecules that are able to interact selectively with the target analytes, thus providing the selectivity of the sensor. The role of the transducer is to convert the variation of a physical property associated with a chemical interaction into a measurable signal which is proportional to the analyte concentration.

An active area of research in electrochemical sensors is the development of electrodes produced by chemical modification called chemically modified electrodes (CMEs) using a various type of materials of desired qualities. Such electrodes have been tailored to accomplish a broad range of functions. Modifications include applying irreversibly adsorbing substances with desired functionalities, covalent bonding of components to the surface and coating the working electrode with polymer films or films of other substances. One of the most important properties of CMEs is their ability to catalyze the oxidation or reduction of solute species that exhibits high over potential at unmodified surfaces. Thus CMEs play an important role in reducing the over potential required for the voltammetricsdetermination of analyte without its major interferences.

Modified electrodes have many applications. A primary interest has been in the area of electrocatalysis. Another application is in the production of electrochromic devices that change colour on oxidation and reduction. Finally the most important analytical use for such electrodes is the development of analytical sensors those are selective for particular species or functional groups. Various substrates such as carbon nanotubes (CNT), gold nanoparticles (AuNPs), polymer films, metalloporphyrins, calixarenes etc. are used for the modification of electrode surface. For the present study, the modification techniques adopted are CNT based modifications incorporating AuNPs, AgNPs and electropolymerization.

Modifications based on Carbon Nanotubes

Carbon nanotubes (CNTs), discovered by Iijima,[72] are an interesting class of nanomaterials offering high electrical conductivity, high surface area, significant

mechanical strength and good chemical stability. CNTs constitute a new structure of graphitic carbon consisting of one or several concentric tubules each with a helically wound hexagonal honeycomb lattice and can be divided into multi-wall carbon nanotubes (MWCNT) and single wall carbon nanotubes (SWCNT) according to the carbon atom layers in the wall of the nanotubes. CNTs have an aspect ratio ranging from 100 to 1000.

Carbon nanotubes have been known to promote electron transfer reactions when used as electrode modification material. In addition to enhanced electrochemical reactivity, CNT-modified electrodes have been shown useful to accumulate important biomolecules (e.g., nucleic acids) and to alleviate surface fouling effects. Since the first use of the CNT based electrode by Britto et al. for the detection of dopamine,[73] research on the application of both MWCNT and SWCNT for electrode modification has expanded into many areas. Electrode modification with CNTs usually involves their direct immobilization on the surfaces of carbon electrodes (mostly glassy carbon electrodes, GCEs) via drop-cast or by abrasive immobilization (mostly on pyrolytic graphite electrodes) methods. The remarkable sensitivity of CNT conductivity to the surface adsorbates permits the use of CNT as highly sensitive nanoscale sensors. These properties make CNT extremely attractive for a wide range of electrochemical biosensors ranging from amperometric enzyme electrodes to DNA hybridization biosensors. To take advantages of the remarkable properties of these unique nanomaterials in such electrochemical sensing applications, the CNT need to be properly functionalized and immobilized.

After synthesis, CNTs may be treated to functionalize their surfaces. The most common treatment with strong acids removes the end caps and may also shorten the length of the CNTs. Acid treatment also adds oxide groups, primarily carboxylic acids, to the tube ends and defect sites. Further chemical reactions can be performed at these oxide groups to functionalize with groups such as amides, thiols or others. Altering the nanotube surface strongly affects solubility properties, which can affect the ease of fabrication of CNT sensors. Non-covalent functionalization by small molecules, grafting to or wrapping nanotubes with polymers or DNA can also alter the electrochemical properties of the material, as reviewed by Zhao and Stoddart.[74] A review by Balasubramanian and Brughand discusses many of the functionalizations that have commonly been used[75]. The CNT ends and sidewall “defect” sites have been proposed

to act similar to pyrolytic graphite edge planes and therefore have greater electrochemical activity. Recent works however have contended that the sidewall defects may be responsible for the electrochemical activity of CNTs. Covalent and non-covalent sidewall and defect site functionalizations have also been demonstrated to play a role in the electrocatalytic properties of CNTs.

Modifications based on metal nanoparticles

The design of new nanoscale materials has acquired great importance in recent years owing to their wide-ranging applications in various fields. Among these materials, metallic nanoparticles such as gold, silver, platinum, palladium, etc. are of great interest due to their important properties and their numerous possible applications. The metal nanoparticles have size-dependent unique chemical, electrical and optical properties and are very promising for practical applications in diverse fields [76–79]. The nanoparticles are very different from bulk materials and their electronic, optical and catalytic properties originate from their quantum scale dimensions. The electrocatalytic activity of metal nanoparticles is strongly dependent on their composition, size, surface area and surface morphology.[80,81] Noble metal nanoparticles have been extensively utilized in recent years, owing to their extraordinary catalytic activities for both oxidation and reduction reactions. To obtain high surface area, metal nanoparticle catalysts are usually dispersed in organic polymers such as nafion, colloids, surfactants and porous substrates, which enable metal particles to be highly dispersed and stable against aggregation[82–85]. In recent years, metal nanoparticles (MNPs) have been extensively studied in electrochemistry because of their special physico-chemical characteristics. The use of MNP based superstructures for the creation of electrochemical devices is an extremely promising prospect. Various methodologies have been used for tailoring MNPs on electrode surfaces, which include the anchoring by electrostatic interaction, covalent linkage, electrochemical deposition etc. Arrays of MNPs have been utilized for electrochemical sensors as they exhibit excellent catalytic activity towards various reactions. Here, the MNPs function as electron antennae efficiently tunnelling electrons between the electrode and electrolyte.

The catalytic activity of metal nanoparticles is known to depend highly on their dispensability and surface properties. As usual, for many catalytic processes, a high degree of dispensability and large surface area are desirable. Conducting polymers are

often considered to be useful matrices for the immobilization of the dispersed nano metal catalysts.[82] Because of a relatively high electrical conductivity of some polymers, it is possible to shuttle the electrons through polymer chains between the electrodes and dispersed metal nano particles, where the electrocatalytic reaction occurs.

In addition to linker molecules, capping reagents should also affect the electron-transfer reactions and electrocatalytic functions of metal NPs. In the development of the synthesis of AuNPs, the Brust–Schiffrin[86] method would really be a breakthrough to prepare a large amount of very small AuNPs with uniform-size utilizing thiols. Because the synthesized MNPs get easily segregated, the thiol-capped gold or silver NPs might be assumed to be a component of the MNP-modified electrode.[87,88] However, thiol capping is too strong to obtain good electrochemical results, though the electrochemistry of thus-formed monolayer-protected Au/Ag clusters was extensively studied. Along with the thiol capping, stabilization of NPs with amine functional groups is also good for electrocatalytic activity[89–91]. To enhance the performance of metal NP-modified electrodes toward electrocatalysis, we should also take note the selection of capping or stabilizing reagents. The electrocatalytic activities of CMEs are further increased by using composites of MNPs with various other electrocatalytic materials such as CNTs, graphene, conducting polymers, metal oxide frameworks, etc.[92–97]

Modifications based on conducting polymers

Since the discovery of organic conducting polymers more than 20 years ago, these materials are finding an increasing use in various branches of technology, such as metallization of dielectrics, primary and secondary batteries, antistatic coatings, electromagnetic shielding, electrochromic systems, etc. Organic conjugated polymers (conducting polymers) are mainly organic compounds that have an extended p-orbital system, through which electrons can move from one end of the polymer to the other.[98] Common classes of organic conducting polymers include polyacetylenes, polypyrroles, polythiophenes, polyanilines, poly(3-alkylthiophene)s, poly(p-phenylene sulfide), etc. One of the most striking properties of conducting polymers is their ability to catalyze some electrode reactions. A thin layer of a conducting polymer deposited onto the surface of substrate electrode is able to enhance the kinetics of electrode processes.[99–102] In an electrochemical polymerization, the monomer, dissolved in an appropriate solvent, is oxidized at the surface of an electrode by applying of an anodic potential (oxidation). Choice of the solvent and electrolyte is of particular importance in electrochemistry

since both should be stable at the oxidation potential of the monomer and provide an ionically conducting medium.

Electropolymerization is generally achieved by potentiostatic (constant potential), galvanostatic (constant current) and potentiodynamic (potential scanning *i.e.* cyclic voltammetry) methods. These techniques are easier to be described quantitatively and therefore have been commonly utilized to investigate the nucleation mechanism and the macroscopic growth. Potentiodynamic techniques such as cyclic voltammetry have been mainly used to obtain qualitative information about the redox processes involved in the early stages of polymerization reaction and to examine the electrochemical behaviour of the polymer film after electrodeposition. Polymer modified electrodes (PMEs) prepared by electropolymerization have received extensive interest in the detection of analytes because of their selectivity, sensitivity and homogeneity in electrochemical deposition, strong adherence to electrode surface and chemical stability of the film.[103–105] Selectivity of PMEs as sensors can be attained by different mechanisms such as size exclusion, ion exchange, hydrophobic interaction and electrostatic interaction. Information concerning the hydrophobicity of coating films can help in better evaluation of the sensitivity of the examined sensor to the desired analytes.

Along with above CNT, metal nanoparticles and conducting polymers, there are a good number of other materials that the researchers focused are listed in the below figure.

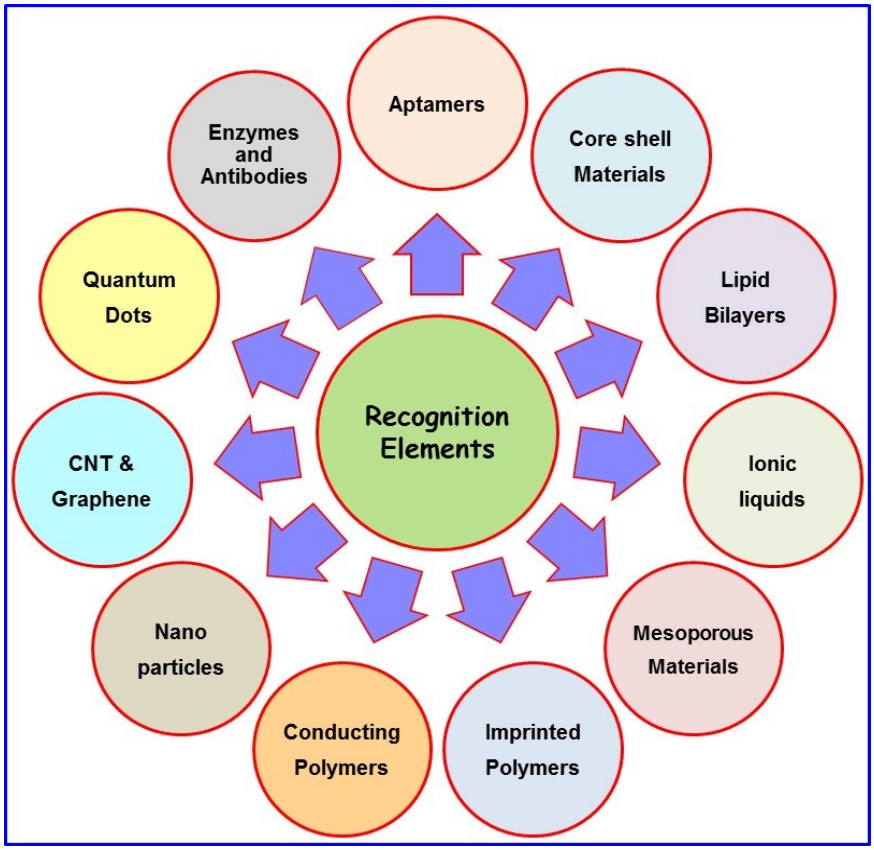

Figure 1.6. *Various types of materials used in CMEs.*

1.5. Literature reports on CMEs as Sensors for Pharmaceutical Drugs

In this section, literature reports are critically reviewed on the applications of biosensors for the detection of pharmaceutical drugs. Both research and development of pharmaceutical analysis embraces innovative procedures in a bid to combine accuracy, precision, selectivity and sensitivity with simplicity, rapidity and low cost. Hence, the interest in biosensors has increased over recent years, since such devices consolidate many of these qualities, including simplicity and rapidity. Indeed, due to these characteristics, biosensors have been applied to many fields of chemical analysis including biomedical, pharmaceutical, food and environmental.

The electrochemical techniques, especially voltammetry, have gained steadily an importance during recent years. They have been applied for the determination of pharmaceutical compounds in dosage forms (tablets, capsules, injections and suspension) and biological samples (real and spiked urine samples, blood and serum). There are various reviews available in the literature on electrochemical detection of pharmaceutical compounds. Cavalheiro, in his review, outlined on the detection of various pharmaceutical drugs on different types of electrode materials and on modified

electrodes.[106] Gil and Melo has reported a review on the use of electrochemical biosensors on pharmaceutical drugs and the development of new material transducers as well as immobilization techniques of recognizing agents can be found on the literature.[107] Siddiqui et al. have discussed the various analytical techniques including electrochemical methods towards the detection of pharmaceutical drugs of different categories.[108] Various types of pharmaceutical compounds analyzed by voltammetric techniques at different CMEs using various electrochemical techniques have been discussed by Farghaly et al.[109] Hereby, we have reviewed some electrochemical sensors for pharmaceutical compounds of selected categories analyzed by voltammetric techniques and CMEs.

Anti-inflammatory and analgesic drugs

The drugs belonging to NSAID (Non-Steroidal Anti-inflammatory Drug) therapeutical class are the most consumed in the world. In view of the number of analyses carried out every day, extensive research further in the development of alternative methods that combine rapidity and simplicity with low cost is needed.

Acetaminophen, also known as paracetamol, is a medication used to treat pain and fever. Mohsen et al. reported a simple, rapid and sensitive electrochemical method for simultaneous determination of acetaminophen and atenolol in Britton-Robinson buffer on a gold nanoparticles incorporated carbon paste electrode [110]. Sanghavi et al. have fabricated a carbon nanotube paste electrode modified in situ with Triton X 100 for the individual and simultaneous determination of acetaminophen, aspirin and caffeine[111]. Recently, Gui Ting et al. developed an electrochemical sensor of acetaminophen based on an electrochemically reduced graphene (ERG) loaded nickel oxides (Ni_2O_3-NiO) nanoparticles coated onto glassy carbon electrode (ERG/Ni_2O_3-NiO/GCE) prepared by a one-step electrodeposition process[112]. Very recently, Adhikari et al. published a high-performance electrochemical sensor for the sensitive detection of acetaminophen based on graphene, which was simultaneously electrochemically reduced and deposited onto a glassy carbon electrode (GCE) [113]. There is a plenty of research has been done on the electrochemical detection of paracetamol [114–116].

Ibuprofen, from isobutylphenylpropanoic acid, is another important nonsteroidal anti-inflammatory drug (NSAID) used for treating pain, fever and inflammation. Sorina et al. describes the electrochemical behaviour of ibuprofen on two types of multi-walled

carbon nanotubes based composite electrodes comprising epoxy resin and silver-modified zeolite[117]. Later, Sidra and group reported the potential of square wave voltammetry for the determination of ibuprofen in aqueous solution with screen printed graphite electrodes, especially pretreated for this purpose, and to investigate the electrochemical oxidation of ibuprofen[118]. Recently, two groups have reported on aptasensor based electrochemical detection of ibuprofen, one is reported by Roushani and Shahdost-fard on the development of an ultrasensitive nanoaptasensor based on the covalent attachment of an aptamer to gold-nanoparticles deposited on glassy carbon electrode as the unique platform[119] and another is reported by Shahdost-fard and Roushanion on an impedimetric aptasensor for ultrasensitive detection of ibuprofen using water soluble cadmiumtelluride quantum dots as the efficient electrochemical platform[120].

Naproxen, [(+)-2-(6-metoxy-2naphthyl)propionic acid], is a non-steroidal anti-inflammatory drug and it is extensively used in the treatment of many diseases like rheumatoid arthritis, degenerative joint disease, ankylosingspondylits, acute gout and primary dismenorrea. Parviz et al. investigated on the electrochemical oxidation of naproxen and paracetamol using dysprosium nanowire modified carbon paste electrode by square wave voltammetry as a new rapid, convenient and sensitive method [121]. Tashkhourian et al. reported on ZnO nanoparticles and multiwalled carbon nanotubes (MWCNTs) modified carbon paste electrode (CPE) as a fast and sensitive tool for the investigation of electrochemical oxidation of naproxen in biological pH [122]. Later, a chiral electrochemical sensor was developed using a gold electrode modified with gold nanoparticles and L-cysteine self-assembled monolayers to study the difference between the interactions of naproxen enantiomeric composition with the chiral modified electrode surface [123]. Recently, Alizadeh and group reported a nanostructured conducting molecularly imprinted polypyrrole film which electrochemically synthesized on a quartz crystal microbalance (QCM) gold electrode and overoxidized for increased selectivity as recognition element for QCM detection of NAP.[124]

So many other anti-inflammatory drugs investigated were electrochemically by using various types of CMEs, such as *celecoxib* investigated by polyaniline grafted multiwall carbon nanotubes modified electrode[125] and *dextromethorphan* is investigated by reduced graphene oxide modified screen-printed electrode[126] and carbon nanotube-carbon microparticle-ionic liquid composite modified electrode[127].

Anti-cancer drugs

Anticancer, or antineoplastic, drugs are used to treat malignancies and to control the growth of cancerous cells. There is a variety of electrochemical sensors developed to detect anticancer drugs by chemically modified electrodes. Liu and group developed an enzyme modified electrodes with Glutathione-s-transferase for detecting various anticancer drugs such as glutahione, 1-chloro-2,4-dinitrobenzene, cis-diamminedichloro platinum (II), pirarubicin, gemcitabine hydrochloride, carboplatin, oxaliplatin, pirarubicin, doxorubicin hydrochloride[128].

Doxorubicin also known as daunomycin is an anthracycline glycoside used in treatment of a variety of cancer diseases. Flechsig et al. examined the analytical response of daunomycin at different types of electrodes such as hanging mercury drop, gold, gold/bismuth, gold/mercury and silver mercury[129]. Zima et al. has reported on differential pulse voltammetric determination of doxorubicin at a carbon paste electrode[130]. Junjie and group developed a sensitive electrochemical method for the determination of doxorubicin using a glassy carbon electrode modified with a nano-titania/nafion composite film as sensor platform[131]. Later, Zanoni et al. developed a sensor for doxorubicin using poly-L-glutamic acid modified glassy carbon electrode as a sensor interface[132]. Chuan and research group have proposed an electrochemical sensor based on a cyclodextrin-graphene hybrid nanosheet modified glassy carbon electrode for the ultrasensitive simultaneous determination of doxorubicin and methotrexate[133].

Mitoxantrone is an anthracycline used as an antitumour antibiotic for leukaemia and breast cancer treatment, due to its interaction with DNA. Initially, Brett and group established the electrochemical oxidation of mitoxantrone, as a complex, pH-dependent, irreversible electrode process involving several metabolites at glassy carbon electrode and at DNA biosensor[134,135]. Hong and Cheng developed a novel chitosan dispersed graphene modified glassy carbon electrode to study the electrochemical characteristics of mitoxantrone [136]. Afterwards, Agrawal et al. fabricated a nanobiosensor to determine the toxicological behaviour of mitoxantrone and to study its interaction with DNA[137].

5-Fluorouracil is an antineoplastic agent which acts as an antimetabolite to uracil and used primarily for the treatment of solid tumours of breast, colon and rectum. Khodari developed a cathodic stripping voltammetry method to determine 5-fluorouracil in the presence of traces of Cu(II) to enhance the peak current of the adsorbed

molecule[138]. Mirceski et al. reported the electrochemical behaviour of 5-fluorouracil at a hanging mercury drop electrode by employing square-wave voltammetry method[139]. Hou and group fabricated an electrochemical sensor for 5-fluorouracil using an ionic liquid modified carbon paste electrode,[140] and Wang developed a disposable gold nanoparticles modified screen-printed electrode for sensitive determination of 5-fluorouracil[141]. Prasad and Co-researchers have developed two types of molecularly imprinted polymer (MIP) based modified electrodes for 5-fluorourcil detection, one is MIP-modified hanging mercury drop electrode[142] and another is nonhydrolytic sol–gel derived imprinted polymer–multiwalled carbon nanotube composite fiber electrode[143].

Topotecan is an anticancer drug and has been widely used in the treatment of ovarian and cervical cancers. Li et al. reported a sub-picomolar level determination of topotecan and have first proposed sodium dodecyl sulfate as a sensitizing reagent at an improved disposable wax-impregnated graphite electrode[144]. Recently, Srivastava and his research group fabricated a highly sensitive and stable TiO_2/graphene/chitosan modified glassy carbon electrode and the sensor exhibited excellent electrocatalytic activity with fast response and convenient determination of topotecan[145].

Dacarbazine, an important chemotherapeutic agent, in particular for the treatment of malignant melanoma. Ordieres et al. have investigated the electrochemical behaviour of dacarbazine by differential pulse polarography at the dropping mercury electrode[146]. Rodriguez and Co-researchers have studied the electrochemical behaviour of the dacarbazine and its major metabolite, 5-aminoimidazole-4-carboxamide, on carbon paste electrodes using linear sweep voltammetry and differential pulse voltammetry[147]. Temerk et al. have developed an indirect method to examine the electrochemical reduction of the dacarbazine-Cu^{2+} complex using cyclic voltammetry and square wave voltammetry at a hanging mercury drop electrode. Along with this, many of the researchers focused on the electrochemical studies on dacarbazine and DNA interactions and binding behaviour at various modified electrodes[148–150].

Various other anticancer drugs were also examined at various CMEs for their sensitive detections. G*emcitabine* was electrochemically studied at gold electrode and at polyaniline-gold nanocomposite modified electrode[151,152]. *Carboplatin* examined at DNA modified glassy carbon electrode[153] and electrochemical sensor for cisplatin was

developed using several metals (Ag, Co, Ru, Pd, Os, Pt, Cu, Pb) deposited carbon paste electrodes[154] and multi-walled carbon nanotubes modified screen-printed electrodes[155].

Cardiovascular agents

Cardiovascular agents are drugs, which are used to treat the conditions of heart or the circulatory or vascular system.

Atenolol is one of the most widely used β1-receptor blocking agent, which is of immense therapeutic use in the treatment of various cardiovascular disorders, such as angina pectoris, cardiac arrhythmia and hypertension. Cervini has developed a graphite-polyurethane composite electrode as an amperometric detector in the flow injection determination of atenolol in pharmaceutical formulations [156]. Electrochemical behaviour of atenolol at a carbon paste electrode modified with mordenite zeolite was described by Arvand and group[157]. Pruneanu fabricated a novel nanostructured assembly based on poly(glutamic) acid/cysteine/gold nanoparticles to study the atenolol oxidation [158]. Ghoreishi et al. developed a differential pulse voltammetry method for simultaneous determination of betaxolol and atenolol at the surface of a multi-walled carbon nanotube modified carbon paste electrode[159].

Verapamil, is commonly used for the treatments of supraventricular arrhythmias, angina and hypertension. The electrooxidative behavior and determination of verapamil on a glassy carbon disc electrode were investigated by S Demircan and group[160]. Brett et al. developed a solid graphite-polyurethane composite electrode to determine the release profiles and the characteristics of electro-oxidation process of verapamil [161]. Oliveira and co-researchers described the individual determination of verapamil and propranolol in pharmaceutical formulations using a glassy carbon electrode modified with functionalized multiwalled carbon nanotubes within a poly (allylamine hydrochloride) film[162]. Jouyban et al. investigated the electrochemical behavior of verapamil using cyclic voltammetry, differential pulse voltammetry and square wave voltammetry at the sulfonic acid functionalized magnetic mesoporous silica impregnated carbon paste electrode[163].

Clopidogrel, an oral thienopyridine-class antiplatelet agent used to inhibit blood clots in coronary artery disease, peripheral vascular disease, cerebrovascular disease, and to prevent myocardial infarction (heart attack) and stroke. A very few reports found on

this drug. Dermis et al. examined the electroanalytical behaviour of clopidogrel bisulfate was investigated by cyclic voltammetry and differential pulse voltammetry techniques using a glassy carbon electrode[164]. Later, Khorshid fabricated a carbon paste electrode comprised of an ion-pair based on clopidogrel with silicotungstate for sensitive, selective, simple, and rapid determination of clopidogrel bisulfate[165].

Another important cardiovascular agent *Acebutolol* was investigated electrochemically at various CMEs. Electrochemical detection of acebutolol was carried out at a hanging mercury drop electrode[166] and at the three types of modified electrodes viz. conventional polymer, carbon paste and modified carbon nanotubes carbon paste electrodes[167].

Gastro-intestinal drugs

Gastro-intestinal drug is a medicine for the gastrointestinal organs and diseases relating to them. This includes any part of the digestive tract from mouth to anus, liver, biliary tract and pancreas.

Ranitidine, a very important drug in this category, is a histamineH2 receptor antagonist and has been used for the short-term treatment of active duodenal ulcer. Many researchers have focused on the electrochemical detection of ranitidine. Salimi et al. fabricated a SWCNT modified glassy carbon electrode for efficient electrocatalytic reduction of ranitidine and metronidazole with relatively high sensitivity, stability and life time[168]. Araujo and Paixao have developed a simple analytical method for ranitidine quantification based on the electrocatalytic oxidation of ranitidine on a glassy carbon electrode modified with the electrochemical deposition of ruthenium oxide hexacyanoferrate[169]. Lee et al. developed a sensitive electrochemical sensor for simultaneous and quantitative detection of ranitidine and metronidazole using poly(thionine)-modified anodized glassy carbon electrode [170].

Omeprazole, a substituted benzimidazole compound and prototype anti-secretary agent, belongs to a new class of potent and clinically active inhibitors of gastric acid secretion. Radi has studied the electrochemical oxidations of lansoprazole and omeprazole at a carbon paste electrode.[171] Later, Jorge et al. was investigated the electrochemical redox behavior of omeprazole at a glassy carbon electrode[172]. Salimi et al. reported a sensitive amperometric sensor of omeprazole and pantoperazole at electrodeposited nickel oxide nanoparticles modified glassy carbon electrode[173].

Priyanka et al. have developed a simple, sensitive and highly selective omeprazole sensor based on the synergistic effect of polyaniline (PANI) and multiwalled carbon nanotubes (MWCNTs)[174]. Recently, Shahrokhian et al. investigated the voltammetric performance of edge-plane pyrolytic graphite (EPG) electrode via adsorptive stripping voltammetry for the study of electrochemical behavior of omeprazole (OMZ) in aqueous solution[175].

Zheng Li et al examined the voltammetric behavior and electrochemical reaction mechanism of *cisapride,* another important gastro-intestinal drug, at a multi-wall carbon nanotube paste electrode using cyclic and differential pulse voltammetry[176].

Anti-depressant drugs

Antidepressants are drugs used for the treatment of major depressive disorder and other conditions, including dysthymia, anxiety disorders, obsessive compulsive disorder, eating disorders, chronic pain and neuropathic pain.

Thioridazine is a phenothiazine neuroleptic drug used in the treatment of schizophrenia, psychiatric disorders and short-term treatment of adults with major depression. Shahrokhian et al. fabricated a cobalt nanoparticle bound multi-walled carbon nanotube modified glassy carbon electrode for the electrochemical oxidation of thioridazine[177]. Mashhadizadeh and Afshar have fabricated a novel ZnS nanoparticle-modified carbon paste electrode and used to study the electrooxidation of thioridazine[178]. Recently Amiri et al. synthesized the nickel (II) incorporated aluminophosphate and it was used as a modifier in carbon paste electrode for the selective determination of thioridazine[179].

Fluvoxamine is a selective serotonin re-uptake inhibitor (SSRI), primarily used as an antidepressant drug but also used to treat other psychological problems, such as obsessive–compulsive, panic, and post-traumatic stress disorders. Nouws et al. examined the electrochemical behaviour of fluvoxamine at a mercury drop electrode[180]. Recently, Madrakian et al. introduced an effective electrochemical sensor for the determination of fluvoxamine using mercury nanoparticles multi walled carbon nanotube modified glassy carbon electrode[181].

Along with the above, several other anti-depressant drugs also examined at different types of CMEs. *Desipramine* was determined electrochemically at nanoTiO_2-amberlite XAD-2 modified glassy carbon paste electrode[182] and at lipid modified carbon paste

electrode[183]. *Citalopram* was examined at zinc oxide nanoparticles and multi-walled carbon nanotubes modified carbon paste electrode[184].

1.6. The aims, scope and objectives of the research

The quality of a drug is determined after establishing its authenticity by testing its purity and quality of the pure substance in the drug and its formulations. A number of methods including physical, chemical, physico-chemical and biological ones are employed for determining the quality of the drugs. Among the physico-chemical methods, electrochemical methods are the most widely used one. In continuation to the development of spectrophotometric and electrochemical methods for the determination of drugs in our laboratory, the present investigation involve the fabrication of electrochemical sensors for drugs such as Isoniazid, 5-Fluorouracil, Clopidogrel and Dacarbazine. For all the sensors developed, the various parameters studied include linear response range, detection limit, effect of pH, scan rate study and interference study. Along with these are the mechanistic parameters of the electrodic reactions such as number of electrons involved, electrochemical reaction rate, diffusion coefficient and reaction mechanism. The developed sensors have been then applied for the determination of the drugs in pharmaceutical formulations and in artificial physiological solutions to establish the applicability of these sensors for direct, on-site determination in real-world samples.

Electroanalytical chemistry can play a very important role in the protection of our environment. In particular, electrochemical sensors and detectors are very attractive for on-site monitoring of priority pollutants and as well as for addressing other environmental needs. Such devices satisfy many of the requirements for on-site environmental analysis. They are inherently sensitive and selective towards electroactive species, fast and accurate, compact, portable and inexpensive. A central advantage of electrochemical signal transduction is the promise of the sampling, analysis, detection and readout of biological binding data in a self-contained portable system.

The purpose of an electrochemical sensor is to provide real-time reliable information about the chemical composition of its surrounding environment. Ideally, the sensor is capable of responding continuously and reversibly and does not agitate the sample. Such devices consist of a transduction element covered with a biological or chemical recognition layer. In the case of electrochemical sensors, they are concerned

with the interplay between electricity and chemistry, namely the measurements of electrical quantities, such as current, potential or charge and their relationship to chemical parameters. Analytical information is obtained from the electrical signal that results from the interaction of the target analyte with the recognition layer.

The main ***objectives*** of the present study are as follows. The overall goal of the present study is to design and present a novel electrochemical sensor technology that can rapidly detect the specified pharmaceutical drugs in real samples such as formulations and urine samples at applicable/physiological concentration limits.

1. To fabricate an electrochemical sensor for the detection of **Isoniazid** using bionanocomposite (MWCNT-Chitosan) based electrodes.

2. To develop an electrochemical sensor for the detection of **5-Fluorouracil** using biopolymer stabilized nanogold decorated carbon nanotube based electrodes.

3. To fabricate an electrochemical sensor for the detection of **Clopidogrel** using silver nanoparticles embedded chitosan layered carbon nanotube based electrodes.

4. To fabricate an electrochemical sensor for the detection of **Dacarbazine** using a conducting polymer coated carbon nanotube paste electrodes.

The developed electrochemical sensors with the above mentioned objectives would offer a substantial scope towards the real time analysis of the specified drug molecules from artificial urine samples and pharmaceutical formulations successfully.

1.7. Research framework

In line with the study objectives, the research framework is shown in the scheme below.

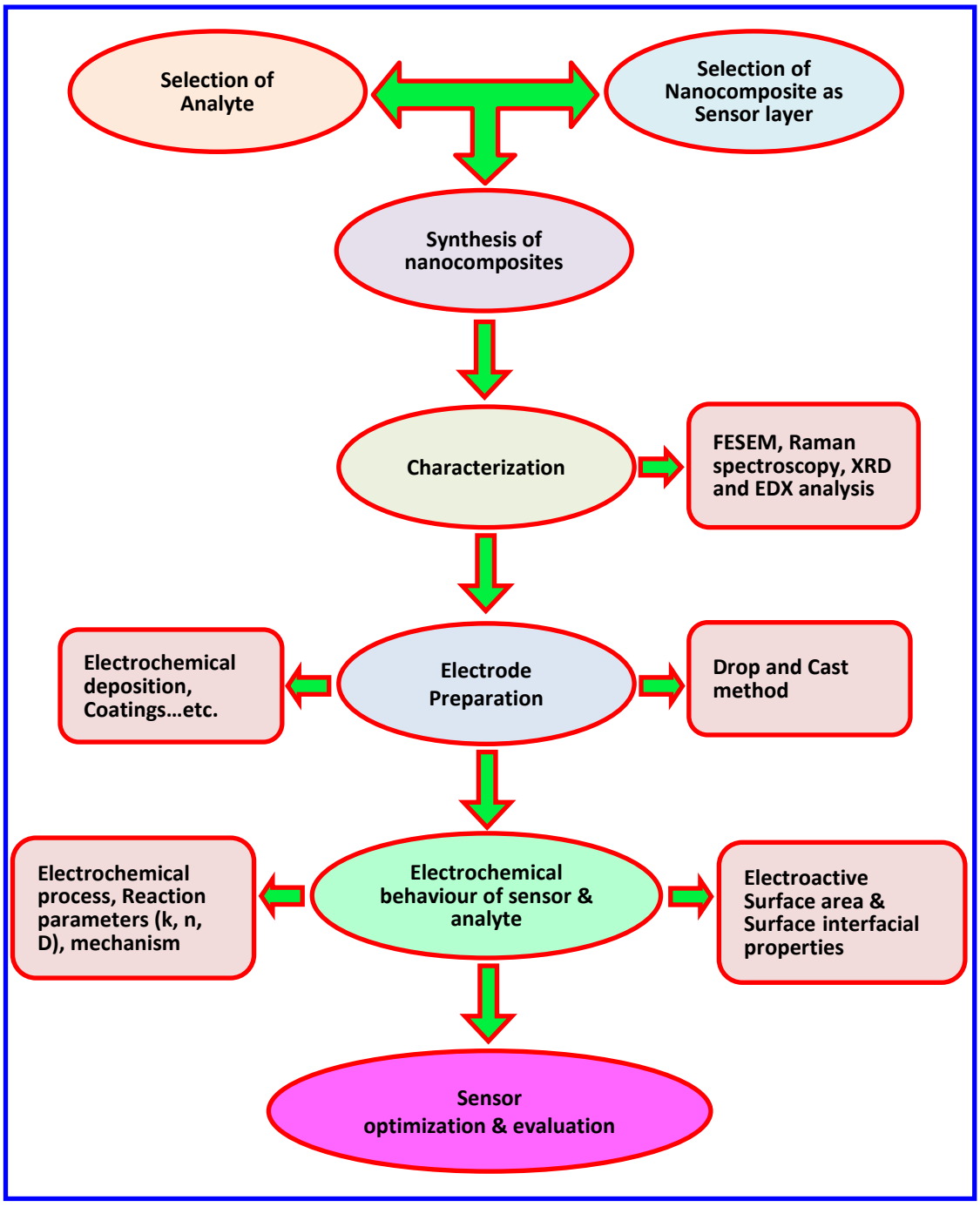

Scheme 1.1. Research framework.

1.8. References

[1] A. Hulanicki, S. Glab, F. Ingman, *Pure appl. chem.* **1991**, *63*, 1247–1250.

[2] J. C. Pickup, F. Hussain, N. D. Evans, O. J. Rolinski, D. J. S. Birch, *Biosens. Bioelectron.* **2005**, *20*, 2555–2565.

[3] R. Thompson, *Fluorescence Sensors and Biosensors*, CRC Press, **2005**.

[4] G. Gauglitz, *Anal. Bioanal. Chem.* **2005**, *381*, 141–155.

[5] A. Lobnik, *Sensors (Peterborough, NH)* **2000**, 77–98.

[6] J. Goicoechea, C. R. Zamarreño, I. R. Matías, F. J. Arregui, *Sensors Actuators, B Chem.* **2008**, *132*, 305–311.

[7] K. Peters, *Smart Mater. Struct.* **2011**, *20*, 013002.

[8] Š. Zajko, I. Klimant, *Sensors Actuators B Chem.* **2013**, *177*, 86–93.

[9] A. Buvailo, Y. Xing, J. Hines, E. Borguet, *Sensors Actuators B Chem.* **2011**, *156*, 444–449.

[10] C. Y. Shen, C. P. Huang, W. T. Huang, *Sensors Actuators, B Chem.* **2004**, *101*, 1–7.

[11] M. J. Vellekoop, *Sensors Actuators A Phys.* **1997**, *63*, 79.

[12] S. K. Vashist, P. Vashist, *J. Sensors* **2011**, 1–13.

[13] A. Tlili, A. Abdelghani, S. Hleli, M. A. Maaref, *Sensors* **2004**, *4*, 105–114.

[14] E. Uttenthaler, M. Schräml, J. Mandel, S. Drost, *Biosens. Bioelectron.* **2001**, *16*, 735–743.

[15] F. Eichelbaum, R. Borngräber, J. Schröder, R. Lucklum, P. Hauptmann, J. Schro, R. Borngra, *Rev. Sci. Instrum.* **1999**, *70*, 2537–2545.

[16] H. P. Lang, C. Gerber, *Top. Curr. Chem.* **2008**, *285*, 1–27.

[17] A. Kooser, R. L. Gunter, W. D. Delinger, T. L. Porter, M. P. Eastman, *Sensors Actuators B Chem.* **2004**, *99*, 474–479.

[18] H.-F. Ji, B. D. Armon, *Anal. Chem.* **2010**, *82*, 1634–42.

[19] K. M. Hansen, T. Thundat, *Methods* **2005**, *37*, 57–64.

[20] B. Xie, K. Ramanathan, B. Danielsson, in *Adv. Biochem. Eng. Biotechnol.*, **1999**, pp. 1–33.

[21] C. F. Mandenius, B. Danielsson, in *Immobil. Enzym. Cells Part D*, **1988**, pp. 307–318.

[22] K. Ramanathan, B. Danielsson, *Biosens. Bioelectron.* **2001**, *16*, 417–423.

[23] B. Danielsson, B. Xie, in *Front. Biosensorics II*, Birkhäuser Basel, Basel, **1997**,

pp. 71–85.

[24] P. T. Walsh, T. A. Jones, in *Sensors Set*, Wiley-VCH Verlag GmbH, Weinheim, Germany, **1991**, pp. 529–572.

[25] J. Lerchner, D. Caspary, G. Wolf, *Sensors Actuators B Chem.* **2000**, *70*, 57–66.

[26] J. Lerchner, J. Seidel, G. Wolf, E. Weber, *Sensors Actuators B Chem.* **1996**, *32*, 71–75.

[27] I. Satoh, Y. Iijima, *Sensors Actuators B Chem.* **1995**, *24*, 103–106.

[28] V. Raghavan, K. Ramanathan, P. V. Sundaram, B. Danielsson, *Clin. Chim. Acta* **1999**, *289*, 145–158.

[29] T. Carlsson, U. Adamson, P. E. Lins, B. Danielsson, *Clin. Chim. acta* **1996**, *251*, 187–200.

[30] D. W. Kimmel, G. LeBlanc, M. E. Meschievitz, D. E. Cliffel, *Anal. Chem.* **2012**, *84*, 685–707.

[31] N. R. Stradiotto, H. Yamanaka, M. V. B. Zanoni, *J.Braz.Chem.Aoc.* **2003**, *14*, 159–173.

[32] A. Z. Sadek, W. Wlodarski, K. Kalantar-Zadeh, C. Baker, R. B. Kaner, *Sensors Actuators A Phys.* **2007**, *139*, 53–57.

[33] G. Di Francia, B. Alfano, V. La Ferrara, *J. Sensors* **2009**, *2009*, 1–18.

[34] I. Castro-Hurtado, G. G. Mandayo, E. Castaño, *Thin Solid Films* **2013**, *548*, 665–676.

[35] C. Chouteau, S. Dzyadevych, J.-M. M. Chovelon, C. Durrieu, *Biosens. Bioelectron.* **2004**, *19*, 1089–1096.

[36] A. A. Shul'ga, A. P. Soldatkin, A. V. El'skaya, S. V. Dzyadevich, S. V. Patskovsky, V. I. Strikha, *Biosens. Bioelectron.* **1994**, *9*, 217–223.

[37] I. Lee, X. Luo, J. Huang, X. T. Cui, M. Yun, *Biosensors* **2012**, *2*, 205–20.

[38] N. Jaffrezic-Renault, S. V. Dzyadevych, *Sensors* **2008**, *8*, 2569–2588.

[39] J. Bobacka, A. Ivaska, A. Lewenstam, *Chem. Rev.* **2008**, *108*, 329–351.

[40] E. Bakker, E. Pretsch, *TrAC - Trends Anal. Chem.* **2005**, *24*, 199–207.

[41] T. Yin, W. Qin, *TrAC - Trends Anal. Chem.* **2013**, *51*, 79–86.

[42] E. Bakker, E. Pretsch, P. Bühlmann, *Anal. Chem.* **2000**, *72*, 1127–1133.

[43] C. C. Rundle, *Data Process.* **2011**, 1–30.

[44] J. Bobacka, *Electroanalysis* **2006**, *18*, 7–18.

[45] R. De Marco, G. Clarke, B. Pejcic, *Electroanalysis* **2007**, *19*, 1987–2001.

[46] E. Lindner, B. D. Pendley, *Anal. Chim. Acta* **2013**, *762*, 1–13.

[47] V. S. Bhat, V. S. Ijeri, A. K. Srivastava, *Sensors Actuators B Chem.* **2004**, *99*, 98–105.

[48] S. M. Usman Ali, O. Nur, M. Willander, B. Danielsson, *Sensors Actuators B Chem.* **2010**, *145*, 869–874.

[49] G. Broncová, T. V. Shishkanova, M. Krondak, R. Volf, V. Král, *Sensors* **2008**, *8*, 594–606.

[50] A. Bratov, N. Abramova, A. Ipatov, *Anal. Chim. Acta* **2010**, *678*, 149–159.

[51] S. D. Caras, J. Janata, *Anal. Chem.* **1985**, *57*, 1924–1925.

[52] L. Torsi, M. Magliulo, K. Manoli, G. Palazzo, *Chem. Soc. Rev.* **2013**, *42*, 8612.

[53] C. S. Lee, S. Kyu Kim, M. Kim, *Sensors* **2009**, *9*, 7111–7131.

[54] J. Locklin, Z. Bao, *Anal. Bioanal. Chem.* **2006**, *384*, 336–342.

[55] S. Jadhav, E. Bakker, *Anal. Chem.* **1999**, *71*, 3657–3664.

[56] A. Walcarius, C. Gondran, S. Cosnier, *Chem. Biol. Microsens. Appl. Liq. Media* **2013**, 115–171.

[57] A. Heller, *Curr. Opin. Biotechnol.* **1996**, *7*, 50–54.

[58] C. Brett, in *Piezoelectric Transducers Appl.*, Springer Berlin Heidelberg, Berlin, Heidelberg, **2008**, pp. 223–239.

[59] J. O. Bockris, A. K. N. Reddy, M. Gamboa-Aldeco, *Ann. N. Y. Acad. Sci.* **2001**, *1228*, 1–817.

[60] H. L. Lord, W. Zhan, J. Pawliszyn, in *Compr. Sampl. Sample Prep.*, Elsevier, **2012**, pp. 677–697.

[61] M. Opallo, A. Lesniewski, *J. Electroanal. Chem.* **2011**, *656*, 2–16.

[62] S. R. Belding, F. W. Campbell, E. J. F. Dickinson, R. G. Compton, *Phys. Chem. Chem. Phys.* **2010**, *12*, 11208–11221.

[63] A. Walcarius, *Anal. Chim. Acta* **1999**, *384*, 1–16.

[64] L. Gorton, *Electroanalysis* **1995**, *7*, 23–45.

[65] A.-E. Radi, *Comb. Chem. High Throughput Screen.* **2010**, *13*, 728–752.

[66] J.-M. Zen, A. S. Kumar, D.-M. Tsai, *Electroanalysis* **2003**, *15*, 1073–1087.

[67] R. W. Murray, a G. Ewing, R. a Durst, *Anal. Chem.* **1987**, *59*, 379A–390A.

[68] A. J. Bard, L. R. Faulkner, *ELECTROCHEMICAL METHODS Fundamentals and Applications*, John Wiley & Sons, New York, **1944**.

[69] E. Laviron, *J. Electroanal. Chem. Interfacial Electrochem.* **1979**, *101*, 19–28.

[70] D. Grahame, *Chem. Rev.* **1947**, 441–501.

[71] D. D. MacDonald, *Electrochim. Acta* **2006**, *51*, 1376–1388.

[72] S. Iijima, *Nature* **1991**, *354*, 56–58.

[73] P. J. Britto, K. S. V Santhanam, P. M. Ajayan, *Bioelectrochemistry Bioenerg.* **1996**, *41*, 121–125.

[74] Y. L. Zhao, J. F. Stoddart, *Acc. Chem. Res.* **2009**, *42*, 1161–1171.

[75] K. Balasubramanian, M. Burghard, *Small* **2005**, *1*, 180–192.

[76] S. Guo, E. Wang, *Nano Today* **2011**, *6*, 240–264.

[77] S. Guo, E. Wang, *Anal. Chim. Acta* **2007**, *598*, 181–192.

[78] F. Wang, S. Hu, *Microchim. Acta* **2009**, *165*, 1–22.

[79] L. Rassaei, F. Marken, M. Sillanpää, M. Amiri, C. M. Cirtiu, M. Sillanpää, *TrAC - Trends Anal. Chem.* **2011**, *30*, 1704–1715.

[80] A. Kolmakov, M. Moskovits, *Annu. Rev. Mater. Res.* **2004**, *34*, 151–180.

[81] P. Mäki-Arvela, D. Y. Murzin, *Appl. Catal. A Gen.* **2013**, *451*, 251–281.

[82] B. C. Sih, M. O. Wolf, *Chem. Commun. (Camb).* **2005**, 3375–3384.

[83] T. Wang, J. S. Hu, W. Yang, H. M. Zhang, *Electrochem. commun.* **2008**, *10*, 814–817.

[84] P. Raveendran, J. Fu, S. L. Wallen, *J. Am. Chem. Soc.* **2003**, *125*, 13940–13941.

[85] T.-F. Kang, F. Wang, L.-P. Lu, Y. Zhang, T.-S. Liu, *Sensors Actuators B Chem.* **2010**, *145*, 104–109.

[86] L. M. Liz-Marzán, *Chem. Commun.* **2013**, *49*, 1994–1996.

[87] S. Bhat, U. Maitra, *J. Chem. Sci.* **2008**, *120*, 507–513.

[88] M. K. Corbierre, R. B. Lennox, *Chem. Mater.* **2005**, *17*, 5691–5696.

[89] A. S. Ramírez-Segovia, J. A. Banda-Alemán, S. Gutiérrez-Granados, A. Rodríguez, F. J. Rodríguez, L. a Godínez, E. Bustos, J. Manríquez, *Anal. Chim. Acta* **2014**, *812*, 18–25.

[90] K. J. Huang, D. J. Niu, X. Liu, Z. W. Wu, Y. Fan, Y. F. Chang, Y. Y. Wu, *Electrochim. Acta* **2011**, *56*, 2947–2953.

[91] P. Rameshkumar, R. Ramaraj, *J. Appl. Electrochem.* **2013**, *43*, 1005–1010.

[92] H. Hosseini, H. Ahmar, A. Dehghani, A. Bagheri, A. R. Fakhari, M. M. Amini, *Electrochim. Acta* **2013**, *88*, 301–309.

[93] V. Kumar, M. Lütfi, M. Saeed, A. Osman, N. Atar, Z. Üstünda, **2013**, *188*, 1201–1211.

[94] J. Lin, C. He, Y. Zhao, S. Zhang, **2009**, *137*, 768–773.

[95] C. Anjalidevi, V. Dharuman, J. S. Narayanan, *Sensors Actuators B. Chem.* **2013**,

182, 256–263.

[96] S. Hu, Y. Wang, X. Wang, L. Xu, J. Xiang, W. Sun, **2012**, *168*, 27–33.

[97] X. Wang, X. Zhang, *Electrochim. Acta* **2013**, *112*, 774–782.

[98] T. A. Skotheim, R. L. Elsenbaumer, J. R. Reynolds, *CRC Press* **2007**, 1680.

[99] A. Malinauskas, *Synth. Met.* **1999**, *107*, 75–83.

[100] J. Heinze, B. A. Frontana-Uribe, S. Ludwigs, *Chem. Rev.* **2010**, *110*, 4724–4771.

[101] J. Janata, M. Josowicz, *Nat. Mater.* **2003**, *2*, 19–24.

[102] N. Gupta, S. Sharma, I. A. Mir, D. Kumar, *J. Sci. Ind. Res. (India).* **2006**, *65*, 549–557.

[103] P. Kalimuthu, S. A. John, *Talanta* **2010**, *80*, 1686–1691.

[104] P. Kalimuthu, S. A. John, *Bioelectrochemistry* **2010**, *79*, 168–172.

[105] L. Zhang, L. Wang, *J. Solid State Electrochem.* **2013**, *17*, 691–700.

[106] É. T. G. Cavalheiro, C. M. a Brett, A. M. Oliveira-Brett, O. Fatibello-Filho, *Bioanal. Rev.* **2012**, *4*, 31–53.

[107] E. D. S. Gil, G. R. de Melo, *Brazilian J. Pharm. Sci.* **2010**, *46*, 375–391.

[108] M. R. Siddiqui, Z. A. AlOthman, N. Rahman, *Arab. J. Chem.* **2013**, doi:10.1016/j.arabjc.2013.04.016.

[109] O. A. Farghaly, R. S. A. Hameed, A.-A. H. Abu-Nawwas, *Int. J. Electrochem. Sci.* **2014**, *9*, 3287–3318.

[110] M. Behpour, S. M. Ghoreishi, E. Honarmand, *Int. J. Electrochem. Sci.* **2010**, *5*, 1922–1933.

[111] B. J. Sanghavi, A. K. Srivastava, *Electrochim. Acta* **2010**, *55*, 8638–8648.

[112] G. T. Liu, H. F. Chen, G. M. Lin, P. P. Ye, X. P. Wang, Y. Z. Jiao, X. Y. Guo, Y. Wen, H. F. Yang, *Biosens. Bioelectron.* **2014**, *56*, 26–32.

[113] B.-R. Adhikari, M. Govindhan, A. Chen, *Electrochim. Acta* **2015**, *162*, 198–204.

[114] T.-L. Lu, Y.-C. Tsai, *Sensors Actuators B Chem.* **2011**, *153*, 439–444.

[115] H. Filik, G. Çetintaş, a. Aslihan Avan, S. N. Koç, I. Boz, *Int. J. Electrochem. Sci.* **2013**, *8*, 5724–5737.

[116] M. Amiri-Aref, J. B. Raoof, R. Ojani, *Sensors Actuators B Chem.* **2014**, *192*, 634–641.

[117] S. Motoc, A. Remes, A. Pop, F. Manea, J. Schoonman, *J. Environ. Sci. (China)* **2013**, *25*, 838–847.

[118] S. Amin, M. T. Soomro, N. Memon, A. R. Solangi, T. Qureshi, A. R. Behzad,

Environ. Nanotechnology, Monit. Manag. **2014**, *1-2*, 8–13.

[119] M. Roushani, F. Shahdost-fard, *Talanta* **2015**, *144*, 510–516.

[120] F. Shahdost-fard, M. Roushani, *J. Electroanal. Chem.* **2016**, *763*, 18–24.

[121] P. Norouzi, F. Dousty, M. R. Ganjali, P. Daneshgar, *Int. J. Electrochem. Sci.* **2009**, *4*, 1373–1386.

[122] J. Tashkhourian, B. Hemmateenejad, H. Beigizadeh, M. Hosseini-Sarvari, Z. Razmi, *J. Electroanal. Chem.* **2014**, *714-715*, 103–108.

[123] A. Afkhami, F. Kafrashi, M. Ahmadi, T. Madrakian, *RSC Adv.* **2015**, *5*, 58609–58615.

[124] N. Alizadeh, M. R. Eslami, *RSC Adv.* **2016**, DOI 10.1039/C5RA21489K.

[125] K. M. Manesh, P. Santhosh, S. Komathi, N. H. Kim, J. W. Park, A. I. Gopalan, K. P. Lee, *Anal. Chim. Acta* **2008**, *626*, 1–9.

[126] A. R. Fakhari, M. H. Koruni, H. Ahmar, A. Shahsavani, S. K. Movahed, *Electroanalysis* **2014**, *26*, 521–529.

[127] H. Heli, S. Majdi, a. Jabbari, N. Sattarahmady, a. a. Moosavi-Movahedi, *J. Solid State Electrochem.* **2010**, *14*, 1515–1523.

[128] E. M. Materon, P.-J. Jimmy Huang, A. Wong, A. A. Pupim Ferreira, M. D. P. T. Sotomayor, J. Liu, *Biosens. Bioelectron.* **2014**, *58*, 232–236.

[129] M. Bučková, P. Gründler, G. U. Flechsig, *Electroanalysis* **2005**, *17*, 440–444.

[130] Z. Jemelková, J. Zima, J. Barek, *Collect. Czechoslov. Chem. Commun.* **2009**, *74*, 1503–1515.

[131] J. J. Fei, X. Q. Wen, Y. Zhang, L. H. Yi, X. M. Chen, H. Cao, *Microchim. Acta* **2009**, *164*, 85–91.

[132] D. Pereira, M. F. Bergamini, M. Valnice, B. Zanoni, *Int. J. Electrochem. Sci.* **2010**, *5*, 1399–1410.

[133] Y. Guo, Y. Chen, Q. Zhao, S. Shuang, C. Dong, *Electroanalysis* **2011**, *23*, 2400–2407.

[134] A. M. O. Brett, T. R. A. Macedo, D. Raimundo, M. H. Marques, S. H. P. Serrano, *Anal. Chim. Acta* **1999**, *385*, 401–408.

[135] a M. Brett, T. R. Macedo, D. Raimundo, M. H. Marques, S. H. Serrano, *Biosens. Bioelectron.* **1998**, *13*, 861–7.

[136] B. Hong, Q. Cheng, *Adv. Chem. Eng. Sci.* **2012**, *02*, 453–460.

[137] A. N. Lad, Y. K. Agrawal, *Appl. Nanosci.* **2013**, *4*, 523–529.

[138] M. Khodari, *Talanta* **1997**, *44*, 305–310.

[139] V. Mirčeski, R. Gulaboski, B. Jordanoski, Š. Komorsky-Lovrić, *J. Electroanal. Chem.* **2000**, *490*, 37–47.

[140] T. Zhan, L. Cao, W. Sun, W. Hou, *Anal. Methods* **2011**, *3*, 2651.

[141] S. Wang, S. Fu, H. Ding, *Sens. Lett.* **2012**, *10*, 974–978.

[142] B. B. Prasad, S. Srivastava, *Sensors Mater.* **2009**, *21*, 291–306.

[143] B. B. Prasad, D. Kumar, R. Madhuri, M. P. Tiwari, *Electrochim. Acta* **2012**, *71*, 106–115.

[144] H. Li, J. Li, Z. Yang, Q. Xu, X. Hu, *Sci. China Chem.* **2011**, *54*, 217–222.

[145] S. Saxena, R. Shrivastava, S. P. Satsangee, S. Srivastava, *J. Electrochem. Soc.* **2014**, *161*, H934–H940.

[146] A. J. M. Ordieres, A. C. Garcia, P. T. Blanco, W. F. Smyth, *Anal. Chim. Acta* **1987**, *202*, 141–149.

[147] J. R. B. Rodriguez, A. Costa-García, A. J. M. Ordieres, P. T. Blanco, *Electroanalysis* **1989**, *1*, 529–534.

[148] Q. Shen, X. Wang, D. Fu, *Appl. Surf. Sci.* **2008**, *255*, 577–580.

[149] M. Song, R. Zhang, X. Wang, *Mater. Lett.* **2006**, *60*, 2143–2147.

[150] A. Radi, A. Eissa, H. M. Nassef, *J. Electroanal. Chem.* **2014**, *717-718*, 24–28.

[151] K. M. Naik, S. T. Nandibewoor, *J. Ind. Eng. Chem.* **2013**, *19*, 1933–1938.

[152] K. Radhapyari, R. Khan, **2015**, *6*, 13–18.

[153] A. M. O. Brett, S. H. P. Serrano, A. Macedo, Tice, D. Raimundo, M. H. Marques, M. A. La-Scalea, *Electroanalysis* **1996**, *8*, 992–995.

[154] D. Hernández-Santos, M. B. González-García, A. Costa-García, *Electrochim. Acta* **2005**, *50*, 1895–1902.

[155] E. M. Materon, A. Wong, S. I. Klein, J. Liu, M. D. P. T. Sotomayor, *Electrochim. Acta* **2015**, *158*, 271–276.

[156] P. Cervini, É. T. G. Cavalheiro, *Anal. Lett.* **2008**, *41*, 1867–1877.

[157] M. Arvand, M. Vaziri, M. Vejdani, *Mater. Sci. Eng. C-Materials Biol. Appl.* **2010**, *30*, 709–714.

[158] S. Pruneanu, F. Pogacean, C. Grosan, E. M. Pica, L. C. Bolundut, A. S. Biris, *Chem. Phys. Lett.* **2011**, *504*, 56–61.

[159] G. S. M. M. S. B. M. Khoobi A., *Bioelectrochemistry* **2013**, *94*, 100–107.

[160] Ş. Demircan, S. Kır, S. A. Ozkan, *Anal. Lett.* **2007**, *40*, 1177–1195.

[161] F. S. Semaan, É. T. G. Cavalheiro, C. M. a. Brett, *Anal. Lett.* **2009**, *42*, 1119–1135.

[162] G. G. Oliveira, D. C. Azzi, F. C. Vicentini, E. R. Sartori, O. Fatibello-Filho, *J. Electroanal. Chem.* **2013**, *708*, 73–79.

[163] M. Hasanzadeh, M. H. Pournaghi-Azar, N. Shadjou, A. Jouyban, *Electrochim. Acta* **2013**, *89*, 660–668.

[164] S. Dermis, E. Aydogan, *Pharmazie* **2010**, *65*, 175–181.

[165] A. F. Khorshid, *Arab. J. Chem.* **2014**, 1–9.

[166] A. F. Al-Ghamdi, M. M. Hefnawy, A. A. Al-Majed, F. F. Belal, *Chem. Cent. J.* **2012**, *6*, 15.

[167] N. A. Alarfaj, M. F. El-Tohamy, *J. Chinese Chem. Soc.* **2014**, *61*, 910–920.

[168] A. Salimi, M. Izadi, R. Hallaj, M. Rashidi, *Electroanalysis* **2007**, *19*, 1668–1676.

[169] W. R. de Araújo, T. R. L. C. Paixão, *Electroanalysis* **2011**, *23*, 2549–2554.

[170] M. M. Rahman, X.-B. Li, Y.-D. Jeon, H.-J. Lee, S. J. Lee, J.-J. Lee, *J. Electrochem. Sci. Technol.* **2012**, *3*, 90–94.

[171] A. Radi, *J. Pharm. Biomed. Anal.* **2003**, *31*, 1007–1012.

[172] S. M. A. Jorge, A. D. R. Pontinha, A. M. Oliveira-Brett, *Electroanalysis* **2010**, *22*, 625–631.

[173] A. Salimi, Z. Enferadi, A. Noorbakhash, K. Rashidi, *J. Solid State Electrochem.* **2012**, *16*, 1369–1375.

[174] P. Karolia, D. C. Tiwari, R. Jain, *Ionics (Kiel).* **2015**, *21*, 2355–2362.

[175] S. Shahrokhian, M. Ghalkhani, M. Bayat, F. Ghorbani-bidkorbeh, **2015**, *14*, 465–471.

[176] P. Xiao, F. Zhao, B. Zeng, *Microchem. J.* **2007**, *85*, 244–249.

[177] S. Shahrokhian, M. Ghalkhani, M. Adeli, M. K. Amini, *Biosens. Bioelectron.* **2009**, *24*, 3235–3241.

[178] M. H. Mashhadizadeh, E. Afshar, *Electroanalysis* **2012**, *24*, 2193–2202.

[179] M. Amiri, S. Sohrabnezhad, A. Rahimi, *Mater. Sci. Eng. C* **2014**, *37*, 342–347.

[180] H. P. A. Nouws, C. Delerue-Matos, A. A. Barros, J. A. Rodrigues, A. Santos-Silva, *Anal. Bioanal. Chem.* **2005**, *382*, 1662–1668.

[181] T. Madrakian, M. Soleimani, A. Afkhami, *Sensors Actuators B Chem.* **2015**, *210*, 259–266.

[182] B. J. Sanghavi, A. K. Srivastava, *Analyst* **2013**, *138*, 1395–404.

[183] M. Khodari, *Int. J. Sci. Res.* **2014**, 1536–1539.

[184] H. Ghaedi, A. Afkhami, T. Madrakian, F. Soltani-Felehgari, *Mater. Sci. Eng. C* **2016**, *59*, 847–854.

CHAPTER 2

Carbon Nanotube Ensembled Biopolymer Electrode for Selective Determination of Isoniazid *in-vitro*

2.1. Introduction

Carbon nanotubes (CNTs) have been recognized as an important material in recent years in various fields due to their unique electrical, mechanical and structural properties. CNTs can easily promote electron transfer between the electroactive species and electrode surface due to its unique long and tubular geometry [1,2]. The remarkable property of CNTs conductivity to the surface adsorbates permits the use of CNTs in the fabrication of highly sensitive nanoscale sensors. Their use as electrode modifiers can lead to a decrease of the overpotential, a decrease in the response time, enhanced electrocatalytic activity and an increase in available active surface area in comparison with conventional carbon electrodes. The electrocatalytic effect of CNTs has been attributed to the activity of edge-plane-like graphite sites at the CNT ends and it would be further increased by functionalization of CNTs. CNTs also reduce the electrode fouling which can greatly improve the reuse of such sensors [3,4]. The low solubility of CNTs in most solvents is the major problem to control for their use as modifiers in the fabrication of chemical sensors and/or biosensors. In order to overcome it, several strategies have been proposed for effective immobilization of CNTs on electrochemical transducers, like dispersion in different solvents or polyelectrolytes or incorporation in composite matrices using distinct binders [5–8].

Chitosan (chit) is a linear β-1,4-linked polysaccharide (similar to cellulose) that is obtained by the partial deacetylation of chitin, which is the structural element in the exoskeleton of crustaceans (such as crabs and shrimp) and cell walls of fungi [9]. It possesses many advantages such as excellent strong film forming ability but with high permeability towards water, biocompatible, good adhesion and high mechanical strength. In this investigation, chitosan has been used as a dispersant to bind CNTs with the electrode surface and to form a stable CNT–chitosan composite film on the GCE surface for sensing isoniazid *in-vitro*.

Isoniazid (Isonicotinylhydrazine, INH) is one of the most widely used first-line clinical drug for the treatment of all kinds of tuberculosis. Overdoses of the drug during the chemotherapy can cause hepatotoxicity, and there has been a global increase in the prevalence of drug–resistant tuberculosis. The large scale therapeutic use of this drug necessitated the need for the development of rapid, simple and on-site analytical method for determining isoniazid in drug formulation for quality control and in biological fluids

for medical diagnosis. Various analytical methods based on titrimetric [10], spectroscopic [11–13], chromatographic [14,15], chemiluminescence [16,17], and electrochemical techniques[18–20] have been aimed for quantitative determination of isoniazid. Electrochemical methods are interesting as they require in expensive, miniaturized portable equipment, and the analytes could be detected in trace levels without any preconcentration steps and without adding any special reagents. The major problem towards the detection of isoniazid using an electrochemical method is the large overpotential required for oxidation/reduction of isoniazid at bare electrodes. Various mediator and polymer based electrodes have been used to decrease the overpotential [21]. Gao et al. have investigated electrocatalytic oxidation of isoniazid using a ferrocenyl derivative as electrocatalyst at Pt electrode [22]. Recently, Jena and Raj have reported nanoAu decorated sol-gel based Au electrode for amperometric detection of isoniazid and the overpotential is reduced here by ~ 450 mV [23]. Carbon nanomaterials are highly interested for tailoring of electrode surface due to the fact that they provide low background currents, low-cost and wide-potential windows. Shahrokhian et al. [24] have investigated CNT based electrode for the determination of isoniazid and have obtained good sensitivity; but the overpotential was not much reduced. Very recently, Yan et al. [25] have investigated hexagonally ordered mesoporous carbon incorporated Nafion polymer electrode for amperometric detection of isoniazid. In this present work, multiwall carbon nanotubes have been ensembled into chitosan biopolymer matrix for the fabrication of a simple and cost effective electrochemical sensor of isoniazid. MWCNT is functionalized and dispersed in chitosan solution to form a stable thin film on GCE. Optimum conditions for highly sensitive and selective determination of isoniazid are established, and this method has been effectively applied to determine isoniazid in drug formulations and physiological liquids.

2.2. Experimental

2.2.1. Chemicals and materials

Isoniazid and ascorbic acid were purchased from Tokyo chemical industry, Japan. Chitosan of low molecular weight range (from crab shells, 60 – 120 kDa, minimum 85 % deacetylation) was obtained from Sigma Aldrich, USA. MWCNTs (95%, 20–50 nm OD and 2–5 μm length) were purchased from Sisco research laboratories, India. All other chemicals were of analytical grade (>99.5 % purity) and were used without further purification. Britton-Robinson buffer (B-R buffer) was

prepared using a mixture of 0.04 M CH_3COOH, 0.04 M H_3BO_3 and 0.04 M H_3PO_4. The desired solution pH was obtained by adding 0.1 M NaOH. Artificial urine solution was prepared according to the procedure provided by Brooks and Keevil [26]. The artificial urine solution was prepared using a mixture of 1.1 mM lactic acid, 2.0 mM citric acid, 25 mM sodium bicarbonate, 170 mM urea, 2.5 mM calcium chloride, 90 mM sodium chloride, 2.0 mM magnesium sulfate, 10 mM sodium sulfate, 7.0 mM potassium dihydrogen phosphate, 7.0 mM dipotassium hydrogen phosphate, and 25 mM ammonium chloride in distilled water. The pH of the solution was adjusted to 6.0 through the addition of 1.0 M hydrochloric acid. All aqueous solutions were prepared using double distilled water.

2.2.2. Functionalization of MWCNTs

MWCNTs were functionalized with –COOH group by using a method similar to that described by Gouveia-Caridade et al.[27]. MWCNTs (120 mg) were added to 10 mL of 3 M nitric acid solution and stirred for 24 h at 60 ºC. The black solid product was filtered and then washed several times with double distilled water until the filtrate solution became neutral (pH = 7). The obtained solid product was collected in a petri dish and dried in an oven at 80 ºC for 24 h. Nitric acid oxidizes CNTs and introduces -COOH groups at the ends and at the sidewall defects of the nanotube structure, which increases the electrocalytic activity of CNTs. In order to characterize the functionalized MWCNT, the number of –COOH groups per gram of functionalized MWCNT has been determined by acid-base back titration method and it is 2.14 ± 0.08 mmol/g (n = 4).

2.2.3. Preparation of MWCNT-chtiosan modified electrodes

At first, GCE (3 mm diameter) was polished with alumina slurry (down to 0.04 μm), and then washed thoroughly with double distilled water, then sonicated in 1:1 aq. HNO3, ethanol and double distilled water consecutively and finally dried at room temperature. A solution of chitosan (1 % w/v) was prepared by dissolving 1 g of chitosan powder in 100 mL aq. acetic acid (1 % v/v) solution and sonicated for 30 min. Different amounts (1, 2, 3 and 4 mg) of oxidized MWCNTs were added to 1 mL chitosan solution and sonicated for 1 h. Then, 10 μL of the resulting homogeneous suspension was cast on the surface of cleaned GCE and dried for 24 – 30 h at room temperature and the resulting electrodes were denoted as MWCNT-Chit/GCE.

2.2.4. Instrumentation

Cyclic voltammetry, chronoamperometry and differential pulse voltammetry measurements were carried out using CHI 6132e electrochemical analyzer, and electrochemical impedance measurements were carried out using Zahner-elektrik workstation (Model IM6e, GmbH, Germany) equipped with Thales 3.08 USB software. All the electrochemical measurements were performed in a conventional electrochemical cell of 20 mL with bare or modified GCE as working electrode, Pt spiral wire as auxiliary electrode and Ag|AgCl (3 M KCl) electrode as reference. All the potentials were referred against Ag|AgCl (3 M KCl) electrode throughout the manuscript. Electrochemical experiments were carried out in B-R buffer at room temperature, and the experimental solution was purged with nitrogen gas for 10 min prior to the start of the experiment to de-aerate the solution.

Pristine- (as received) and functionalized CNT were characterized by vibrational Raman spectroscopy. Raman spectra of the samples were recorded using a HR800 LabRAM confocal Raman spectrometer operating at 20 mW laser power using a peltier cooled CCD detector. The spectra were collected using a He–Ne laser source having an excitation wavelength of 633 nm and with an acquisition time of 10 s using a 5× objective. The Raman spectral data were acquired in a mixture (4:1 v/v) of acetonitrile and water using a quartz cuvette.

Scanning electron microscope (SEM) images of MWCNT-chitosan nanocomposite film were recorded using TESCAN VEGA 3 scanning electron microscope. MWCNT-chitosan nanocomposite film was prepared by casting 1 % w/v chitosan solution dispersed with MWCNT at 4 mg/mL level. A thin layer of gold was sputtered on the nanocomposite film to avoid the charging during SEM analysis.

2.3. Results and discussion

2.3.1. Raman spectra of CNT and functionalized CNT

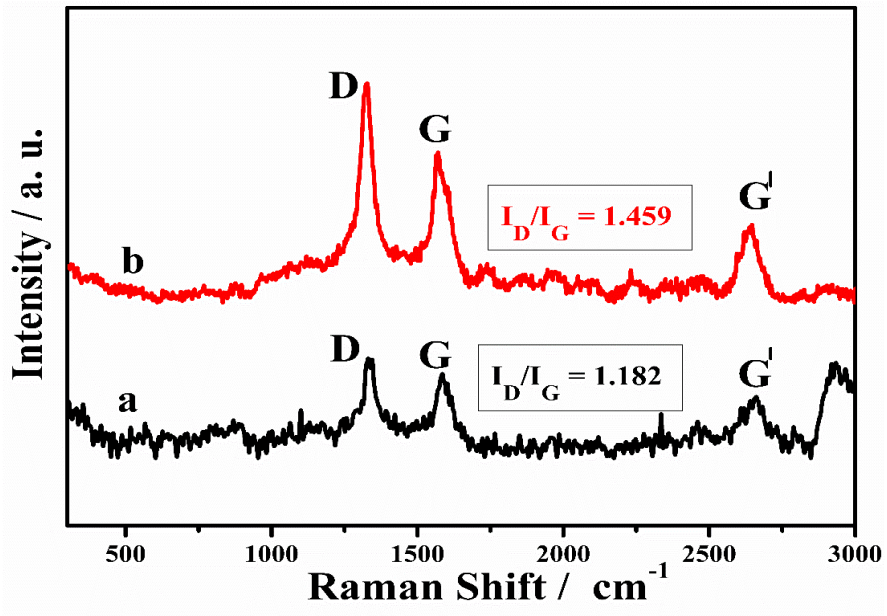

Fig. 2.1: *Raman spectra of pristine MWCNT and functionalized MWCNT.*

Pristine- and functionalized-CNT were characterized by Raman spectroscopy. Both Pristine- and functionalized-CNT each show four characteristic peaks namely D, G, D' and G' bands in their Raman spectral data (Fig. 2.1). The peak at ~1330 cm^{-1} is related to the defect derived D band which represents the defect sites or disordered graphitic structure of MWCNT. The peak at ~1580 cm^{-1} is assigned as graphitic structure derived G band which represents the >C=C< bond nature in the graphitic plane of CNT. The peak at ~1610 cm^{-1} represents D′ band which indicates the defective sites in the manufacture of CNT. The peak at ~2660 cm^{-1} is overtone of the D band originated from a double-resonance process [28–30]. Smaller D band indicates high purity of CNT whereas larger D band is likely due to the influence of terminal groups. Quality of CNT could be decided based on the ratio of these peak intensities, in other words I_D/I_G values would be considered in determining the quality of CNT. When compared the I_D/I_G values of functionalized MWCNT (1.46) with that of pristine MWCNT (1.18), the high I_D/I_G value for functionalized MWCNT suggests that the formation of some sp^3 carbons by oxidation in the case of functionalized MWCNT, which confirms the successful functionalization of MWCNT with –COOH groups.[31–33]

2.3.2. Morphology of MWCNT-chitosan nanocomposite electrode

Figure 1 shows the scanning electron microscope (SEM) images of the MWCNT-chitosan nanocomposite electrode at two different magnifications. As shown in Fig. 1(a), the MWCNT-chitosan film is of porous nature with large surface area, and thus it could enhance the electrodic current for an analyte and thus the sensitivity. The nanocomposite has been distributed uniformly and homogenously all over the electrode. SEM image obtained at the higher magnification (Fig. 2.2b) clearly reveals that the MWCNTs are well dispersed on the electrode surface and have formed a good network on the electrode, which could promote a facile electron transfer. Fine individual strips of MWCNTs with a range of 20 to 50 nm diameter are seen. The porous nature with well dispersed homogenous structure all over the surface is expected to favour the fabrication of reliable and reproducible nanocomposite film on the electrode.

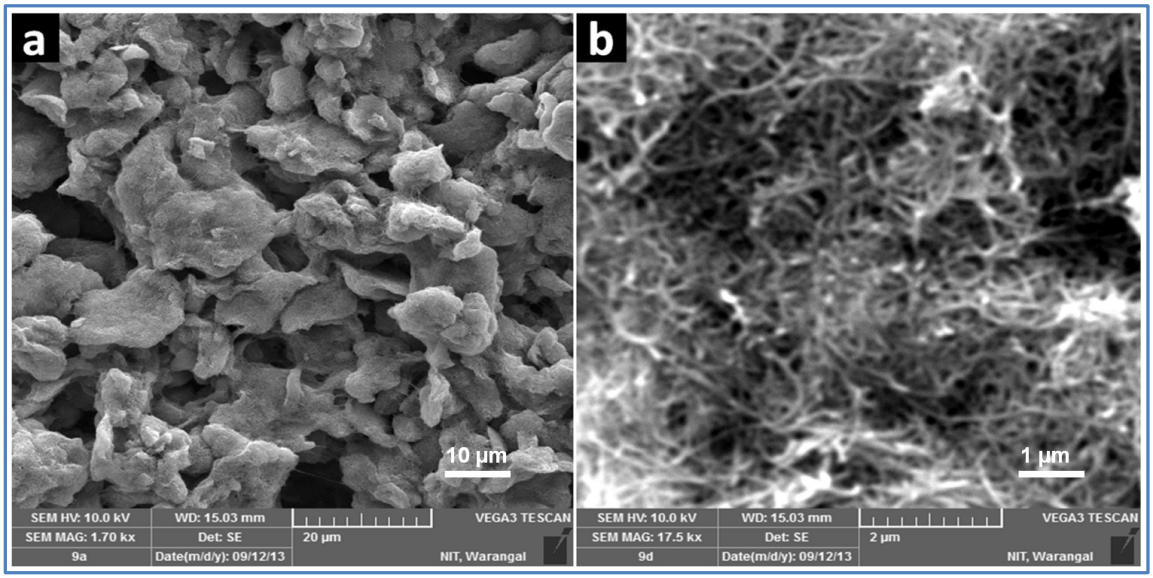

Fig. 2.2. *SEM images of MWCNT-chitosan nanocomposite at two different magnifications.*

2.3.3. Electroactive surface area of MWCNT-Chit/GCE

Active surface area of bare GCE and MWCNT-Chit/GCE was determined by electrochemical method. Cyclic voltammograms of 2 mM $K_3[Fe(CN)_6]$ in aq. 0.1 M KCl were recorded at both MWCNT-Chit/GCE and bare GCE at different scan rates. Further calculations have been carried out using Randles-Sevcik equation (Eq. 2.1) for a reversible process:

$$i_p = 2.69 \times 10^5 A n^{3/2} D^{1/2} C v^{1/2} \quad \ldots\ldots\ldots\ldots\ldots \quad (Eq. 2.1)$$

where i_p refers to the peak current, n is the number of electrons transferred, A is the surface area of electrode, D is diffusion coefficient, c is the concentration of $K_3[Fe(CN)_6]$ and v refers to the scan rate. The surface area can be calculated from the slope of the i_p vs. $v^{1/2}$ plot, using the D value of $K_3[Fe(CN)_6]$, 6.7×10^{-6} cm^2 s^{-1} [34]. Active surface area for bare GCE was found to be 0.071 cm^2 which is equal to the geometrical surface area of a 3 mm diameter electrode, whereas it is 0.262 cm^2 for MWCNT-Chit/GCE. From these observations, we can conclude that the surface area of MWCNT-Chit/GCE was nearly four times higher than that of bare GCE and it is due to the distribution of nanostructural MWCNT on the surface of GCE.

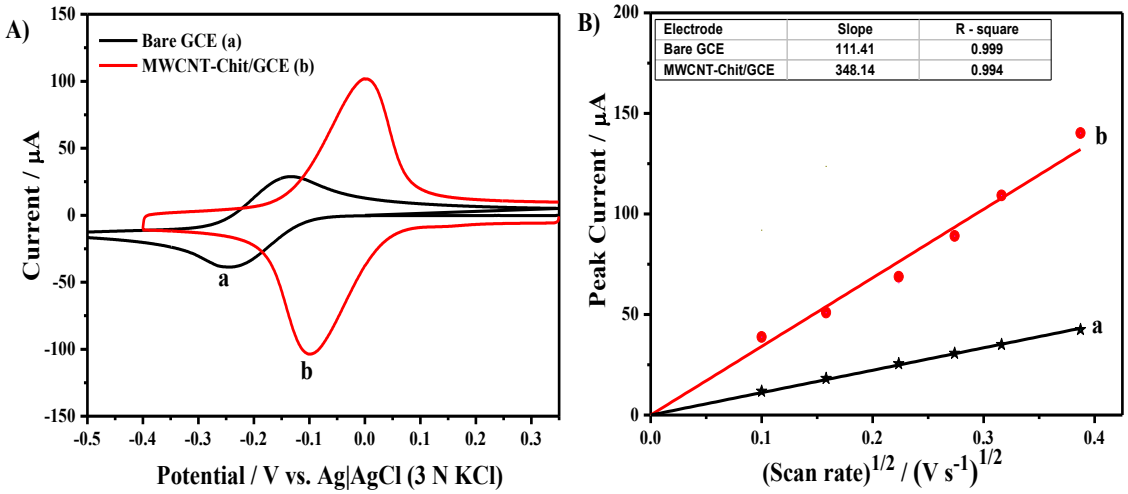

Fig. 2.3. *(A) CVs of $K_3[Fe(CN)_6]$ recorded at bare GCE (a) and MWCNT-Chit/GCE (b) in aq. 2 mM $K_3[Fe(CN)_6]$ + 0.1 KCl; potential scan rate = 100 mV s^{-1}.(B) Plot of the anodic peak current against the square root of scan rate.*

2.3.4. Electrocatalytic oxidation of isoniazid

Cyclic voltammograms (CVs) obtained for the oxidation of isoniazid at bare GCE and MWCNT-Chit/GCE in B-R buffer of pH 6.0 are shown in Fig. 2.4. Isoniazid exhibits irreversible CV with an anodic peak at both GCE and MWCNT-Chit/GCE and no peaks are observed in the reverse scan. While the anodic peak is obtained at ~ + 0.97 V at bare GCE, it is obtained at a very less positive potential of + 0.17 V at MWCNT-Chit/GCE. A large decrease in overpotential for the oxidation of isoniazid is obtained at MWCNT-Chit/GCE, and the decrease in overpotential is as much as 800 mV compared to bare GCE. Moreover, the anodic peak current of isoniazid at MWCNT-Chit/GCE is about 3 times larger than that of bare GCE. These phenomena are clear evidences for electrocatalytic effect of the MWCNT-chitosan modified electrode towards isoniazid oxidation. These results suggest that the MWCNT-chitosan film might be forming a

better electron conducting pathway on the electrode surface and the formed film is able to accelerate the rate of isoniazid electron transfer.

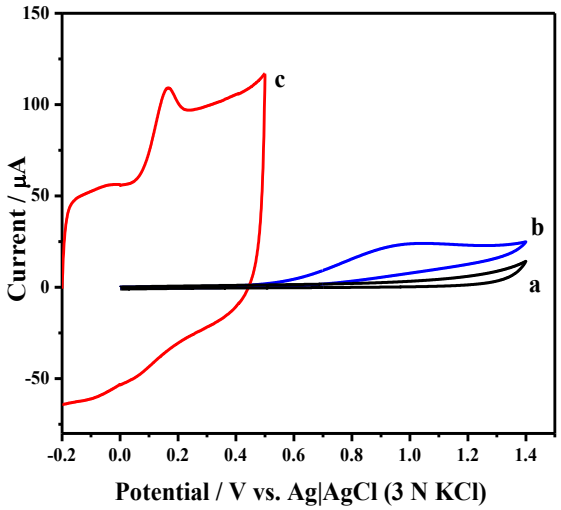

Fig. 2.4. *CVs recorded at (a, b) bare glassy carbon electrode and at (c) MWCNT-Chit/GCE in the (a) absence and (b, c) presence of 0.1 mM isoniazid in B-R buffer (pH 6.0). Scan rate = 100 mV* s^{-1}.

2.3.5. Optimization of pH and the amount of MWCNT

The effect of pH on the electrochemical response of 0.1 mM isoniazid at MWCNT-Chit/GCE was investigated in B-R buffer solution of different pH (pH 4.0 to 10.0) by cyclic voltammetry as shown in Fig. 2.5. The solution pH obviously influenced the oxidation peak of isoniazid. The peak current is maximum in the pH range of 5.0 – 6.0, and it decreased to minimum at pH 9.0 and 10.0. Moreover, in the pH range of 8.0 to 10.0, isoniazid shows an additional irreversible anodic peak with low intensity and the peak currents are relatively low. In the overall pH range of 4.0 to 10.0, the peak currents are very high at pH 6.0. Considering these observations, B-R buffer of pH 6.0 has been chosen for all further experiments.

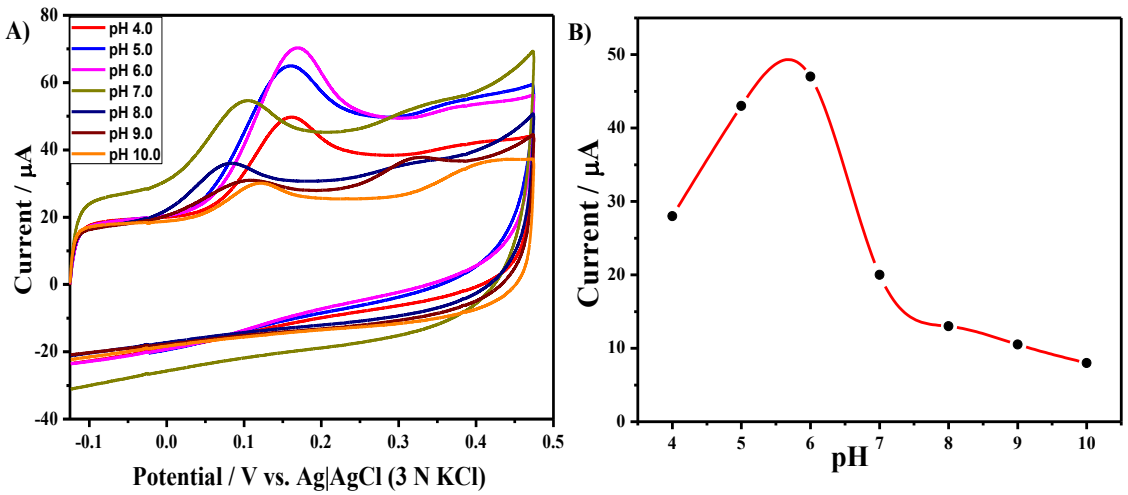

Fig. 2.5. *(A) CVs of 0.1 mM isoniazid recorded at MWCNT-Chit/GCE in B-R buffer at different pH values (4.0 – 10.0). Scan rate = 100 mV s^{-1}. (B) Plot of ip vs. pH of B-R buffer.*

Different amounts of MWCNTs were dispersed in chitosan solution to prepare the modified electrodes, and electrochemical studies have been carried out to optimize the amount of MWCNTs for modification of GCE. Figure 2.6 shows the CVs observed for the oxidation of isoniazid on these modified GCEs. The oxidation peak current is increased with increasing amount of MWCNTs (1 - 3 mg/mL). At further higher amounts (above 3 mg) of MWCNT, solidification of MWCNT suspension takes place which inturn results in less stable MWCNT-chitosan film on the electrode surface. From these results, 3 mg/ml of MWCNTs is found to be optimum for the efficient oxidation of isoniazid at MWCNT-Chit/GCE.

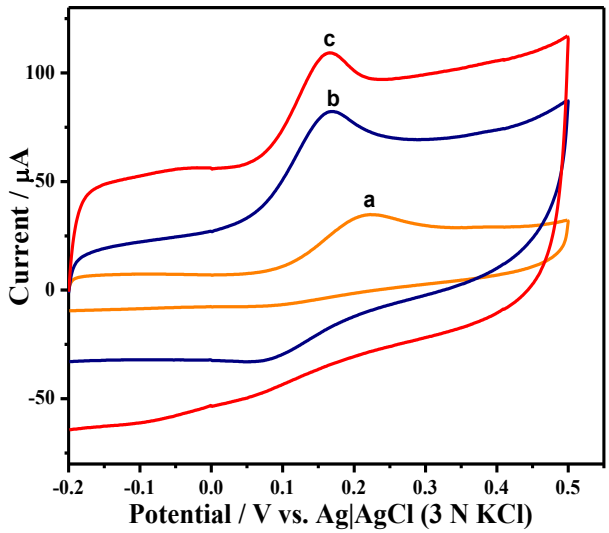

Fig. 2.6. *CVs of 0.1 mM INH in B-R buffer (pH 6.0) using MWCNT-Chit/GCE fabricated with (a) 1 mg mL^{-1} (b) 2 mg mL^{-1} and (c) 3 mg mL^{-1} of MWCNT. Scan rate 100 mV s^{-1}.*

The influence of scan rate on the electrochemical response of 0.1 mM isoniazid at MWCNT-Chit/GCE was investigated by cyclic voltammetry, and the respective results are shown in Fig. 2.7. The oxidation peak currents are gradually increased with increasing scan rate, and the peak current is linearly proportional to the square root of scan rate in the range of 20 to 500 mV s^{-1} (Fig. 2.7(A)). When peak current values were plotted against the square root of scan rate ($\upsilon^{1/2}$), a linear relationship with a regression coefficient of 0.995 was obtained (Fig. 2.7(B)). This behavior suggests that the oxidation of isoniazid at nano-biocomposite MWCNT-chitosan modified electrode is diffusion controlled and that the permeation of isoniazid and electrolyte across the nanocomposite film is very facile (*vide infra*).

For an irreversible electrochemical reaction, the relationship between the peak potential Ep and the scan rate ν is expressed in Eq. (1) by Laviron [35] is shown I Eg. 2.2.

$$\boldsymbol{Ep = E^{\circ} + \frac{RT}{\alpha nF} ln\left[\frac{RTk^{\circ}}{\alpha nF}\right] + \left[\frac{RT}{\alpha nF}\right] ln(\nu)} \quad \ldots\ldots\ldots\ldots \quad \boldsymbol{(Eq.2.2)}$$

where α is the charge transfer coefficient, k° is the standard rate constant for the heterogeneous electron transfer, n is the number of electrons involved in the reaction and E° is the formal potential. According to Eq. (1), the αn value can be determined from the slope of Ep vs. ln(ν) plot (Fig. 2.7(C)), and k° can be calculated from the intercept of the plot if the value of E° is known. The value of E° can be obtained from the intercept of the Ep vs. ν plot (Fig. 2.7(D)) by extrapolation to the vertical axis at ν = 0 and is 0.128 V. From the slope of the Ep vs. ln(ν) plot, αn was calculated to be 0.81. Generally, α can be assumed to be 0.5 for an irreversible electrode process. So the electron transfer number (n) for the electrochemical oxidation of INH becomes 2, and the k° value is determined from the intercept to be 0.55 s^{-1}.

By considering all the above results, we could conclude that the electrochemical oxidation of INH is a two-electron diffusion controlled process and the plausible mechanism for the oxidation of INH has been proposed (Scheme 2.1).

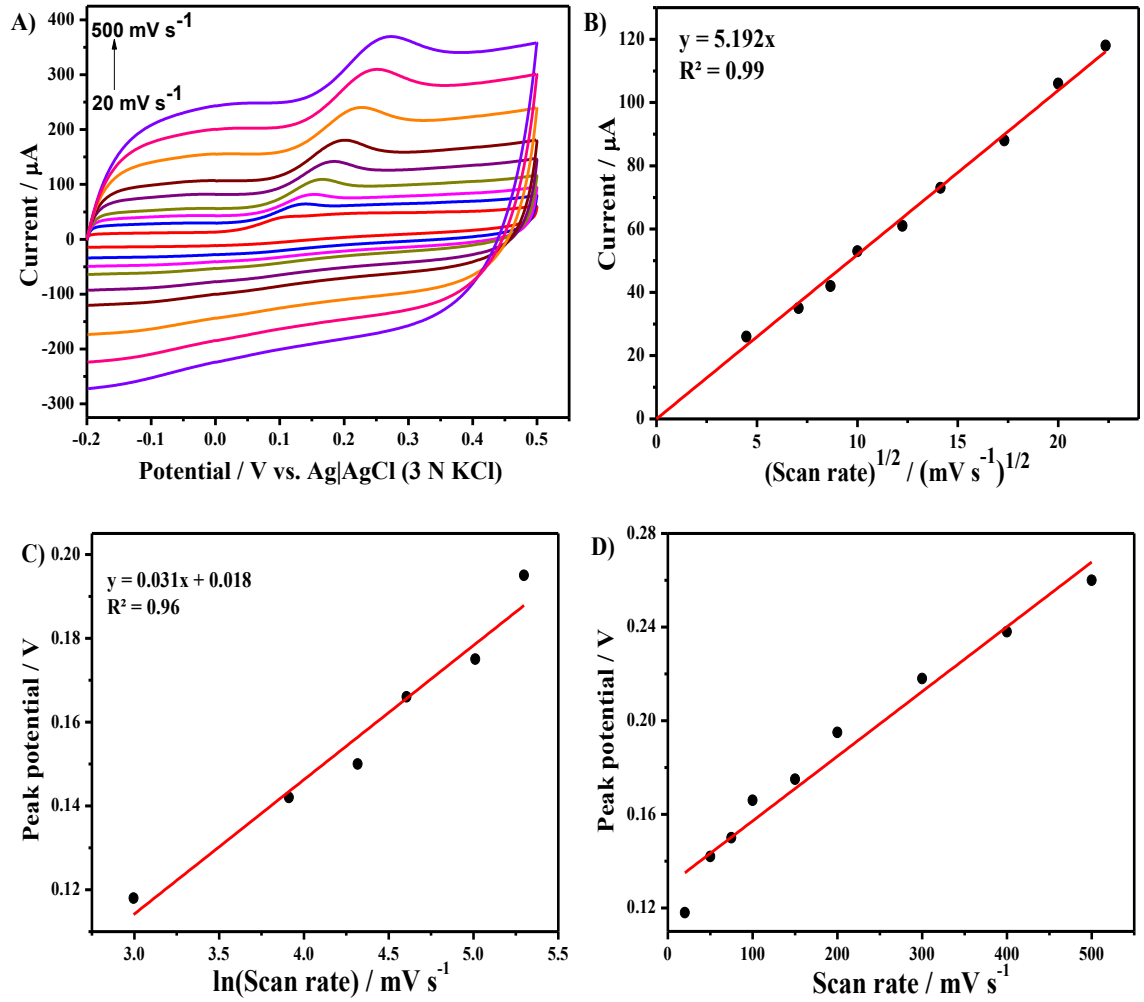

Fig. 2.7. *(A) CVs of 0.1 mM isoniazid in B-R buffer (pH 6.0) using MWCNT-Chit/GCE at scan rates 20, 50, 75, 100, 150, 200, 300, 400 and 500 mV s^{-1}. B) Plot of ip vs. square root of scan rate. (C) Plot of peak potential against ln(scan rate), (D) Plot of peak potential against scan rate.*

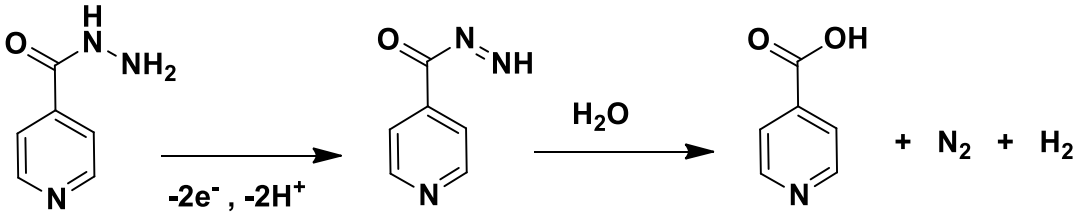

Scheme 2.1*: Mechanism for electrochemical oxidation of INH*

Diffusion coefficient (D) of INH for the electrochemical oxidation at MWCNT-Chit/GCE is determined using chronoamperometric measurements (Figure 2.8(A)) by adopting the Cottrell's equation (Eq. 2.3).[36]

$$i = nFACD^{1/2}\pi^{-1/2}t^{-1/2} \quad \text{..... (Eq. 2.3)}$$

where D and C were the diffusion coefficient (cm^2 s^{-1}) and bulk concentration (mol cm^{-3}) of INH, respectively; A was the electrode area (0.262 cm^2); i was the current controlled by the diffusion of INH from the bulk solution to the electrode/solution interface. The plot of i vs. $t^{-1/2}$ at various INH concentrations was found to be linear (Fig. 2.8(B)). Further, the diffusion coefficient calculated from the slope obtained from the plot of (slope of i vs. $t^{-1/2}$) against concentration of INH (Fig. 2.8(C)) and it is found that the diffusion coefficient of INH at MWCNT-Chit/GCE is 3.7 × 10^{-6} cm^2 s^{-1}. The diffusion coefficient obtained for INH at present electrode is well comparable to the previous reported values (3.6 × 10^{-6} to 5.4 × 10^{-6} cm^2 s^{-1}) at various modified electrodes.[20,37,38]

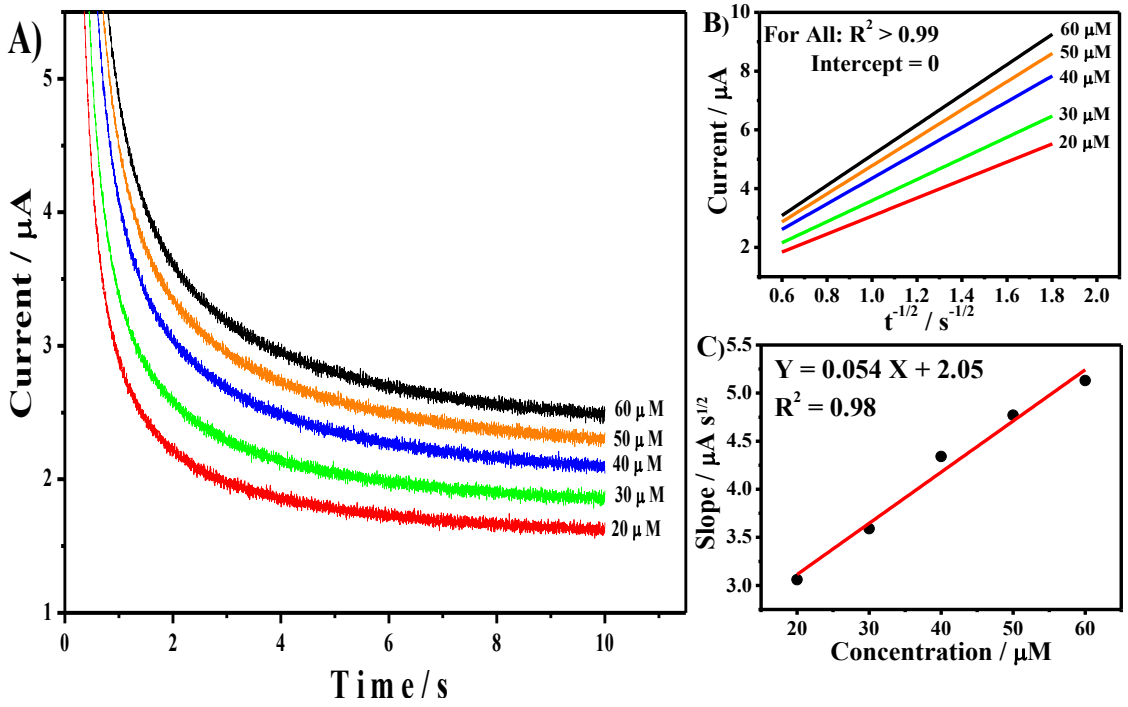

Fig. 2.8. *(A) CA plots of INH in B-R buffer (pH 6.0) at different concentrations (20, 30, 40, 50, 60 µM) at MWCNT-Chit/GCE. (B) i vs. $t^{-1/2}$ plot and (C) plot of slope of (i vs. $t^{-1/2}$) against concentration of INH.*

2.3.6. Electrochemical Impedance Spectroscopy (EIS)

Electrochemical impedance spectroscopy (EIS) is a powerful tool for studying the interfacial properties of surface-modified electrodes[39,40]. The charge transfer resistance (R_{ct}) of the electrode provides vital insight into the nature of interface. EIS analysis of bare GCE and MWCNT-Chit/GCE is carried out 1 mM $K_3[Fe(CN)_6]$ + 0.1 M KCl in the frequency range of 60 kHz to 10 mHz. The results were found to best fit with a simple Randles equivalence circuit. The Randles circuit consists of the ohmic

resistance (R_s) of the electrolyte solution, the double layer capacitance (C_{dl}), electron transfer resistance (R_{ct}) and the Warburg impedance (Z_w) resulting from the diffusion of analyte molecules from the bulk of the electrolyte to the interface. Figure 2.9 shows the Nyquist plots of the MWCNT–chitosan modified electrode and bare GCE in aqueous 1 mM $K_3[Fe(CN)_6]$ + 0.1 M KCl. The Nyquist plot of MWCNT-Chit/GCE (Fig. 2.9a) is nearly a straight line and represents Warburg impedance alone, which indicates the good conductivity of the modified electrode whereas a large electron-transfer resistance was observed at bare GCE (Fig. 2.9b).

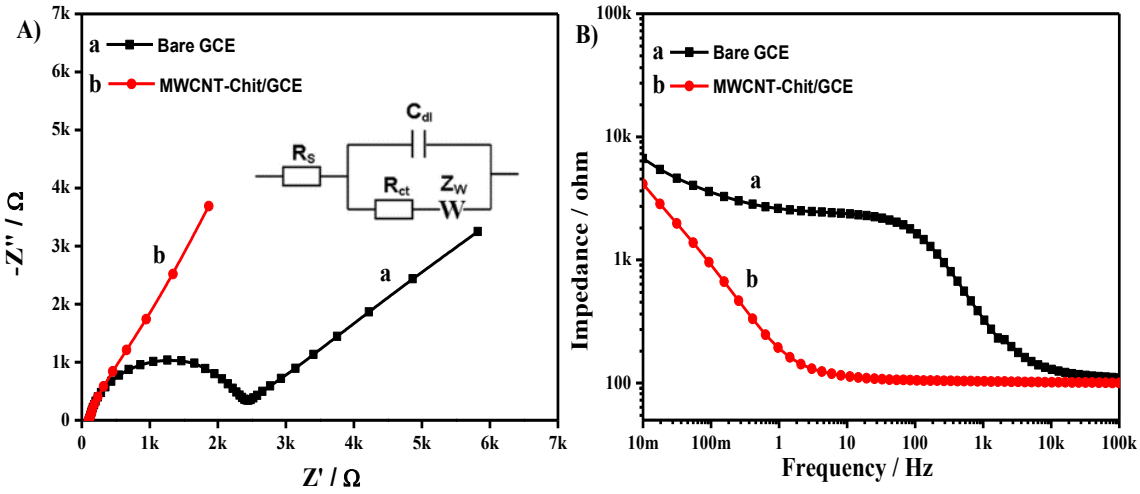

Fig. 2.9. *A) Nyquist B) Bode plots for EIS measurements of bare GCE (a), and MWCNT-Chit/GCE (b) in 1 mM $K_3[Fe(CN)_6]$ in 0.1 M KCl.*

The cyclic voltammetric and EIS experimental results show that the CNTs–chitosan composite film formed a better electron conduction pathway on the electrode surface. That is to say, the CNTs played an important role as electron-transfer mediator thus made the electron-transfer easier. This is due to the nano level surface structural and morphological features of the modified CNTs, the large surface area and excellent electrical conductivity. The fabricated MWCNT-Chit/GCE is investigated further for quantitative analysis of isoniazid.

2.3.7. Differential pulse voltammetry (DPV)

The voltammetric response of the MWCNT–Chit/GCE electrode to the presence of INH was investigated by DPV. At the MWCNT-chitosan modified electrode, the anodic peak at +0.15 V was monitored and the experimental conditions were optimized to obtain a good voltammetric profile with high peak current, low background current and sharp peak with low full-width-half-maximum values. The optimized experimental

parameters for a good voltammetric profile were scan rate of 50 mV s^{-1}, pulse amplitude of 50 mV and pulse period of 0.5 s. After optimizing the operating conditions, differential pulse voltammetric measurements were carried out at the MWCNT–Chit/GCE in B-R buffer containing different INH concentrations and the results are shown in Fig. 2.10(A). The dependence of the oxidation peak currents on the concentration of isoniazid is shown in Fig. 2.10(B). The results showed that the oxidation peak current (i_p) linearly increased with the concentration of isoniazid. The linear regression equation is expressed as: i (μA) = 1.1104 + 1.673 C_{INH} (μM) with the regression coefficient R^2= 0.987; the detection limit is found to be 5.5 × 10^{-8} M (S/N = 3) which is equivalent to ~7.5 ng mL^{-1} with a linear determination range of 1.0 × 10^{-7} M to 1.0 × 10^{-5} M. The performance of the present electrochemical sensor is compared with other electrochemical sensors and also with other analytical methods reported in the literature (Table 2.1).

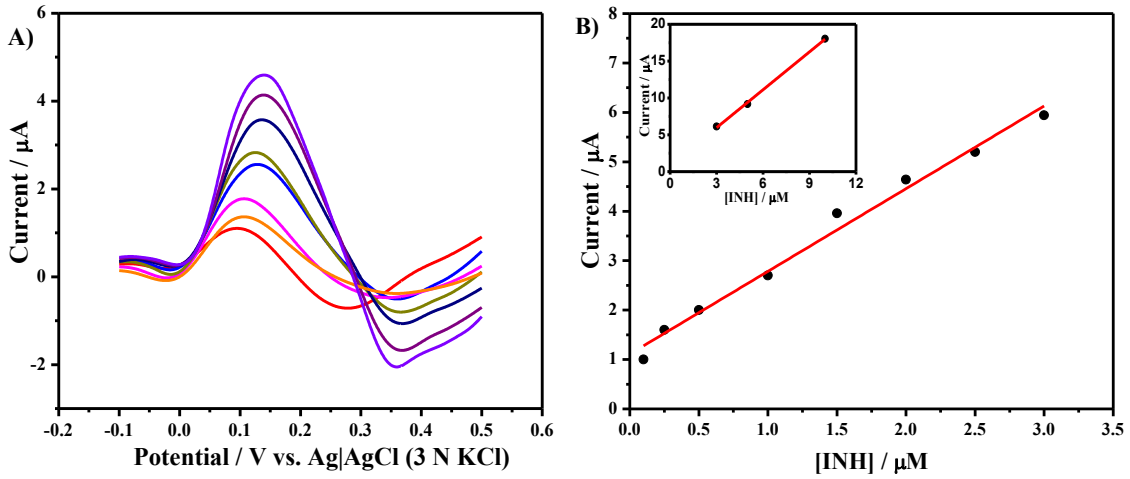

Fig. 2.10. *(A) DPVs of different concentrations of INH (0.1, 0.2,….3 μM) in B-R buffer (pH 6.0) using MWCNT-Chit/GCE. (B) Plot of the peak current against the concentration of INH. Inset shows the plot of peak current at higher concentrations of isoniazid.*

Table 2.1. Detection of INH using electrochemical and various analytical methods

Method	Electrode	Decrease in overpotential (mV)	Linear range	Limit of detection	Reference
DPV	Carbon paste / Poly-L-histidine		$5.0 \times 10^{-7} – 1.1 \times 10^{-4}$ M	1.7×10^{-7} M	Bergamini et al., 2010 [30]
SWV[a]	Pt / Ferrocene mediator		$5.0 \times 10^{-5} – 6.0 \times 10^{-4}$ M	--	Gao et al., 2006 [22]
DPV	MWCNT / Thionine		$1.0 \times 10^{-6} – 1.0 \times 10^{-4}$ M	5.0×10^{-7} M	Shahrokhian et al., 2010 [31]
Amperometry	GC / Polypyrrole	345	$4.0 \times 10^{-6} – 2.0 \times 10^{-3}$ M	3.2×10^{-6} M	Majidi et al., 2006 [20]
Amperometry	GC / Nafion-Ordered Mesoporous carbon	480	$1.0 \times 10^{-7} – 3.7 \times 10^{-4}$ M	8.4×10^{-8} M	Yan et al., 2011 [25]
DPV	GC / MWCNT-carbon paste	150	$1.0 \times 10^{-6} – 1.0 \times 10^{-3}$ M	5.0×10^{-7} M	Shahrokhian et al., 2007 [24]
HPLC	n.a.	n.a.	0.002 – 20 μg mL^{-1}	0.5 ng mL^{-1}	Zhou et al., 2009 [32]
MEKC	n.a.	n.a.	3.0 – 100.0 mg mL^{-1}	1.0 mg mL^{-1}	Nemutlu et al., 2007 [33]
UV-VIS Spectrophotometry	n.a.	n.a.	0.3 – 3.5 μg mL^{-1}	0.26 μg mL^{-1}	Safavi et al., 2004 [12]
UV-VIS Spectrophotometry	n.a.	n.a.	0.6 – 6.2 μg mL^{-1}	0.15 μg mL^{-1}	Safavi et al., 2008 [34]
DPV	MWCNT-Chit/GCE	800	$1.0 \times 10^{-7} – 3.0 \times 10^{-6}$ M (0.014 – 0.411 μg mL^{-1})	5.5×10^{-8} M (7.5 ng mL^{-1})	Present Work

[a] SWV – Square-wave voltammetry, MEKC – micellar electrokinetic capillary chromatography, n.a. – Not applicable

The low-detection-limit of INH obtained by the present electrochemical sensor using MWCNT-Chit/GCE is highly significant and superior compared to the detection-limits reported previously by using various electrochemical[20,30,31], chromatographic[43,44] and spectrophotometric[12,45] methods.

2.3.8. Interference studies

Electrochemical response of INH in the presence of the possible electroactive physiological components such as ascorbic acid (AA), uric acid (UA) and dopamine (DA) has been carried out at MWCNT-chitosan modified electrode using DPV method. Figure 2.11 shows the DPVs at MWCNT-chitosan modified electrode at different concentrations of INH in the presence of ~4 times higher concentration of 20 µM of AA, and the results show that the concentration of INH could be determined accurately even in the presence of higher concentrations of AA. Higher concentrations of other interferents UA and DA also did not influence the current response of INH significantly (signal change < 5%). From the experimental observations, it is clearly evident that the proposed electrochemical method using MWCNT-Chit/GCE can be used effectively for the detection of INH even in the presence of higher concentrations of possible interferents.

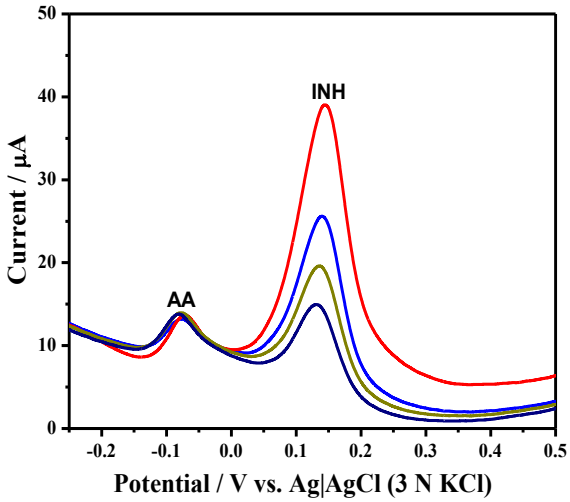

Fig. 2.11. *DPVs of different concentrations of isoniazid (5 µM, 10 µM, 15 µM, 20 µM) in B-R buffer (pH 6.0) using MWCNT-Chit/GCE in the presence of 20 µM ascorbic acid.*

2.3.9. Repeatability and Reproducibility

Reusability of the MWCNT-chitosan modified electrode towards the electrochemical oxidation of INH was investigated by repetitively recording DPV at a fixed INH concentration of 5 µM. The relative standard deviation (RSD) for the anodic

peak currents in six determinations is only 2.5 %, indicating excellent reusability of the nanocomposite modified electrode. Furthermore, the anodic peak currents for the determination of INH in multiple experiments over a time period of 10 days decreased only by 3.0 %. Also, no much change is observed in the oxidation peak potential of INH at modified electrode even after one month of its fabrication though the modified electrode kept at ambient conditions. Moreover, the reproducibility of the MWCNT-chitosan nanocomposite electrode was investigated by analyzing the DPV response of five different electrodes prepared independently. The peak potential for the oxidation of isoniazid is identical with all the electrodes, and the peak currents of the DPVs recorded by using the five independent electrodes at the isoniazid concentration of 1 μM vary only a little with a standard deviation of 2.2 %, indicating that the MWCNT-chitosan nanocomposite electrode is highly reproducible. From the results, it is clear that the MWCNT-chitosan composite formed a stable and reproducible nanobiocomposite film on GCE for the determination of isoniazid.

2.3.10. Determination of INH in pharmaceutical and artificial urine samples

Pharmaceutical samples of isoniazid (300 mg/tablet), which were diluted appropriately, were analyzed with the proposed electrochemical method by the standard addition method. In Fig. 2.12, the curve "e" shows the DPV of analytical sample containing 0.5 μM of pure INH and 0.5 μM of INH from pharmaceutical tablet at MWCNT-Chit/GCE, which gives a good recovery of 102 % with low RSD (1.6 %). The recovery of isoniazid from tablet samples at different concentrations was listed in Table 2 and it varies from 96.7 % to 102.0 %. Recovery of INH in artificial urine was also examined by direct addition of INH into undiluted artificial urine without any buffer. Isoniazid metabolizes rapidly with a half-life of 1 – 3 h. Isoniazid and its derivatives are excreted in urine with 75 – 95% of the drug excreted in 24 h. The concentration of isoniazid in urine 10 h after administration of the drug decreases to as low as 0.26 μg mL^{-1}, i.e., 1.9 μM[43,46]. Lactic acid and uric acid present in urine would interfere effectively in the electrochemical analysis. Artificial urine sample was prepared with the presence of lactic acid and uric acid, etc. at normal urine concentrations levels (see Experimental section) and was examined by DPV analysis. The MWCNT-Chit/GCE did not show any peak to the artificial urine sample in the absence of isoniazid (Fig. 2.12c). It clearly shows that the fabricated nano-biocomposite electrode did not respond to any

of the electroactive interferents present in the urine sample. The nanocomposite matrix comprising –COOH groups in the functionalized MWCNTs might have strongly retarded the electroactive interferences in urine such as lactic acid and uric acid. The electrode was then investigated for detection of isoniazid directly in artificial urine sample. DPV of MWCNT-Chit/GCE electrode in artificial urine sample with the presence of 0.5 µM INH was recorded (Fig. 2.12d), and it shows one peak corresponding to the oxidation of isoniazid. These results clearly indicate that the developed sensor chip could detect INH selectively from urine sample as low as 5 x 10^{-7} M. This detection limit is nearly four times superior compared to the concentration of isoniazid in urine 10 h after administration, and thus diluted urine samples could also be investigated for the determination of isoniazid by the present method. The recovery of isoniazid from undiluted artificial urine samples at different concentrations (5.0 – 15.0 × 10^{-7} M) was listed in Table 2.2, and it varies from 97.0 % to 101.4 %. From the results of the recovery analysis, we conclude that the fabricated sensor can be used efficiently for selective determination of isoniazid from pharmaceutical formulations and from urine samples *in-vitro*.

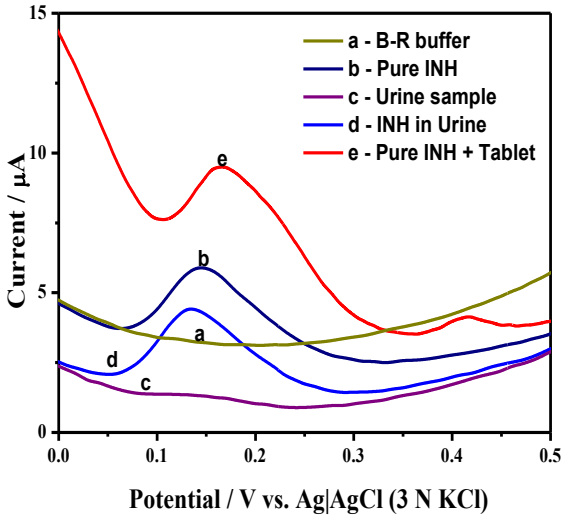

***Fig. 2.12**. DPVs in the (a, c) absence and (b, d) presence of 0.5 µM INH in (a, b) B-R buffer of pH 6.0 and in (c, d) artificial urine. e) Mixture of 0.5 µM pure INH and 0.5 µM INH from tablet in B-R buffer (pH 6.0) at MWCNT-Chit/GCE.*

Table 2.2. Determination of INH in pharmaceutical tablet and in artificial urine samples using MWCNT-Chit/GCE.

Sample	INH ($\times 10^{-7}$ M)	Tablet Added ($\times 10^{-7}$M)	[a]Found ($\times 10^{-7}$M)	Average Recovery (%)	[a]RSD of recovery (%)
Tablet (Solonex, 300 mg)	5.0	5.0	10.20	102.0	1.6
	5.0	10.0	14.50	96.7	2.4
	5.0	15.0	20.10	100.5	1.8
Urine Sample	5.0	-	5.07	101.4	0.8
	10.0	-	9.80	98.0	1.2
	15.0	-	14.55	97.0	3.1

[a] Mean value of six measurements

2.4. Conclusions

In this work, we fabricated a stable and effective electrochemical sensor for sensitive determination of INH with MWCNT-chitosan nanocomposite modified electrode using simple drop and cast method. MWCNT-chitosan nanocomposite film remarkably enhances the voltammetric signal response and lowers the oxidation overpotential of INH. In this nanocomposite modified electrode, the MWCNTs act as good electrocatalytic mediator and MWCNT–chitosan composite film generates a better electron conduction pathway on the GCE surface. The nanocomposite film was highly stable for multiple analysis over a long period due to the unique binding character of chitosan biopolymer. The fabricated MWCNT-chitosan modified electrode can be used for the detection of ppb levels (ng/mL) of INH in the presence of biological interferents. The proposed sensor has good stability, high sensitivity and simple fabrication procedure. From all these advantages, we conclude that this nanocomposite electrode could be extended to the determination of pharma drugs in biological fluids and pharmaceutical formulations.

2.5. References

[1] G. A. Rivas, M. D. Rubianes, M. C. Rodríguez, N. F. Ferreyra, G. L. Luque, M. L. Pedano, S. A. Miscoria, C. Parrado, *Talanta* **2007**, *74*, 291–307.

[2] L. Agüí, P. Yáñez-Sedeño, J. M. Pingarrón, *Anal. Chim. Acta* **2008**, *622*, 11–47.

[3] M. E. Ghica, R. Pauliukaite, O. Fatibello-Filho, C. M. A. Brett, *Sensors Actuators B Chem.* **2009**, *142*, 308–315.

[4] S. Murugesan, K. Myers, V. Ravi Subramanian, *Appl. Catal. B Environ.* **2011**, *103*, 266–274.

[5] Y. Li, X. Shi, J. Hao, *Carbon N. Y.* **2006**, *44*, 2664–2670.

[6] K.-J. Huang, X. Liu, W.-Z. Xie, H.-X. Yuan, *Colloids Surf. B. Biointerfaces* **2008**, *64*, 269–274.

[7] S. W. Kim, T. Kim, Y. S. Kim, H. S. Choi, H. J. Lim, S. J. Yang, C. R. Park, *Carbon N. Y.* **2012**, *50*, 3–33.

[8] A. Salimi, B. Kavosi, F. Fathi, R. Hallaj, *Biosens. Bioelectron.* **2013**, *42*, 439–446.

[9] G. O. Phillips, P. A. Williams, *Handbook of Hydrocolloids*, Woodhead Publishing Limited, **2000**.

[10] A. M. El-Brash, L. A. El-Hussain, *Arch. Pharm. Res.* **1997**, *20*, 597–601.

[11] S. A. Benetton, E. R. M. Kedor-Hackmann, M. I. R. M. Santoro, V. M. Borges, *Talanta* **1998**, *47*, 639–643.

[12] A. Safavi, M. A. Karimi, M. R. Hormozi Nezhad, R. Kamali, N. Saghir, *Spectrochim. Acta. A. Mol. Biomol. Spectrosc.* **2004**, *60*, 765–769.

[13] G. Krishnamurthy Naidu, K. Suvardhan, K. Suresh Kumar, D. Rekha, B. S. Sastry, P. Chiranjeevi, *J. Anal. Chem.* **2005**, *60*, 822–827.

[14] H. I. Seifart, W. L. Gent, D. P. Parkin, P. P. van Jaarsveld, P. R. Donald, *J. Chromatogr. B. Biomed. Appl.* **1995**, *674*, 269–275.

[15] P. J. Smith, J. Van Dyk, A. Fredericks, *Int. J. Tuberc. Lung Dis.* **1999**, *3*, S325–S328.

[16] Z. Song, J. Lü, T. Zhao, *Talanta* **2001**, *53*, 1171–1177.

[17] S. Zhang, H. Li, *Anal. Chim. Acta* **2001**, *444*, 287–294.

[18] G. Yang, C. Wang, R. Zhang, C. Wang, Q. Qu, X. Hu, *Bioelectrochemistry* **2008**, *73*, 37–42.

[19] M. . Ghoneim, K. . El-Baradie, A. Tawfik, *J. Pharm. Biomed. Anal.* **2003**, *33*, 673–685.

[20] M. R. Majidi, A. Jouyban, K. Asadpour-Zeynali, *J. Electroanal. Chem.* **2006**, *589*, 32–37.

[21] J. Tong, X.-J. Dang, H.-L. Li, *Electroanalysis* **1997**, *9*, 165–168.

[22] Z.-N. Gao, X.-X. Han, H.-Q. Yao, B. Liang, W.-Y. Liu, *Anal. Bioanal. Chem.* **2006**, *385*, 1324–1329.

[23] B. K. Jena, C. R. Raj, *Talanta* **2010**, *80*, 1653–1656.

[24] S. Shahrokhian, M. Amiri, *Microchim. Acta* **2007**, *157*, 149–158.

[25] X. Yan, X. Bo, L. Guo, *Sensors Actuators B Chem.* **2011**, *155*, 837–842.

[26] T. Brooks, C. W. Keevil, *Lett. Appl. Microbiol.* **1997**, *24*, 203–206.

[27] C. Gouveia-Caridade, R. Pauliukaite, C. M. A. Brett, *Electrochim. Acta* **2008**, *53*, 6732–6739.

[28] C. H. An Wong, M. Pumera, *J. Mater. Chem. C* **2014**, *2*, 856–863.

[29] E. Nossol, A. J. Gorgatti Zarbin, *J. Mater. Chem.* **2012**, *22*, 1824–1833.

[30] P. Li, Y. Ding, A. Wang, L. Zhou, S. Wei, Y. Zhou, Y. Tang, Y. Chen, C. Cai, T. Lu, *ACS Appl. Mater. Interfaces* **2013**, *5*, 2255–2260.

[31] X. Wu, X. Chen, J. Wang, J. Liu, Z. Fan, X. Chen, J. Chen, *Ind. Eng. Chem. Res.* **2011**, *50*, 891–897.

[32] J. Fan, Z. Shi, M. Tian, J. Wang, J. Yin, *ACS Appl. Mater. Interfaces* **2012**, *4*, 5956–5965.

[33] L. G. Bulusheva, A. V. Okotrub, I. A. Kinloch, I. P. Asanov, A. G. Kurenya, A. G. Kudashov, X. Chen, H. Song, *Phys. status solidi* **2008**, *245*, 1971–1974.

[34] S. Hrapovic, E. Majid, Y. Liu, K. Male, J. H. T. Luong, *Anal. Chem.* **2006**, *78*, 5504–12.

[35] E. Laviron, *J. Electroanal. Chem.* **1979**, *101*, 19–28.

[36] A. J. Bard, L. R. Faulkner, *Electrochemical Methods: Fundamentals and Applications, 2nd Ed.*, John Wiley & Sons, New York, **2001**.

[37] U. P. Azad, N. Prajapati, V. Ganesan, *Bioelectrochemistry* **2015**, *101*, 120–125.

[38] U. P. Azad, V. Ganesan, *J. Solid State Electrochem.* **2012**, *16*, 2907–2911.

[39] Y. Feng, T. Yang, W. Zhang, C. Jiang, K. Jiao, *Anal. Chim. Acta* **2008**, *616*, 144–151.

[40] R. Pauliukaite, M. E. Ghica, O. Fatibello-Filho, C. M. A. Brett, *Electrochim. Acta* **2010**, *55*, 6239–6247.

[41] M. F. Bergamini, D. P. Santos, M. V. B. Zanoni, *Bioelectrochemistry* **2010**, *77*, 133–138.

[42] S. Shahrokhian, E. Asadian, *Electrochim. Acta* **2010**, *55*, 666–672.

[43] Z. Zhou, D. Zhao, J. Wang, W. Zhao, M. Yang, *J. Chromatogr. A* **2009**, *1216*,

30–35.

[44] E. Nemutlu, M. Çelebier, B. Uyar, S. Altınöz, *J. Chromatogr. B* **2007**, *854*, 35–42.

[45] A. Safavi, M. Bagheri, *Spectrochim. Acta Part A Mol. Biomol. Spectrosc.* **2008**, *70*, 735–739.

[46] A. Sj, P. Sj, K. Kw, S. Gy, C. Mp, H. Kim, J. Kwon, R. Ch, C. Hs, K. Mm, et al., *Tuberc Respir Dis.* **1999**, *47*, 442–450.

CHAPTER 3

Gold Nanoparticles Decorated Carbon Nanotubes based Sensor for Electrochemical Detection of 5-Fluorouracil *in-vitro*

3.1. Introduction

In recent years, various antitumor active compounds are widely used in the treatment of cancer, and one of the most widely used drugs for chemotherapy of solid tumours is 5-fluorouracil (5-FU). It is an antineoplastic agent used for the treatment of solid tumour based cancers. Generally, high serum concentrations of drugs are necessitated to effect a pharmacological activity against tumours, but 5-FU metabolizes rapidly in the body. Determining safe and effective dosage of drugs for chemotherapy is still a substantial challenge in the treatment of neoplastic diseases. Frequent measurement of the concentration of 5-FU in physiological fluids is extremely demanded to maintain an optimal concentration of 5-FU. It is noteworthy that an overdose of 5-FU may cause very high toxicity by accumulation in cancer patients. Controlling the amount of 5-FU in a given formulation and the dose to the sufferers is important in pharmaceutical quality control and for clinical diagnosis. Various analytical methods have been aimed for the detection of 5-FU based on spectroscopic [1,2], chromatographic capillary [3,4], electrophoresis [5] and electrochemical methods [6–8]. Electrochemical transduction methodologies are advantageous because they offer miniaturization, portable analysis, rugged instrumentation with no movable parts, high sensitivity, on-site analysis, etc. However, the major problem towards the detection of 5-FU by an electrochemical method is the poor oxidation of 5-FU at bare electrodes and only a few electrochemical sensors have been reported so far for the detection of 5-FU. Therefore, highly sensitive and selective sensor systems are still in need for the determination of 5-FU at nano molar levels.

Carbon nanotubes (CNTs) are investigated immensely in a wide variety of research fields because of their salient features, such as high mechanical strength, nanowires of few hundred micrometer long tubular geometry and chemically inert nature with high electrical conductivity [9,10]. However, low dispersion and high aggregation impediment the effective usage of CNTs for electrochemical sensor applications. Incorporation of functional reactive groups into the backbone of CNTs and combined use with ionic liquids, polymer electrolytes, etc. could alleviate the drawbacks. In electrochemical sensor systems, CNT based electrodes are less susceptible to electrode fouling and thus the reuse of such sensors would be greatly improved [11,12].

Another interesting nanomaterial for the modification of electrode surface is gold nanoparticles (GNPs), because of the high surface area along with high conductivity.

GNPs allow electrons to flow freely into the material and have demonstrated high catalytic activity for both oxidation and reduction reactions. The major problem with the nanoparticles is aggregation of particles, which could lead to the decrease of both active surface area and also conductivity. Therefore, it is necessary to develop effective methods to synthesize gold nanoparticles which could be free from aggregation. Several strategies have been developed to prevent the nanoparticles from aggregation such as polymer coatings, surfactant stabilizers, thiol-ligand coatings and polymer agents capping [13–15]. Considering the advantages of both MWCNTs and GNPs towards electrode modification, a hybrid composite between MWCNTs and GNPs is intended to avoid aggregation and also to bring some special features by synergistic effect.

Chitosan (chit) obtained by partial deacetylation of the natural biopolymer, chitin, is used here to form a linkage between MWCNTs and GNPs. Chitosan polymer has attracted here for the dispersion of CNTs because of the presence of a large number of functional groups such as hydroxyl and amine groups in addition to its very good film forming ability, hydrophilicity and biocompatibility. In our previous work, we fabricated a MWCNT-chitosan nanocomposite based electrode which exhibited an excellent catalytic activity, and there chitosan formed a very good linkage between MWCNT and electrode substrate [16]. In this investigation, MWCNT decorated with GNPs is synthesized in the presence of chitosan. The functional groups present in chitosan are responsible for both the reduction and stabilization of the GNPs with which the nanoparticles become stable and free from aggregation. Chitosan can also be chosen to avoid the use of toxic reductants such as hydrazine and sodium borohydride. By combining these advantages of chitosan, we fabricated an electrochemical sensor for the important anti-cancer drug 5-flourouracil using a nanocomposite of MWCNT and GNPs.

3.2. Experimental

3.2.1. Chemicals

5-Fluorouracil, ascorbic acid, uric acid, dopamine and serotonin were obtained from Tokyo chemical industry, Japan. Chitosan (60 – 120 kDa, 85% deacetylation) and gold (III) chloride ($HAuCl_4$) were purchased from Sigma Aldrich, USA. MWCNTs (95%, 20–30 nm OD and 10–30 μm length) were purchased from Sisco research laboratories, India. Other chemicals used in this investigation were analytical grade reagents (minimum 99% purity). Britton-Robinson buffer (B-R buffer) was prepared by mixing boric acid, phosphoric acid and acetic acid 40 mM each, followed by the addition

of 0.1 M NaOH to adjust the pH (pH 4.0 to 11.0). Artificial urine solution was prepared following a procedure reported in the literature [17]. It consists urea (170 mM), citric acid (2.0 mM), lactic acid (1.1 mM), sodium chloride (90 mM), ammonium chloride (25 mM), sodium sulphate (10 mM), sodium bicarbonate (25 mM), calcium chloride (2.5 mM), potassium dihydrogen phosphate (7.0 mM) and dipotassium hydrogen phosphate (7.0 mM), and the solution was adjusted to pH 8.0 by the addition of 1.0 M NaOH. Double distilled water filtered finally through a 0.2 µm Millipore cartridge was used to prepare aqueous solutions throughout the experiment.

3.2.2. Functionalization of MWCNTs

Functionalization of MWCNT with carboxyl groups was carried out by treating with hot nitric acid, following a procedure reported in the literature [18]. MWCNT (120 mg) was taken in 10 mL of 3 M nitric acid and heated at 60 °C for one day. Then, the black solid product was filtered, washed with water until the filtrate becomes neutral and dried at 80 °C for one day. On treatment with nitric acid, MWCNT is introduced with carboxyl groups at the sidewall defects and at the ends of the nanotubes. The resultant functionalized MWCNT was characterized by Raman spectroscopy. The number of carboxyl groups present in the functionalized MWCNT was determined by acid-base titration method, and it is 2.1 mmol g^{-1}.

3.2.3. Synthesis of GNP-MWCNT nanocomposite

The nanocomposite of GNP and MWCNT was prepared by adopting major changes in the recipe reported previously for GNP [19]. A solution of chitosan (1% w/v) was prepared by dissolving it in aqueous acetic acid (1% v/v). MWCNT (5 mg) was added to 10 mL of the chitosan solution and ultrasonicated until a homogeneous black suspension was obtained. Then, 5 mL of aq. 10 mM $HAuCl_4$ was added to the resultant MWCNT–chitosan mixture and heated for 1 h at ~80 ºC. Wine red coloured gold nanoparticles can be observed in the black suspension which are protected by chitosan biopolymer. The homogeneous mixture was then stirred for 1 h to allow the chitosan protected GNPs to attach with MWCNTs through the functional –COOH groups of MWCNT and the amine groups of protecting chitosan layer. The GNP-attached MWCNTs are collected by centrifugation of the above mixture, and the GNPs which are not attached to MWCNTs and remaining in the supernatant are discarded. The collected solid product is denoted hereafter as GNP-MWCNT nanocomposite.

3.2.4. *Fabrication of modified electrodes*

Glassy carbon electrodes of 3 mm diameter (CH Instruments, USA) were polished with alumina powder of 1 µm size and down to 50 nm and washed well under ultrasonication with water, aq. 1:1 nitric acid, ethanol and finally with water. GNP-MWCNT nanocomposite or MWCNT (3 mg) was dispersed into a solution of chitosan (1% w/v, 1 mL) under ultrasonication at RT for about 30 min. The resultant dispersions of GNP-MWCNT and MWCNT (10 µL) were used to form a thin film on the GCE surface by drop-casting method. The resultant electrodes were dried at RT for 24 h and denoted hereafter as GNP-MWCNT-Chit/GCE and MWCNT-Chit/GCE.

3.2.5. *Instrumentation*

UV-Visible spectra were recorded on PerkinElmer LAMBDA25 spectrophotometer. Raman spectra of MWCNT samples were recorded using a confocal spectrometer (Model: LabRAM, HR800). A He-Ne laser source (633 nm; 20 mW power) was used for excitation, and the data were collected for 10 s using a 5× objective. Powder X-ray diffraction (XRD) of GNP-MWCNT composite was recorded in the range of 10° – 90° 2θ on a Brucker AXS D8 diffractometer, and Cu was used as the target (K = 1.5406 Å) with a step size of 0.002° and a scan speed of 0.5 s per step. Surface morphological studies were carried out on an FEI Quanta 200F field emission scanning electron microscope (FESEM) operating at 15 kV. For FESEM analysis, the samples were cast on a conducting carbon tape and sputtered with a thin layer of gold to avoid charging during the analysis.

3.2.6. *Electrochemical analysis*

Voltammetry, chronoamperometry experiments were carried out using an Electrochemical Potentiostat/Galvanostat (Model 6132e, CH Instruments, USA). Electrochemical impedance measurements were carried out using an electrochemical workstation (Model: IM6e, Zahner, Germany) equipped with Thales software. A conventional two-compartment three-electrode cell of 20 mL volume was used with bare or modified GCE as the working electrode, spiral Pt electrode as the counter electrode and Ag|AgCl (3 N KCl) as reference electrode. Electrode potentials were referred against Ag|AgCl (3 N KCl) throughout the manuscript. B-R buffer (pH 4.0 – 11.0) was used as the electrolyte for electrochemical experiments. For electrochemical analysis, the experimental solutions were purged with nitrogen gas for 10 min prior to the start of the experiment.

3.3. Results and Discussion

3.3.1. Characterization of GNP-MWCNT nanocomposite

Formation of gold nanoparticles is usually first examined by UV–Visible spectra of the colloidal gold solution. UV-Visible spectra of the colloidal solution of chitosan protected GNPs, chitosan solution and aq. $HAuCl_4$ solution were recorded. The absorption maxima (λ_{max}) of the GNP colloidal solution is observed at 525 nm (Fig. 3.1(A)), which indicates that the size of gold nanoparticles is about ~30 nm in diameter[20,21].

XRD was used to further confirm the size of GNP in the GNP-MWCNT composite. The powder XRD patterns of MWCNT and GNP-MWCNT are shown in Fig. 3.1(B). XRD pattern of GNP-MWCNT has all Bragg's reflections associated to crystalline gold, which were observed at 38.2°, 44.4°, 64.6°, 77.5° and 81.8°, representing (1 1 1), (2 0 0), (2 2 0), (3 1 1) and (2 2 2) planes of FCC crystalline gold (JCPDS No. 04 - 0784). The crystalline size of GNP was calculated using Scherrer formula, and the average crystalline size obtained from the calculation is ~28.7 nm. The results clearly indicate that the GNPs are of finite size and that the aggregation of nanoparticles is well controlled.

Raman spectroscopy is an important and powerful technique for characterization of CNTs and other nanomaterials[22,23]. Structural changes caused by the functionalization of MWCNT and by the decoration with GNPs can be observed by changes in Raman spectroscopy bands. Figure 3.1(C) shows the Raman spectra recorded for pristine MWCNT, functionalized MWCNT and GNP-decorated MWCNT, where all the three samples are exhibiting D-band (~1,330 cm^{-1}) related to structural disorders of carbon based materials, G-band (~1,580 cm^{-1}) related to graphitized carbon and G^1-band (~2,660 cm^{-1}) is the first overtone of the D-band. The intensity ratio (I_D/I_G) is an indicator of the quantitative measure of structural defects. Functionalization of MWCNTs is evident from the I_D/I_G peak intensity ratio, where we observed a remarkable increase in I_D/I_G value from pristine (1.18) to functionalized MWCNT (1.46). This observation clearly confirms that the graphitized carbon content relatively decreased in functionalized MWCNT obviously owing to the functionalization process, which involves in the formation of carboxyl groups at the defect sites and at the end of the nanotubes. Further, the decoration with GNPs on functionalized MWCNT is confirmed by the peak position and intensities of D, G, and G^1 bands. At first, there was

no significant difference in the I_D/I_G ratio between GNP-MWCNT and functionalized MWCNT. It indicates that the decoration of GNPs onto the surface of functionalized MWCNTs did not affect the core CNT structure. However, there is a little shift in the G-band to higher wavenumber by GNP decoration onto MWCNT (Fig. 3.1(C) inset), and it indicates the chemical interaction between GNPs and the functionalized MWCNT. A similar trend is also observed with the G^1 band.

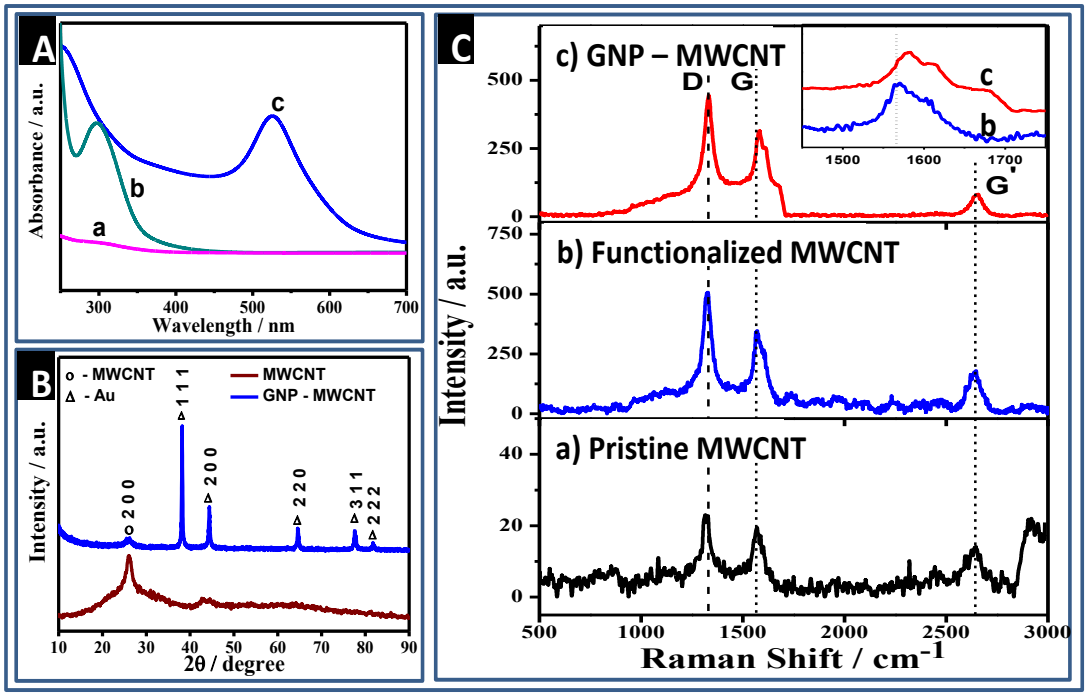

Fig. 3.1. *A) UV-Visible spectra of a) aq. 1 wt.% chitosan, b) aq. $HAuCl_4$, c) gold colloid in aq. 1 wt.% chitosan. (B) XRD spectra of MWCNT and GNP-MWCNT composite. (C) Raman spectra of pristine MWCNT, functionalized MWCNT and GNP-MWCNT.*

The field emission scanning electron microscope (FESEM) was used to characterize the surface morphology of GNP-MWCNT nanocomposite. Figure 3.2 shows the FESEM images of MWCNT and GNP-MWCNT nanocomposite. The FESEM image of GNP-MWCNT composite is seen to have sharp crystallites continuously throughout the CNT structure. Obviously, the FESEM image of plain MWCNT shows simple thread like structures of MWCNT. Figure 3.2 clearly illustrates that the gold nanoparticles are distributed all over the surface of MWCNT as sharp crystallites and have formed a good network on MWCNT. Furthermore, the GNP-MWCNT film is of very much porous nature with a fine distribution of MWCNTs all over the matrix, and in overall the nanocomposite could promote the electron transfer across the film efficiently.

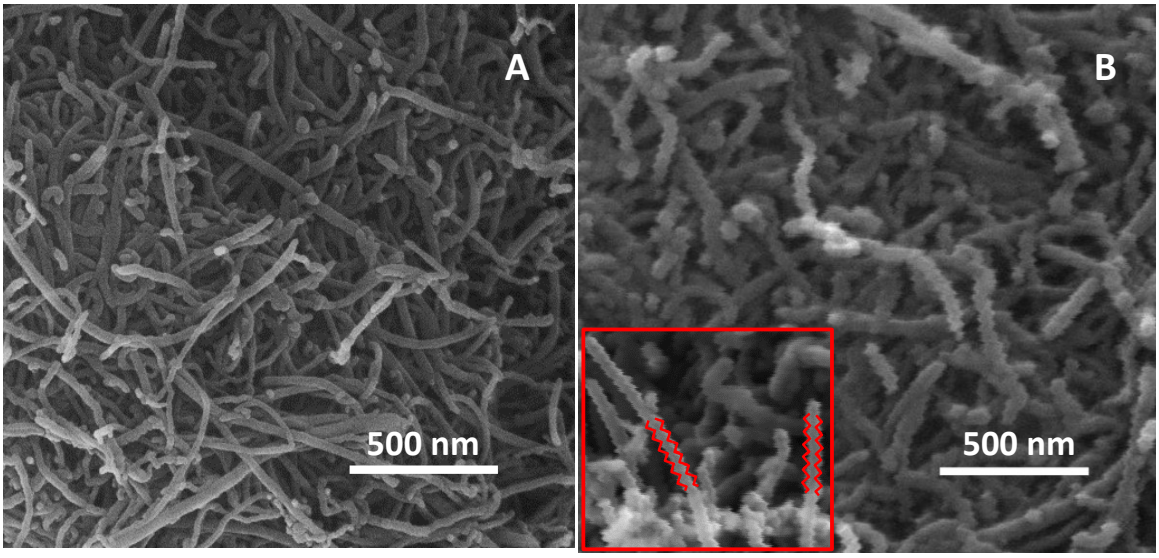

Fig. 3.2. *FESEM image of (A) MWCNT (B) GNP-MWCNT nanocomposite; Inset shows a magnified section of the image.*

3.3.2. Electroactive surface area of modified electrodes

The cyclic voltammetry analysis is a very basic method to study the electrochemical characteristics of an analyte at modified electrodes. At first, the electroactive areas of the modified electrodes were estimated by cyclic voltammetry and compared with that of bare GCE. For the purpose, cyclic voltammograms (CVs) of $K_3[Fe(CN)_6]$ were recorded at bare GCE, MWCNT-Chit/GCE and GNP-MWCNT-Chit/GCE electrodes in aq. 2 mM $K_3[Fe(CN)_6]$ + 0.1 M KCl at various scan rates (10 to 150 mV s^{-1}). For the three electrodes, the CVs obtained at the scan rate of 100 mV s^{-1} and the plot of peak currents against the square root of scan rate are shown in Fig. 3.3(B). The peak currents observed with the modified electrodes are higher than that observed with bare GCE. The results were analyzed, and the effective surface areas of the modified electrodes were determined by applying the Randles-Sevcik equation and by considering the diffusion coefficient of $K_3[Fe(CN)_6]$ as 6.7×10^{-6} cm^{-2} s^{-1}, according to the procedure recorded elsewhere [24]. The effective surface area of bare GCE is 0.078 cm^2, which is nearly equal to the geometrical surface area of 3 mm diameter electrode. The electroactive surface areas of MWCNT-Chit/GCE and GNP-MWCNT-Chit/GCE are nearly 4 to 7 times higher than that of bare GCE and are 0.26 and 0.58 cm^2, respectively.

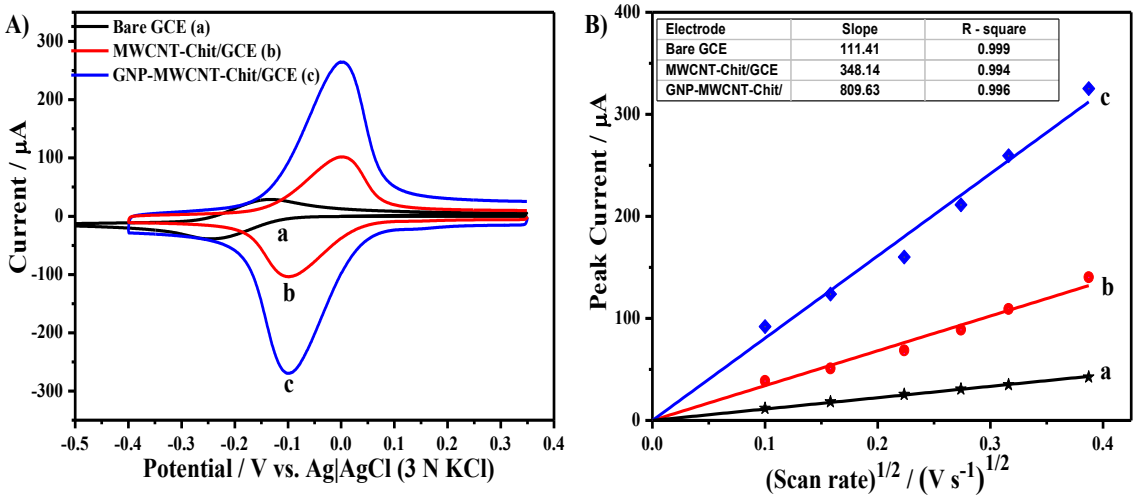

***Fig. 3.3**. (A) CVs of $K_3[Fe(CN)_6]$ recorded at bare GCE (a), MWCNT-Chit/GCE (b) and GNP-MWCNT-Chit/GCE (c) in aq. 2 mM $K_3[Fe(CN)_6]$ + 0.1 KCl; scan rate = 100 mV s^{-1}. (B) Plot of the anodic peak current against the square root of scan rate.*

3.3.3. Electrocatalytic oxidation of 5-fluorouracil

Cyclic voltammograms of 5-fluorouracil were recorded at bare GCE, MWCNT-Chit/GCE and GNP-MWCNT-Chit/GCE in B-R buffer (pH 8.0) containing 0.5 mM 5-FU, and the CVs are shown in Fig. 3.4. In the absence of 5-FU, no characteristic peak was observed at any of the electrodes in B-R buffer. In the presence of 5-fluorouracil, an irreversible anodic peak was observed at all the electrodes. The anodic peak potential for the oxidation of 5-FU at bare GCE is ~ +1.25 V. At both MWCNT-Chit/GCE and GNP-MWCNT-Chit/GCE electrodes, a well-defined anodic peak was observed at a less positive potential, +1.10 V. The decrease in the overpotential for the oxidation of 5-FU at GNP-MWCNT-Chit/GCE is advantageous. Furthermore, the peak currents for the oxidation of 5-FU at MWCNT-Chit/GCE and GNP-MWCNT-Chit/GCE electrodes are respectively higher by 4 and 15 times than that at bare GCE. These observations are clear evidences for the enhanced effect of GNP-MWCNT nanocomposite towards 5-FU oxidation. Moreover, the GNP-MWCNT modified electrode shows a large background charging current compared with MWCNT-Chit/GCE and bare GCE, owing to a significant increase in the active surface area of the electrode. These results clearly reveal that the GNP-MWCNT nanocomposite film formed a better electron conduction pathway for the oxidation of 5-FU and helped to accelerate the electron transfer across the electrode interface.

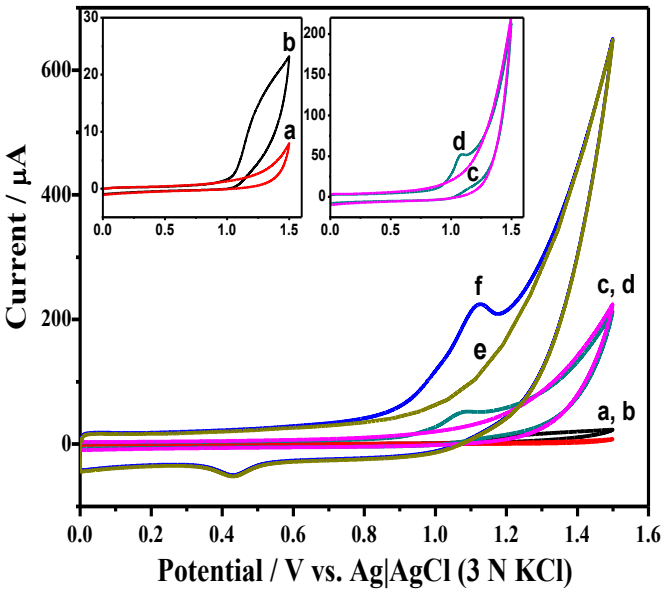

Fig. 3.4. *CVs of 5-FU recorded in B-R buffer (pH 8.0) in the presence (b, d, f) and absence (a, c, e) of 0.5 mM 5-FU at bare GCE (a, b), MWCNT-Chit/GCE (c, d) and GNP-MWCNT-Chit/GCE (e, f). Scan rate = 100 mV s^{-1}.*

Effect of pH on the electrochemical characteristics of 5-FU at GNP-MWCNT-Chit/GCE was investigated by cyclic voltammetry in B-R buffer of different pH values (pH 4.0 to 11.0) (Fig. 3.5). The pH of the buffer solution obviously influenced the

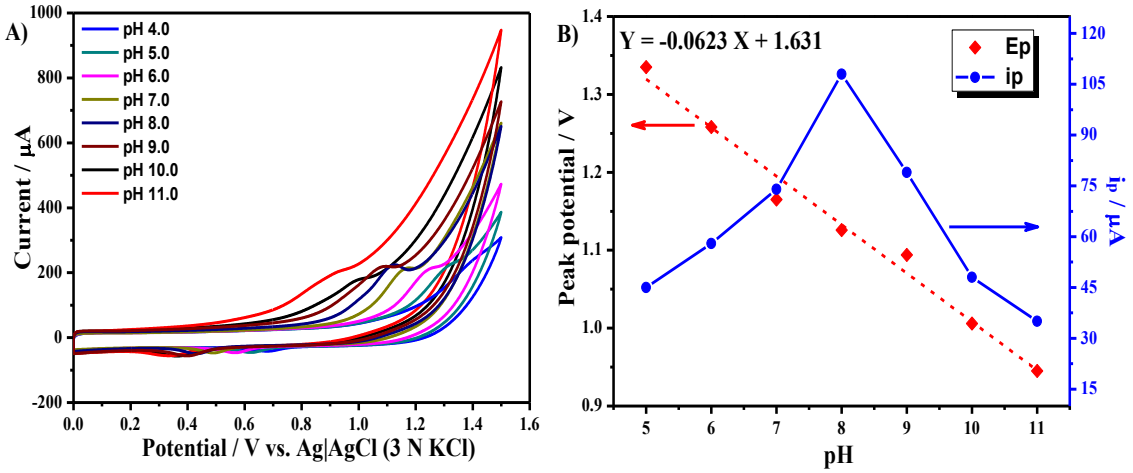

Fig. 3.5. *(A) CVs of 0.5 mM 5-FU in B-R buffer of different pH values (4 – 11) at GNP-MWCNT-Chit/GCE; scan rate = 100 mV s^{-1}. (B) Plot of peak potential and peak current against pH.*

oxidation peak of 5-FU. The peak currents are high in the pH range of 7.0 – 9.0, and it decreased to a minimum at pH ≥ 10.0. The peak potential (Ep) was gradually changing to less positive potentials as the pH varied from 5.0 to 11.0. The plot between Ep and pH (Fig. 3.5(B)) shows that Ep is linearly dependent on pH. The slope of the Ep vs. pH plot is 0.062 V and is very close to the theoretical Nernstian value of 0.059 V, which

indicates that the number of protons and the number of electrons transferred in the electrochemical oxidation of 5-FU are equal to each other. In the overall pH range of 4.0 to 11.0, the peak current was very high at pH 8.0. Considering these observations, B-R buffer of pH 8.0 has been chosen for further analysis.

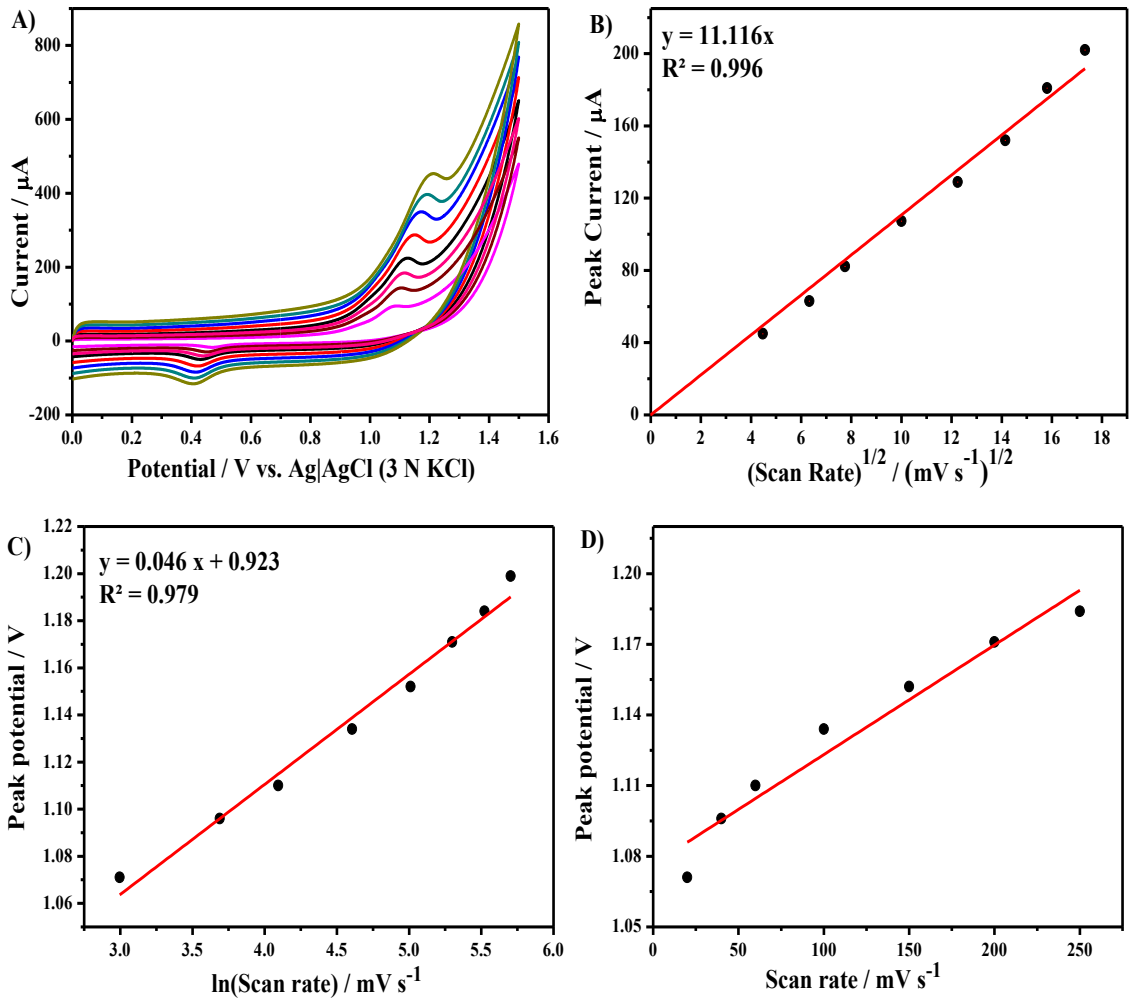

Fig. 3.6. *(A) CVs of 0.5 mM 5-FU in B-R buffer (pH 8.0) at GNP-MWCNT-Chit/GCE with different scan rate (20, 40, 60, 100, 150, 200, 250, 300, 350 mV s^{-1}) (B) Plot of peak current against square root of scan rate. (C) Plot of peak potential against ln(scan rate), (D) peak potential against scan rate.*

Influence of the scan rate on the voltammetric behaviour of 5-FU was studied. Cyclic voltammograms of 0.5 mM 5-FU at GNP-MWCNT-Chit/GCE were recorded with different scan rates (20 – 350 mV s^{-1}) and are shown in Fig. 3.6(A). The peak currents for the oxidation of 5-FU gradually increased with the scan rate. The plot between the anodic peak current and the square root of scan rate was linear, passing through the origin (Fig. 3.6(B)). It clearly indicates that the electrochemical oxidation of

5-FU is a diffusion controlled process and that the permeation of 5-FU across the GNP nanocomposite film is very facile (*vide infra*).

For an irreversible electrochemical reaction, the relationship between the peak potential Ep and the scan rate ν expressed by Laviron[25] is shown in Eq. 2.2 of Chapter 2. According to the equation, the αn value can be determined from the slope of Ep vs. ln(ν) plot (Fig. 3.6(C)), and k° can be calculated from the intercept of the plot if the value of E° is known. The value of E° can be obtained from the intercept of the Ep vs. ν plot (Fig. 3.6(D)) by extrapolation to the vertical axis at ν = 0 and is 1.08 V. From the slope of the Ep vs. ln(ν) plot, αn was calculated to be 0.56. Generally, α can be assumed to be 0.5 for an irreversible electrode process. So the electron transfer number (n) for the electrochemical oxidation of 5-FU becomes 1, and the k° value is determined from the intercept to be 0.82 s^{-1}. Diffusion coefficient of 5-FU for the electrochemical oxidation at GNP-MWCNT-Chit/GCE is determined using chronoamperometry (Figure 3.7) by adopting the Cottrell's equation[26] and its value is determined to be 9.62 × 10^{-6} cm^2 s^{-1}. The diffusion coefficient obtained for 5-FU at the present electrode is well comparable to the previous reported values (7.60 × 10^{-6}, 7.02 × 10^{-5} cm^2 s^{-1}) at different modified electrodes[6,7]. Taking into consideration of the results obtained in Ep vs. ν and Ep vs. pH (vide supra) studies together, we could conclude that the electrochemical oxidation of 5-FU is a one-electron one-proton transfer process, and these results are in well agreement with the mechanism for the oxidation of 5-FU (Scheme 3.1)[7] proposed in previous reports.

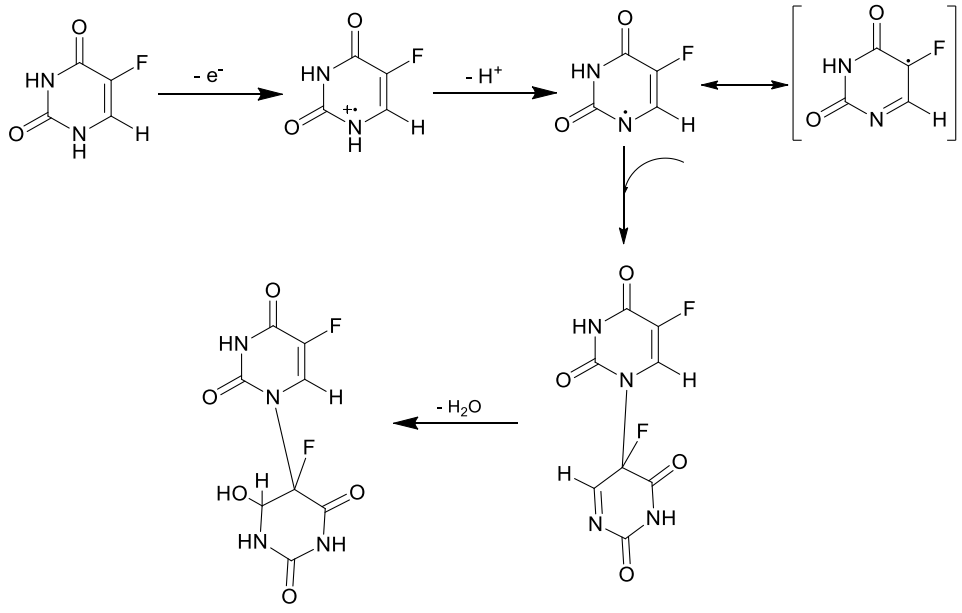

***Scheme 3.1**: Mechanism for electrochemical oxidation of 5-FU*

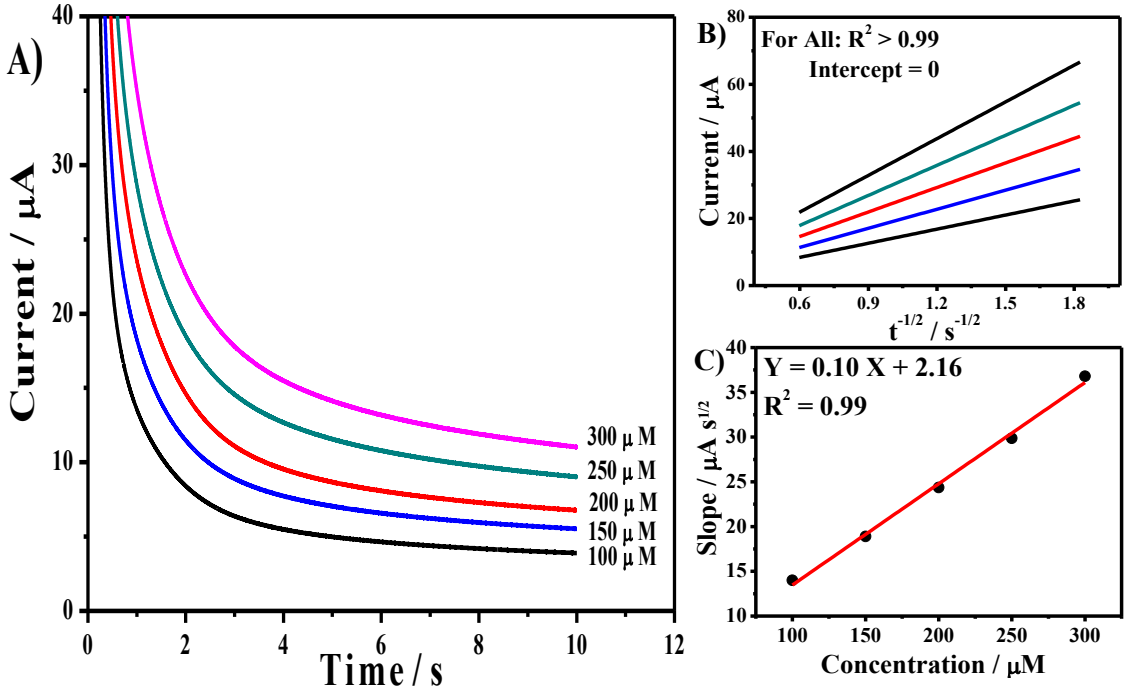

Fig. 3.7. *(A) CA plots of 5-FU in B-R buffer (pH 8.0) at different concentrations (100, 150, 200, 250, 300 µM) at GNP-MWCNT-Chit/GCE. (B) i vs. $t^{-1/2}$ plot and (C) plot of the slope of (i vs. $t^{-1/2}$) against the concentration of 5-FU.*

3.3.4. Electrochemical Impedance Spectroscopy (EIS)

Electrochemical impedance spectroscopy of the GNP nanocomposite electrode was examined to study the interfacial properties of the electrode and to examine the characteristics of the nanocomposite film. Charge transfer resistance (R_{ct}) determined here is an important characteristic of electron-transfer across the electrode interface. Electrochemical impedance spectra of bare GCE, MWCNT-Chit/GCE, GNP-MWCNT-Chit/GCE in aq. 1 mM $K_3[Fe(CN)_6]$ + 0.1 M KCl were examined at the open circuit potential over the frequency range of 100 kHz to 10 mHz. The open circuit potential was approximately equal to the redox potential of $K_3[Fe(CN)_6]$ at its respective electrode. The results were analyzed with various equivalent circuit models, and the observed results were found to best fit with Randles equivalent circuit. The resulting Nyquist and Bode plots are shown in Fig. 3.8. The Nyquist plot of bare GCE shows a semi-circular pattern followed by a linear plot, and the charge-transfer resistance (R_{ct}) for electron-transfer at bare GCE is determined to be 2.3 kohm. However, the Nyquist plots of both MWCNT-Chit/GCE and GNP-MWCNT-Chit/GCE (Fig. 3.8(A)) exhibit only a linear plot relevant to a mere diffusion behaviour alone, indicating the very good conductivity of the nanocomposite modified electrode with negligible charge transfer resistance. The Bode plots clearly show that the diffusion behaviour of redox species towards the GNP-

MWCNT-Chit/GCE was very high compared to MWCNT-Chit/GCE and that the active surface area was increased by decorating MWCNT with gold nanoparticles.

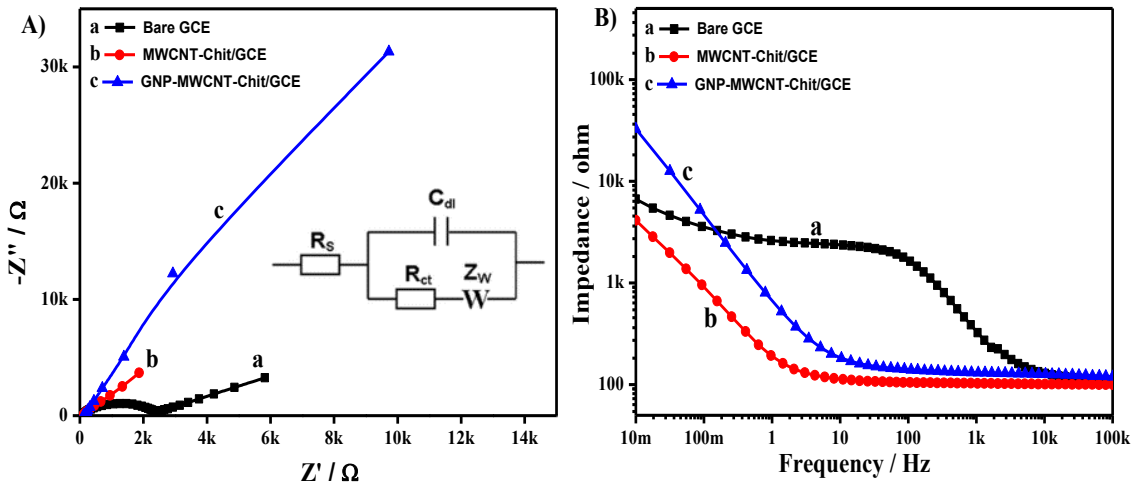

Fig. 3.8. *(A) Nyquist and (B) Bode plots of EIS analysis at bare GCE, MWCNT-Chit/GCE and GNP-MWCNT-Chit/GCE in aq. 1 mM $K_3[Fe(CN)_6]$ + 0.1 M KCl. Inset: Randles circuit.*

Both the cyclic voltammetry and EIS analysis results show that the GNP-MWCNT nanocomposite film provided a facile electron conduction pathway for catalyzed oxidation of 5-FU. That is to say, the GNP-MWCNT-Chit composite comprising long tubular conductive CNT coupled with gold nanoparticles and the fine dispersion of nanotubes in the chitosan matrix together made the electron transfer easier. The enhanced electron transfer could be ascribed to the nanolevel surface structural and morphological features of GNP and MWCNT, such as porous surface structure, continuous network of GNPs on MWCNT and excellent electrical conductivity of the GNP-MWCNT composite. The fabricated GNP-MWCNT-Chit/GCE is investigated for quantitative analysis of 5-FU.

3.3.5. Differential pulse voltammetry (DPV)

Differential pulse voltammetric analysis of 5-FU at the GNP nanocomposite electrode was carried out for quantitative analysis of 5-FU. Optimum experimental parameters for a good voltammetric profile with high peak current and minimal background current are established to be 100 mV pulse amplitude, 100 ms pulse width and 10 mV step increment. Differential pulse voltammograms of 5-FU at GNP-MWCNT-Chit/GCE electrode were recorded in B-R buffer (pH 8.0) over the concentration range of 0 – 10 µM 5-FU, and the results are shown in Fig. 3.9(A). A well-

defined anodic peak was observed at +0.95 V. The peak current increased gradually with the increase in the concentration of 5-FU. The DPV measurements were repeated four times with independent electrodes, and the peak current was plotted against the concentration of 5-FU. A linear plot with a regression coefficient of 0.99 was obtained, as shown in Fig. 3.9(B). Low-detection-limit of the sensor system is defined as the change in peak current by three relative standard deviations, and it is determined from the plot to be 20 nM. The linear determination range is 3×10^{-8} – 10×10^{-6} M. The performance of the GNP nanocomposite electrode were compared with those reported previously [1,2,4,6–8,27–30], as shown in Table 1. The low-detection-limit of our study is very much comparable with those reported by various electrochemical methods, different modified electrodes and chromatographic and other analytical methods (Table 3.1).

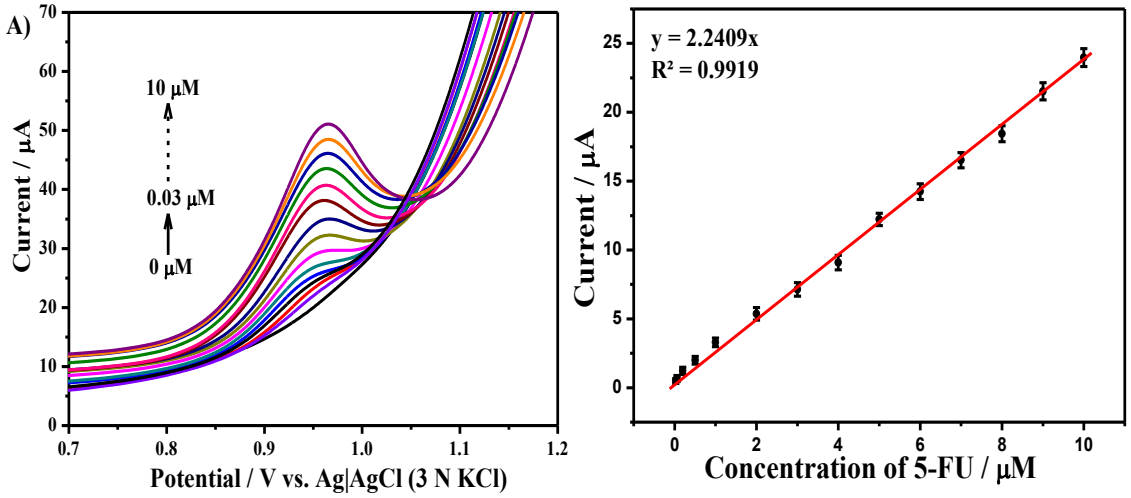

Fig. 3.9. *(A) DPVs of 5-FU in B-R buffer (pH 8.0) at different concentrations (0, 0.03, 0.06, 0.2, 0.5, 1, 2, 3, 4, 5, 6, 7, 8, 9, 10 µM) at GNP-MWCNT-Chit/GCE. (B) Plot of peak current against concentration of 5-FU.*

Table 3.1: Detection of 5-FU using electrochemical and various analytical methods

Method	Electrode	Linear range	Limit of detection	Reference
SWV	AuNP-SPE	0.2 – 50 μg mL^{-1}	0.1 μg mL^{-1}	S. Wang et al. (2012)
Potentiometry	Membrane electrode	1.3 – 130 μg mL^{-1}	10 μM	S.S. Hassan et al. (1998)
DPASV	MIP-fiber electrode	9.99–426.46 ng mL^{-1}	1.30 ng mL^{-1}	B.B. Prasad et al.(2012)
DPV	IL-CPE	0.5 μM – 800 μM	13 nM	W.Hou et al. (2011)
Cyclic voltammetry	MWNT/BTB/GCE	0.8 μM – 5 mM	0.26 μM	S. Guijun et al. (2013)
SWV	HMDE	10 pM – 90 pM	7.7 pM	V. Mirceski et al. (2000)
Vibrational Spectroscopy	n.a.	--	2 μg mL^{-1}	S. Farquharson et al.(2005)
Spectrophotometry	n.a.	30 – 100 μg mL^{-1}	0.5 μg mL^{-1}	M. M. Amer et al. (1997)
HPLC	n.a.	4–160 μg L^{-1}	4 μg L^{-1}	D. Chu et al. (2003)
HPLC	n.a.	0.2–40 μg mL^{-1}	0.6 ng mL^{-1}	W. Chen et al. (2012)
DPV	GNP-MWCNT-Chit/GCE	50 nM – 10 μM (6.5 ng mL^{-1} – 1.3 μg mL^{-1})	2×10^{-8} M (2.6 ng mL^{-1})	Present work

BTB – Bromothymol blue, SWV – Square-wave voltammetry, HMDE – Hanging mercury drop electrode, AuNP-SPE - Gold nanoparticle-modified screen-printed electrode, DPASV – Differential pulse adsorptive stripping voltammetry, HPLC – High performance liquid chromatography, n.a. – Not applicable.

3.3.6. *Interferences*

Electrochemical response of 5-FU in the presence of potentially electroactive biological compounds such as ascorbic acid (AA), uric acid (UA), dopamine (DA) and 5-hydroxytryptamine (5-HT) has been investigated at the GNP-MWCNT nanocomposite electrode by DPV method. Figure 3.10 shows the DPVs at the GNP-MWCNT nanocomposite electrode in the mixture of AA, UA, DA and 5-HT 5 µM each and different concentrations of 5-FU at micromolar concentration levels (2, 4, 6, 8 µM) in B-R buffer (pH 8.0). At the GNP-MWCNT-Chit/GCE, distinct peaks for AA, DA, 5-HT and 5-FU each were observed with a merged peak of UA (Fig. 3.10). The peak currents for 5-FU increased as the concentration of 5-FU increases in the presence of these interferences. Even higher concentrations of AA, DA, UA and 5-HT together could not affect the current response of 5-FU in B-R buffer. From the experimental results, it is clearly evident that the proposed electrochemical sensor can be used effectively for the detection of 5-FU even in the presence of various possible electroactive interferents.

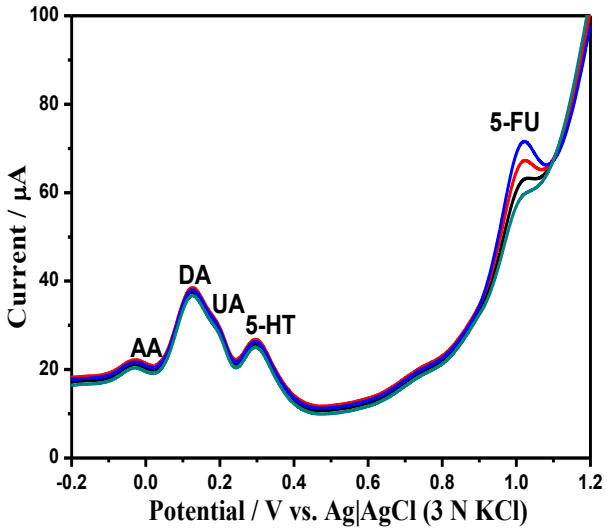

Fig. 3.10. *DPVs recorded at GNP-MWCNT-Chit/GCE with 5-FU at different concentrations (2.0, 4.0, 6.0, 8.0 µM) in the presence of AA, DA, UA and 5-HT 5 µM each in B-R buffer (pH 8.0).*

3.3.7. *Reproducibility and Reusability*

The stability, reusability and reproducibility of the GNP nanocomposite electrodes for the detection of 5-FU was investigated by DPV analysis. DPVs of 20 µM 5-FU were recorded at a single GNP-MWCNT-Chit/GCE electrode over a period of 7 days, while storing the modified electrode at ambient laboratory conditions. The peak currents of the recorded DPVs decreased merely by 3.8% in about 25 measurements, and

this observation clearly indicates the stability and reusability of the fabricated GNP nanocomposite electrode. Further, reproducibility of the modified electrode was examined by recording DPVs of 5-FU in multiple measurements with the use of six GNP-MWCNT-Chit/GCE electrodes fabricated independently. The peak currents of the DPVs of 20 µM 5-FU recorded at these electrodes varied to an extent of only 2.4%. It clearly reveals that the nanocomposite electrode is highly reproducible for the analysis of 5-FU. In overall, all the observations conclude that the reusability and reproducibility of the GNP nanocomposite electrode are quite satisfactory.

3.3.8. Determination of 5-FU in pharmaceutical and artificial urine samples

Pharmaceutical samples of 5-FU (Fluracil 250 mg/5 mL injection) were analyzed by using the fabricated nanocomposite sensor with the standard addition method. In Fig. 3.11, curves "a, b and c" show the DPVs of the analytical samples containing 0.5 µM of pure 5-FU together with different concentrations (0.5, 1 and 3 µM) of 5-FU of the pharmaceutical injection at the GNP-MWCNT-Chit/GCE. The experimental time for a DPV analysis is as low as 25 s. The recovery values obtained in these experiments varied from 98.3% to 102.6% (Table 3.2) and are quite satisfactory. Recovery of 5-FU from artificial urine was examined by the addition of 5-FU into undiluted artificial urine of pH 8.0 without any buffer. In Fig. 3.11, curves "d, e and f" show the DPVs of the GNP-MWCNT-Chit/GCE electrode recorded in the artificial urine sample in the presence of 1.0, 2.0 and 4.0 µM 5-FU. The recovery of 5-FU from undiluted artificial urine samples at different concentrations of 5-FU (1.0 - 4.0 µM) varied from 97.6% to 101.4% (Table 32). In physiological samples of clinical patients, the mean concentration of 5-FU varies over a wide concentration range of 0.106 – 3.77 µg mL^{-1} (0.82 – 29.2 µM) in serum samples [31,32] and as high as 10 – 60 µg mL^{-1} (77.4 – 464.2 µM) in urine samples [3,33]. The linear determination range of the developed sensor (0.03 – 10 µM) along with the very good recovery limits for physiological urine and pharmaceutical samples clearly confirms that the developed nanocomposite sensor would of biomedical interest.

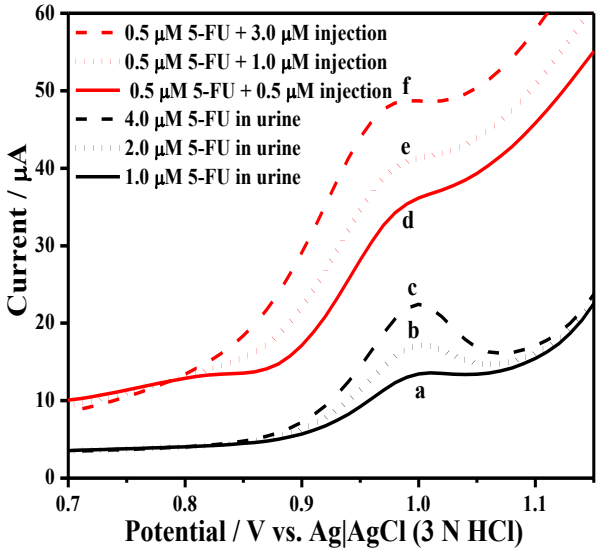

Fig. 3.11. *DPVs recorded at GNP-MWCNT-Chit/GCE in the presence of a mixture of 0.5 µM pure 5-FU and different concentrations of 5-FU (a = 0.5 µM, b = 1.0 µM and c = 3.0 µM) from pharmaceutical formulation in B–R buffer (pH 8.0) and in the presence of (d = 1.0, e = 2.0 and f = 4.0 µM) 5-FU in artificial urine.*

Table 3.2: Determination of 5-FU in pharmaceutical injection and in artificial urine samples using the GNP-MWCNT–Chit/GCE

Sample	5-FU ($\times 10^{-6}$ M)	Injection Added ($\times 10^{-6}$ M)	[a]Found ($\times 10^{-6}$ M)	Average Recovery (%)	[a]RSD (%)
Injection (Fluracil, 250 mg/5 ml)	1.0	1.0	2.06	102.6	1.8
	1.0	2.0	3.05	100.7	1.3
	1.0	3.0	3.96	98.3	1.4
Urine Sample	1.0	-	0.98	98.9	0.9
	2.0	-	1.98	97.6	0.7
	4.0	-	4.02	100.2	1.2

[a] Mean of six measurements

3.4. Conclusions

In this work, we synthesized chitosan biopolymer protected GNPs and decorated on the surface of MWCNT with an effective linkage between them. Further, a stable and efficient electrochemical biosensor based on GNP-MWCNT nanocomposite electrode was fabricated for sensitive determination of 5-FU by simple drop-cast method. The GNP-MWCNT nanocomposite film remarkably enhanced the current response and decreased the oxidation overpotential of 5-FU. In the GNP nanocomposite modified

electrode, both fine dispersion of MWCNT in the nanocomposite film and the continuous network of GNPs of finite size (~28.7 nm) on the CNT chain helped for a facile electron-transfer across the film and for a good electrocatalytic activity. The present electrochemical biosensor was efficient for the detection of ppb levels (ng mL^{-1}) of 5-FU despite the presence of potential electroactive interferents and had shown good recovery limits for direct determination from biological fluids and pharmaceutical formulations with the analysis time of as low as 25 s. The fabricated biosensor exhibited good stability, high sensitivity and simple fabrication procedure. All the advantages obtained with the present biosensor system confirm that the nanocomposite based biosensor coupling CNT, nanometallic particle and a green biopolymer chitosan could be explored and extended for selective determination of various pharmaceutical drugs.

3.5. References

[1] S. Farquharson, A. D. Gift, C. Shende, P. Maksymiuk, F. E. Inscore, J. Murran, in *Vib. Spectrosc.*, **2005**, pp. 79–84.

[2] M. M. Amer, S. S. Hassan, S. A. Abd El-Fatah, A. M. El-Kosasy, *J. Pharm. Pharmacol.* **1998**, *50*, 133–138.

[3] M. Barberi-Heyob, J. L. Merlin, B. Weber, *J. Chromatogr. B Biomed. Sci. Appl.* **1992**, *581*, 281–286.

[4] D. Chu, J. Gu, W. Liu, J. P. Fawcett, Q. Dong, *J. Chromatogr. B Anal. Technol. Biomed. Life Sci.* **2003**, *795*, 377–382.

[5] A. Procházková, S. Liu, H. Friess, S. Aebi, W. Thormann, *J. Chromatogr. A* **2001**, *916*, 215–224.

[6] X. Hua, X. Hou, X. Gong, G. Shen, *Anal. Methods* **2013**, *5*, 2470.

[7] T. Zhan, L. Cao, W. Sun, W. Hou, *Anal. Methods* **2011**, *3*, 2651.

[8] V. Mirčeski, R. Gulaboski, B. Jordanoski, Š. Komorsky-Lovrić, *J. Electroanal. Chem.* **2000**, *490*, 37–47.

[9] G. A. Rivas, M. D. Rubianes, M. C. Rodríguez, N. F. Ferreyra, G. L. Luque, M. L. Pedano, S. A. Miscoria, C. Parrado, *Talanta* **2007**, *74*, 291–307.

[10] L. Agüí, P. Yáñez-Sedeño, J. M. Pingarrón, *Anal. Chim. Acta* **2008**, *622*, 11–47.

[11] M. E. Ghica, R. Pauliukaite, O. Fatibello-Filho, C. M. A. Brett, *Sensors Actuators B Chem.* **2009**, *142*, 308–315.

[12] S. Murugesan, K. Myers, V. Ravi Subramanian, *Appl. Catal. B Environ.* **2011**, *103*, 266–274.

[13] R. K. Gupta, M. P. Srinivasan, R. Dharmarajan, *Mater. Lett.* **2012**, *67*, 315–319.

[14] S. S. Nair, S. A. John, T. Sagara, *Electrochim. Acta* **2009**, *54*, 6837–6843.

[15] P. Kannan, S. A. John, *Electrochim. Acta* **2011**, *56*, 7029–7037.

[16] M. Satyanarayana, K. K. Reddy, K. V. Gobi, *Anal. Methods* **2014**, *6*, 3772–3778.

[17] T. Brooks, C. W. Keevil, *Lett. Appl. Microbiol.* **1997**, *24*, 203–206.

[18] C. Gouveia-Caridade, R. Pauliukaite, C. M. A. Brett, *Electrochim. Acta* **2008**, *53*, 6732–6739.

[19] H. Huang, X. Yang, *Biomacromolecules* **2004**, *5*, 2340–2346.

[20] N. R. Jana, L. Gearheart, C. J. Murphy, *Langmuir* **2001**, *17*, 6782–6786.

[21] D. Ghosh, *Opt. Photonics J.* **2013**, *03*, 18–26.

[22] H. Sharma, D. C. Agarwal, a. K. Shukla, D. K. Avasthi, V. D. Vankar, *J. Raman Spectrosc.* **2013**, *44*, 12–20.

[23] D. N. Travessa, F. S. da Silva, F. H. Cristovan, A. M. Jorge Jr., K. R. Cardoso, *Mater. Res.* **2014**, *17*, 687–693.

[24] S. Hrapovic, E. Majid, Y. Liu, K. Male, J. H. T. Luong, *Anal. Chem.* **2006**, *78*, 5504–12.

[25] E. Laviron, *J. Electroanal. Chem.* **1979**, *101*, 19–28.

[26] A. J. Bard, L. R. Faulkner, *Electrochemical Methods: Fundamentals and Applications, 2nd Ed.*, John Wiley & Sons, New York, **2001**.

[27] W. Chen, Y. Shen, H. Rong, L. Lei, S. Guo, *J. Pharm. Biomed. Anal.* **2012**, *59*, 179–183.

[28] B. B. Prasad, D. Kumar, R. Madhuri, M. P. Tiwari, *Electrochim. Acta* **2012**, *71*, 106–115.

[29] S. S. Hassan, M. M. Amer, S. A. Abd El-Fatah, A. M. El-Kosasy, *Anal. Chim. Acta* **1998**, *363*, 81–87.

[30] S. Wang, S. Fu, H. Ding, *Sens. Lett.* **2012**, *10*, 974–978.

[31] G. Bocci, R. Danesi, A. Di Paolo, F. Innocenti, G. Allegrini, A. Falcone, A. Melosi, M. Battistoni, G. Barsanti, P. F. Conte, et al., *Clin. Cancer Res.* **2000**, *6*, 3032–3037.

[32] T. Yoshida, E. Araki, M. Iigo, T. Fujiil, M. Yoshino, Y. Shimadal, D. Saitol, H. Tajiril, H. Yamaguchp, S. Yoshida, et al., *cancer Chemother Pharmacol* **1990**, *26*, 352–354.

[33] W. E. Hull, E. Port, R. Herrmann, W. Kunz, *Cancer Res.* **1988**, *48*, 1680–1688

CHAPTER 4

Silver Nanoparticles Impregnated Chitosan Layered Carbon Nanotubes as a Sensor Interface for Sensitive Detection of Clopidogrel *in-vitro*

4.1. Introduction

In the last decades, a lot of research work has been carried out to incorporate a variety of nanomaterial into sensing layers with unique properties for biosensors to fabricate novel analytical tools. The development of sensing layers in order to detect trace amounts of chemical, biochemical and biological analytes selectively and sensitively have attracted a great interest. Intense research has been developed for the use of biosensors in a wide range of application fields like food industry, environmental monitoring, biotechnology, pharmaceutical chemistry and clinical diagnostics [1–3].

Among various nano structured materials, carbon nanotubes (CNTs) have been recognized as an important material in recent years in various fields due to their unique electrical, mechanical and structural properties. Their use as electrode modifiers can lead to a decrease of the overpotential, a decrease in the response time, enhanced electrocatalytic activity and an increase in available active surface area in comparison with conventional carbon electrodes[4,5]. The electrocatalytic effect of CNTs has been attributed to the activity of edge-plane-like graphite sites at the CNT ends and it would be further increased by functionalization of CNTs and making composites with other electrocatalytic materials such as metal/metal oxide nanoparticles, conducting polymers, and redox mediators [6–9]. CNTs also reduce the electrode fouling which can greatly improve the reuse of such sensors [10–12].

In this research work, we aimed to develop CNT based hybrid nanocomposites by coupling with silver nanoparticles (SNPs) to obtain improved active surface area and amplified flow of electrons across the interface. Our interest on silver nanoparticles for the reason that they demonstrate high catalytic activity for both oxidation and reduction reactions [13]. Moreover, the preparation of SNPs is very inexpensive compare to that of Au and Pt nanoparticles because the precursor for SNPs (silver nitrate or silver acetate) is cheaper than gold and platinum precursors. But, by simply mixing these materials it cannot simply be possible to develop a highly electrochemically active hybrid material. The high performance of these combinations possible only when the SNPs formed on the surface of CNTs by making a strong linkage between CNT and SNPs that can enhance the electron flow with a faster rate. On the other hand, it is necessary to develop simple and effective synthesis route to produce stable SNPs which is protected from aggregation and of homogenous size. In this context, there are various schemes developed for the

stabilization of nanoparticles such as polymer coatings, some surfactant stabilizers, and polymer agents capping [14–19].

Another interesting material, chitosan (chit) is a linear, β-1,4-linked polysaccharide (similar to cellulose) obtained by the partial deacetylation of chitin and provides the above requirements to make an active linkage between the SNP and MWCNT. Along with our requirements, chitosan possesses many other advantages, such as excellent strong film forming ability but has high permeability towards water and biocompatible. It shows good adhesion and high mechanical strength which makes the sensor highly stable and reusable for multiple analysis. In chitosan, the amine groups are responsible to well accommodate the SNPs which make nanoparticles stable and free from aggregation and also facilitate the interactions between MWCNT and SNP.

In the present work, we have tried to develop a highly sensitive and selective SNP embedded chitosan and MWCNT hybrid composite based sensor for important anti-platelet drug, clopidogrel. Clopidogrel (methyl (+)-(*S*)-*α*-(*o*-chlorophenyl)-6,7-dihydrothieno-[3,2-*c*]pyridine-5(4*H*)-acetate) antiplatelet agent used to blood clots in coronary artery disease, peripheral vascular disease and cerebrovascular disease. It is closely related to ticlopidine and appears to have a slightly more favourable toxicity profile with less frequent thrombocytopenia and leukopenia, although TTP (thrombotic thrombocytopenic purpura) has been reported. Considering all these factors, determination of clopidogrel concentration levels in body fluids as well as in pharmaceutical formulations is very important in quality control and in clinical diagnosis.

4.2. Experimental

4.2.1. Chemicals and materials

Clopidogrel bisulphate (CLP), ascorbic acid, uric acid, dopamine and serotonin were purchased from Tokyo chemical industry, Japan. Chitosan of low molecular weight range (from crab shells, 60 – 120 kDa, minimum 85% deacetylation) and silver nitrate were obtained from Sigma Aldrich, USA. MWCNTs (95%, 20–50 nm OD and 2–5 µm length) was purchased from Sisco research laboratories, India. All other chemicals were of analytical grade (>99.5 % purity) and were used without further purification. Britton-Robinson buffer (B-R buffer) was prepared using a mixture of 0.04 M CH_3COOH, 0.04 M H_3BO_3 and 0.04 M H_3PO_4. To dissolve clopidogrel bisulphate, initially the buffer solution was added with 5 ml of methanol for 100 ml of B-R buffer. The desired solution

pH was obtained by adding 0.1 M NaOH. Artificial urine solution was prepared according to the procedure provided by Brooks and Keevil [20] (Chapter 2).

4.2.2. Synthesis of AgChit-CNT nanocomposite

AgChit nanocomposite was prepared by adopting a recipe reported previously [21] with a major change and in the presence of MWCNT. 1 wt% of chitosan solution was first prepared by dissolving chitosan powder in aq. 1.0% (v/v) acetic acid solution. MWCNTs are at first treated with 3 M aqueous nitric acid to remove the impurities and to functionalize the MWCNTs with carboxylic groups. Then 5 mg of this fuctionalized MWCNTs was added into 10 mL of the above chitosan solution and ultrasonicated until homogeneous black suspension obtained. Then, 4 mL of aq. 10 mM $AgNO_3$ solution was added to the resultant CNTs–chitosan mixture and stirred for 30 min. Then 2 ml of 10 mM freshly prepared $NaBH_4$ was added quickly to the above mixture, consequently then a pale green coloured silver nano particles can be observed in the black suspension whereas yellow coloured nanoparticle were observed in the absence of MWCNT. The resulting mixture was kept stirring for another 90 min. The chitosan forms a strong linkage with the $–COO^-$ groups of functionalized MWCNT through the amine groups of chitosan and the SNPs are embedded in the matrix of chitosan. Consequently, the SNPs strongly implanted into the chitosan are bonded with MWCNTs and the AgChit-CNT hybrid composite was centrifuged and collected from the above mixture leaving the SNPs which are not embedded in the chitosan composite in the supernatant. The AgChit-CNT composite was kept in a refrigerator at 4 ºC in the dark for a week before use.

4.2.3. Fabrication of electrode systems

At first, GCE (3 mm diameter) was polished with alumina slurry (down to 0.04 µm), and then washed thoroughly with double distilled water, then sonicated in 1:1 aq. HNO_3, ethanol and double distilled water consecutively and finally dried at room temperature. A solution of chitosan (1 % w/v) was prepared by dissolving 1 g of chitosan powder in 100 mL aq. acetic acid (1% v/v) solution and sonicated for 30 min. A 3 mg of AgChit-CNT nanocomposite was added to 1 mL chitosan solution and sonicated for 1 h. Then, 10 µL of the resulting homogeneous suspension of the nanocomposite was cast on the surface of cleaned GCE and dried for 24 – 30 h at room temperature and the resulting electrode was denoted as AgChit-CNT/GCE. Similarly, CNT alone dispersed in chitosan solution (1% v/v) was used, and resulting electrode was denoted as CNT/GCE.

4.2.4. Characterization

UV-Visible spectra were recorded on Perkin Elmer100 UV-Visible spectrophotometer. Raman spectra of the prepared nanocomposites were recorded using a HR800 LabRAM confocal Raman spectrometer operating at 20 mW laser power using a peltier cooled CCD detector. The spectra were collected using a He–Ne laser source having an excitation wavelength of 633 nm and with an acquisition time of 10 s using a 5× objective. The Raman spectral data were acquired in a mixture of acetonitrile and water (4:1 v/v) using a quartz cuvette. Powder X-ray diffraction (XRD) patterns of the samples were recorded in 2θ range of 10°–90° on a Brucker AXS D8 diffractometer, and Cu was used as the target (k = 1.5406 Å) with a step size of 0.002º and a scan speed of 0.5 second per step. Morphological studies of the samples were carried out on a FEI Quanta 200F scanning electron microscope equipped with energy-dispersive X-ray analyser (EDX) operating at 10 - 20 kV. For the FESEM-EDX analysis, the samples were smeared on a conducting carbon tape and samples were coated with a thin layer of gold by sputtering method to avoid charging during analysis.

4.2.5. Electrochemical analysis

Cyclic voltammetry, chronoamperometry, differential pulse voltammetry and i-t curve measurements were carried out using CHI 6132e electrochemical analyser (CH Instruments, USA), and electrochemical impedance measurements were carried out using Zahner-elektrik workstation (Model IM6e, GmbH, Germany) equipped with Thales 3.08 USB software. All the electrochemical measurements were performed in a conventional electrochemical cell of 20 mL with bare or modified GCE as working electrode, Pt spiral wire as auxiliary electrode and Ag|AgCl (3 N KCl) electrode as reference. All the potentials were referred against Ag|AgCl (3 N KCl) electrode throughout the manuscript. Electrochemical experiments were carried out in B-R buffer at room temperature, and the experimental solution was purged with nitrogen gas for 10 min prior to the start of the experiment to de-aerate the solution.

4.3. Results and Discussion

4.3.1. Characterization of AgChit-CNT composite

Colloidal nanoparticles are initially examined by UV–visible spectroscopic analysis to know the basic confirmation of nanoparticles formation and its size range. In the present study SNP colloidal solution in the presence of MWCNT is in greenish

colour and the absorption maxima (λ_{max}) is about ~396 nm whereas in the absence of MWCNT it is in yellowish colour with the λ_{max} about ~408 nm (Fig. 4.1). From UV–visible spectroscopic studies, it is inferred that the presence of MWCNTs decreased the particle size of SNPs and it is in the range of 30–40 nm diameters[22].

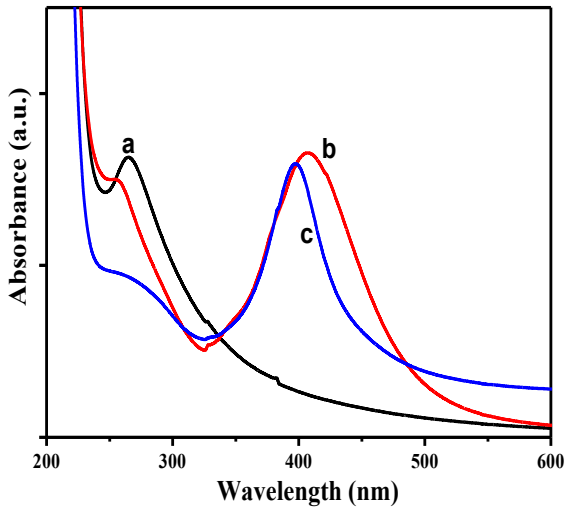

Fig. 4.1. *UV-Visible spectra of aq. $AgNO_3$ (a), silver colloid prepared in chitosan in the absence (b) and presence (c) of MWCNT.*

XRD was used to further confirm the presence of silver nanoparticles in AgChit-CNT composite. The powder XRD patterns of CNT and AgChit-CNT are shown in Fig. 4.2. XRD pattern of AgChit-CNT has all Bragg's reflections due to crystalline silver, which were observed at 38.2°, 44.4°, 64.6°, 77.5° and 81.8° representing (1 1 1), (2 0 0), (2 2 0), (3 1 1) and (2 2 2) planes of face centred cubic crystalline silver nanoparticles (JCPDS No. 04-0783). The SNP size was calculated using Scherrer formula, and the average crystalline size determined from the calculation is about 35.6 nm.

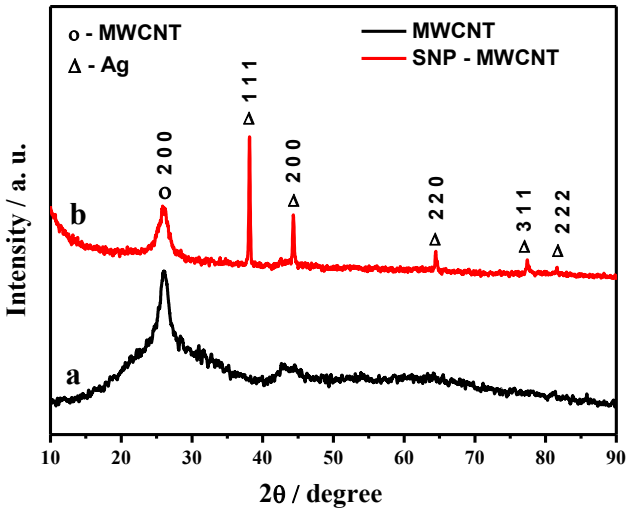

Fig. 4.2*. XRD spectra of MWCNT and AgChit-CNT composite.*

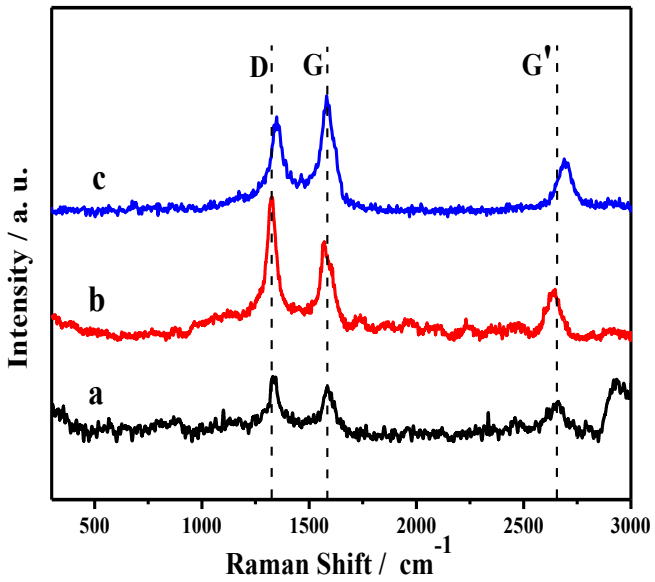

Fig. 4.3. *Raman spectra of pristine MWCNT (a), functionalized MWCNT (b) and AgChit-CNT (c).*

Structural changes caused by functionalization of the hybrid composite with AgChit can be observed by changes in Raman spectroscopy bands. Figure 4.3 shows the obtained spectra from pristine CNT, functionalized-CNT and AgChit-CNT, where all the three samples are exhibiting D-band (~ 1,330 cm^{-1}) related to structural disorders of carbon based materials, G-band (~1,580 cm^{-1}) related to graphitized carbon and G^{l}-band (~ 2,660 cm^{-1}) is the first overtone of the D mode peaks. The I_D/I_G ratio is an indication of the quantitative measure of structural defects. Functionalization of pristine CNTs was confirmed by the peak intensity ratios of D-band and G-band (I_D/I_G), where we could observe a remarkable increase in I_D/I_G values from pristine (1.18) to functionalized CNT (1.46). Further, the SNPs decoration on functionalized-CNTs was confirmed by the peak shift of D and G^{l} bands. The Raman shift of D band for AgChit-CNT composite is at 1348 cm^{-1} and it is higher than the D band of functionalized CNT (1325 cm^{-1}) which indicates the formation of AgChit layer over the surface of functionalized CNTs.

Surface morphological studies of CNT and AgChit-CNT nanocomposite has been examined by Field emission scanning electron microscope (FESEM). Figure 4.4 (A & B) shows FESEM images of plain CNT and AgChit-CNT nanocomposite respectively. Figure 4.4(B) clearly illustrates that the SNPs which have been embedded in the chitosan are well-distributed along the surface of CNTs and have formed a good network on CNTs, which could promote a facile electron transfer. Figure 4.4(B) also shows that the

AgChit-CNT film is of porous nature with large surface area, and thus it could enhance the electrodic current of the nanocomposite electrode.

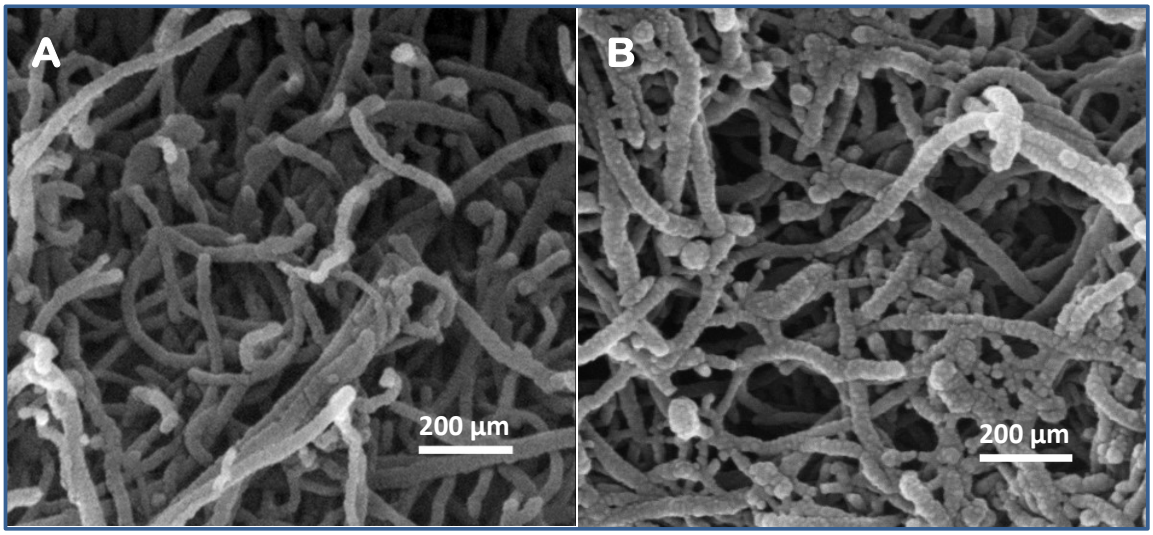

Fig. 4.4. *FESEM image of (A) MWCNT and (B) AgChit-CNT.*

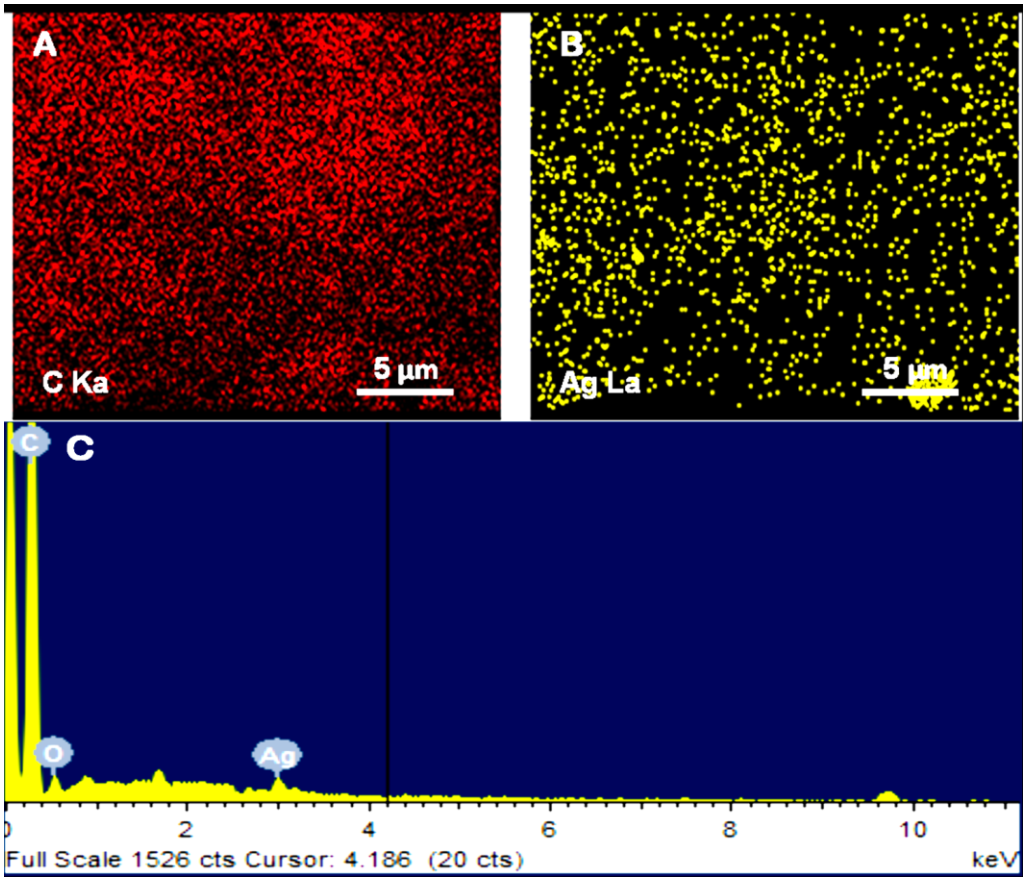

Fig. 4.5. *EDX elemental mapping of (A) carbon and (B) silver in AgChit-CNT composite. (C) Elemental composition of the AgChit-CNT composite from EDX analysis.*

The chemical composition of the AgChit-CNT was determined using EDX measurements. As shown in Fig. 4.5, EDX elemental mapping clearly reveals that the Ag

element is evenly distributed throughout the AgChit-CNT matrix. The elemental composition of the AgChit-CNT composite obtained from EDX analysis is shown in Fig. 4.5 and it indicated the presence of C, O, and Ag as the major elemental components with the weight percentage of 91.29%, 5.11%, and 3.60%, respectively, over the entire region of the prepared sample.

4.3.2. Electroactive surface areas of modified electrodes

Initially, the electroactive surface areas of the modified and bare GCE were determined by cyclic voltammetry. Here, aq.2 mM $K_3[Fe(CN)_6]$ in 0.1 M KCl was taken as a probe to measure the active surface area of bare GCE, CNT/GCE and AgChit-CNT/GCE electrodes, and CVs of $K_3[Fe(CN)_6]$ were recorded with these electrodes at different scan rates. The CVs of $K_3[Fe(CN)_6]$ at bare GCE, CNT/GCE and AgChit-CNT/GCE electrodes at 100 mV s^{-1} and the plot of peak currents against the square root scan rate are shown in Fig. 4.6. The peak currents observed at the modified electrodes were higher than that of bare GCE. The results were analyzed, and the effective surface area of the modified electrodes was determined by applying the Randles-Sevcik equation and by considering the diffusion coefficient of $K_3[Fe(CN)_6]$ as 6.7×10^{-6} cm^2 s^{-1}, according to the procedure recorded elsewhere [23]. The effective surface area of bare GCE is 0.074 cm^2, which is nearly equal to the geometrical surface area of a 3 mm diameter electrode. The electroactive surface areas of CNT/GCE and AgChit-CNT/GCE are calculated to be 0.26 and 0.48 cm^2, respectively, and the active surface areas of the modified electrodes are a few times higher than of bare GCE.

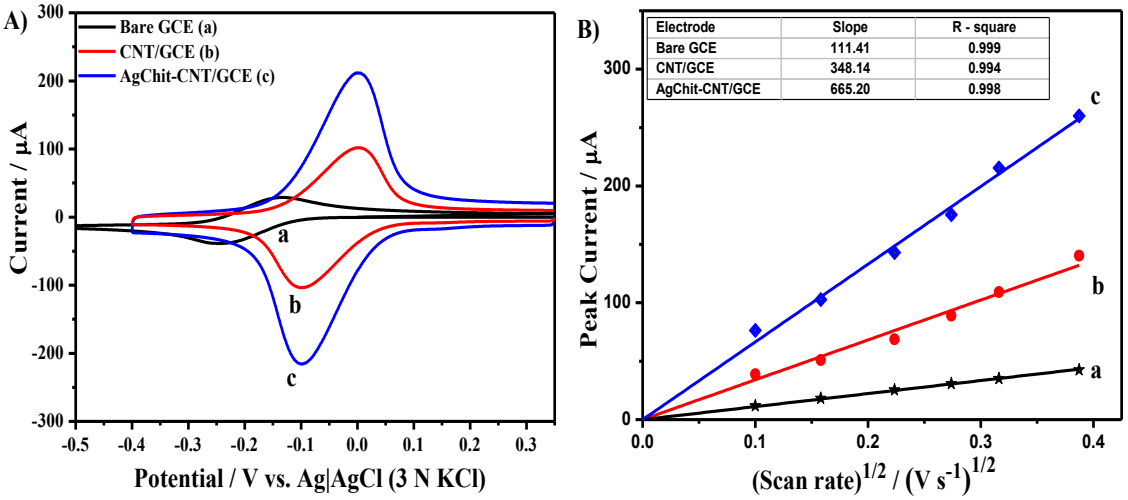

Fig. 4.6. *(A). CVs of $K_3[Fe(CN)_6]$ recorded at bare GCE (a), CNT/GCE (b) and AgChit-CNT/GCE in aq. 2 mM $K_3[Fe(CN)_6]$ + 0.1 KCl; potential scan rate = 100 mV s^{-1}. (B) Plot of the anodic peak current against the square root of scan rate.*

4.3.3. *Electrocatalytic oxidation of Clopidogrel*

Cyclic voltammograms (CVs) obtained for the oxidation of CLP at bare GCE, CNT/GCE, and AgChit-CNT/GCE in B-R buffer are shown in Fig. 4.7(A). Clopidogrel exhibits an irreversible CV with an anodic peak at bare GCE, CNT/GCE and AgChit-CNT/GCE and no peaks was observed in the reverse scan. The anodic peak current of CLP at AgChit-CNT/GCE is about 4 folds higher than that at CNT/GCE and is nearly 10 folds higher than that of bare GCE. These phenomena are clear evidences for enhanced electrochemical behaviour of the AgChit-CNT nanocomposite towards CLP oxidation. These results inferred that the silver nanoparticles embedded nanocomposite film might be forming a highly constructive electric network on the electrode surface and accelerating the electron flow through it.

The amount of silver nanoparticles in the nanocomposite film of AgChit-CNT is optimized by preparing the AgChit-CNT nanocomposite with different amounts of silver precursor (1 – 5 ml of 10 mM $AgNO_3$) during the synthesis, and the respective nanocomposites were examined by cyclic voltammetric analysis in the presence of 0.5 mM CLP (Fig. 4.7(B)). The peak current of nanocomposite prepared with 4 ml of $AgNO_3$ is the highest compared to that of all other composites. So, the sensor system fabricated by using a AgChit-CNT nanocomposite prepared with 4 ml of silver precursor has been considered for the analysis of CLP here after.

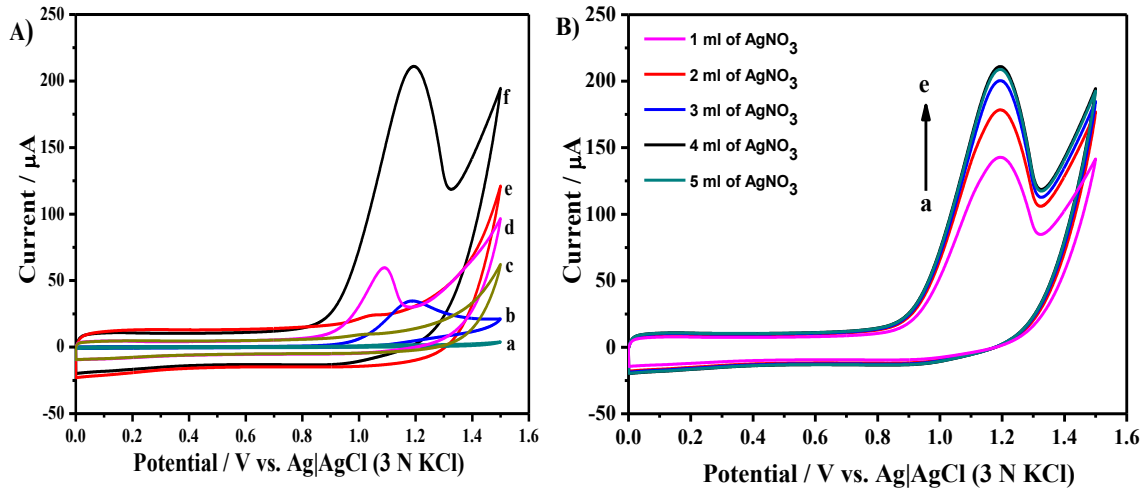

Fig. 4.7. *(A) CVs of 0.5 mM CLP in B-R buffer (pH 3.5) at bare GCE (a, b), CNT/GCE (c, d) and AgChit-CNT/GCE (e, f). (B) AgChit-CNT nanocomposite modified GCE prepared with different amounts of $AgNO_3$ precursor (a=1, b=2, c=3, d=4, e=5 ml of 10 mM $AgNO_3$). Scan rate = 100 mV s^{-1}.*

The effect of pH on the electrochemical response of 0.5 mM CLP at AgChit-CNT/GCE was investigated in B-R buffer solution of different pH (pH 1.8 to 5.0) by cyclic voltammetry (Fig. 4.8(A)). The buffer solution pH is obviously influencing the oxidation peak of clopidogrel and it is observed that the oxidation peak current is maximum at pH 3.5 (Fig. 4.8(B)). Hence, the B-R buffer of pH 3.5 has been chosen for all further investigations. Moreover, the pH of the buffer shows a linear relationship with the oxidation potential of CLP at AgChit-CNT/GCE (Fig. 4.8(C)), and the slope obtained is about 54 mV which infers that the number of protons involved in the oxidation of CLP is equal to the number of electrons.

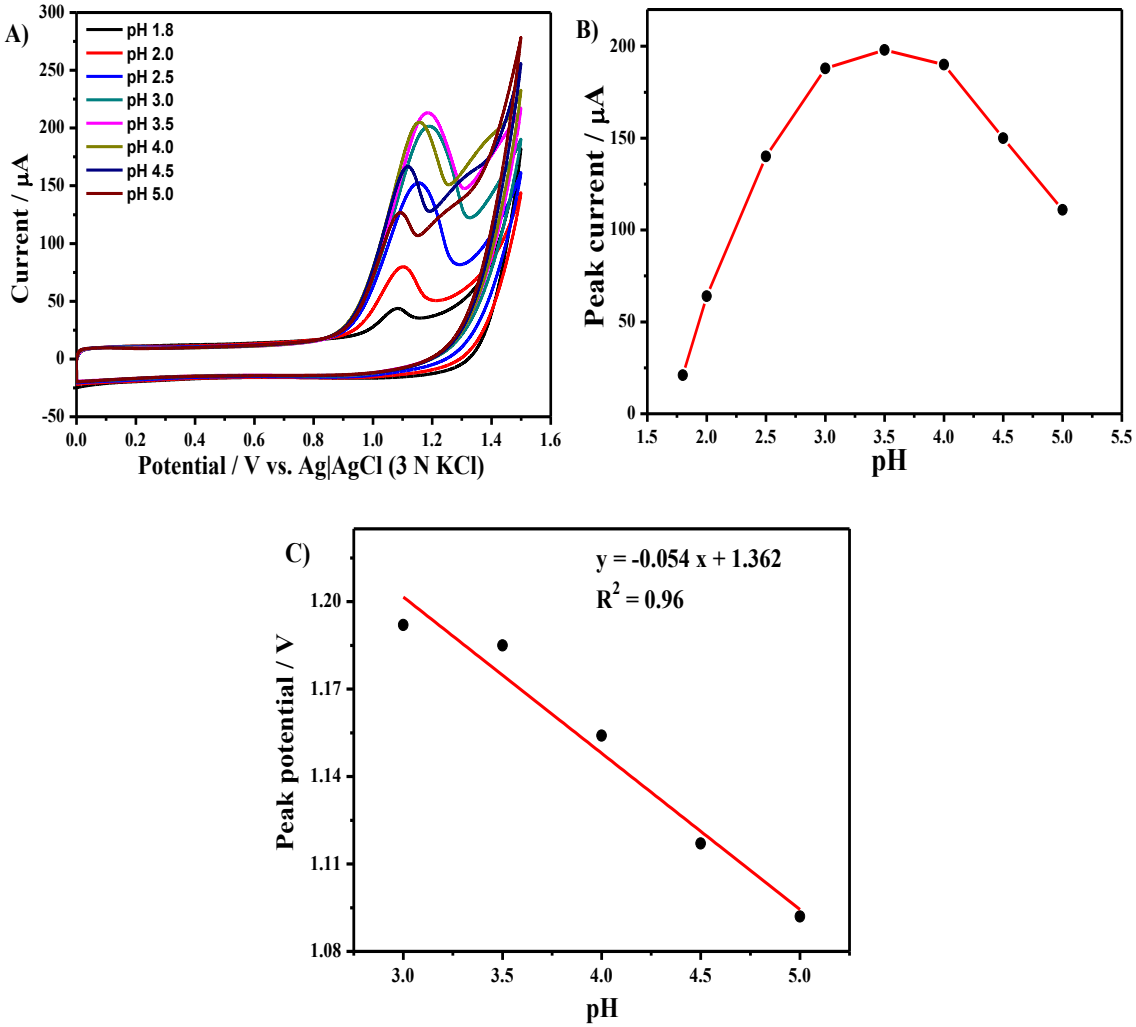

Fig. 4.8. *(A) CVs of 0.5 mM CLP in B-R buffer of different pH values (1.8 – 5.0) at AgChit-CNT/GCE. (B) Plot of peak current against pH. (C) Plot of peak potential against pH.*

The influence of scan rate on the electrochemical response of 0.5 mM CLP at AgChit-CNT/GCE was investigated by cyclic voltammetry, and the respective results

are shown in Fig. 4.9(A). The oxidation peak currents gradually increase with increasing scan rate, and the peak current is linearly proportional to the square root of scan rate in the range of 20 to 250 mV s^{-1} (Fig. 4.9(B)). This behaviour infers that the electrochemical oxidation of CLP at the AgChit-CNT nanocomposite modified electrode is diffusion controlled process.

For an irreversible electrochemical reaction, the relationship between the peak potential Ep and the scan rate ν is as expressed in Laviron equation [24] (Chapter 2, Eq. 2.2). According to that equation, the nα value can be determined from the slope of Ep vs. ln(ν) plot (Fig. 4.9(C)), and heterogeneous electron-transfer rate constant, k°, can be calculated from the intercept of the plot if the value of E° is known. The value of E° can be obtained from the intercept of the Ep vs. ν plot (Fig. 4.9(D)) by extrapolation to the vertical axis at ν = 0 and is 1.08 V. From the slope of the Ep vs. ln(ν) plot, αn was calculated to be 0.56. Generally, α can be assumed to be 0.5 for an irreversible electrode process. So the electron transfer number (n) for the electrochemical oxidation of CLP becomes 1, and the k° value is determined from the intercept to be 0.71 s^{-1}. Considering the results of Ep vs. pH studies together, we could conclude that the electrochemical oxidation of CLP is a one-electron one-proton transfer process

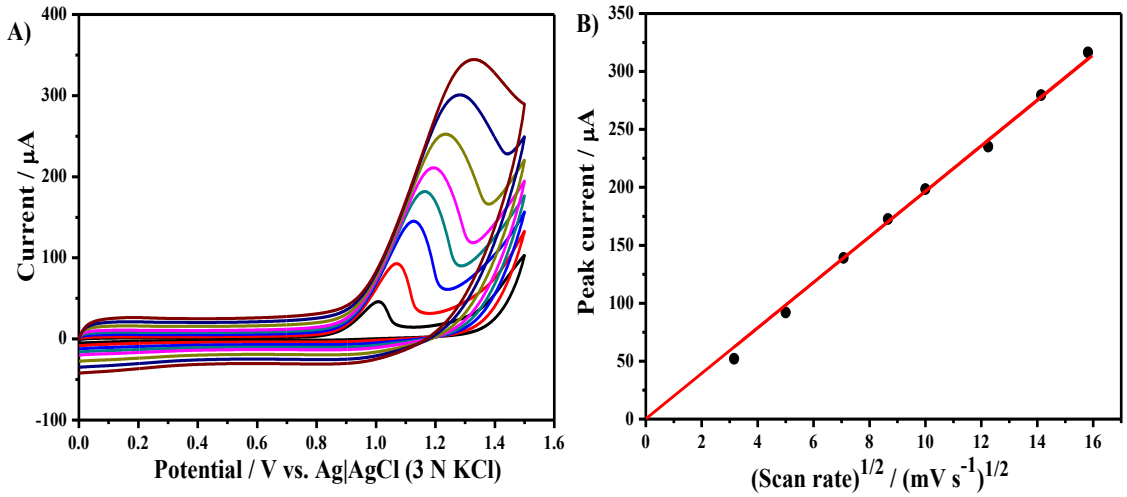

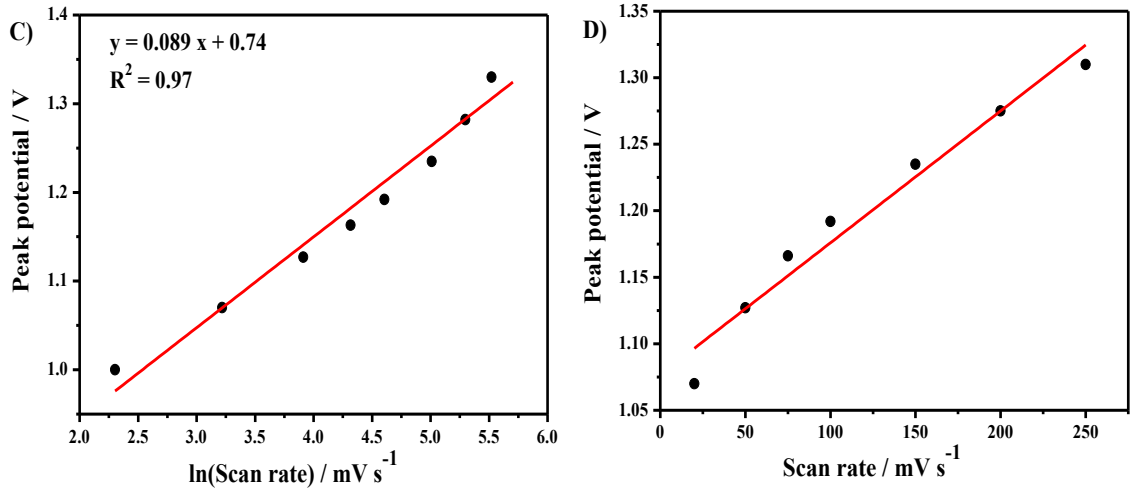

Fig. 4.9. (A) CVs of 0.5 mM CLP in B-R buffer (pH 3.5) at AgChit-CNT/GCE with different scan rates (10, 25, 50, 75, 100, 150, 200, 250 mV s^{-1}). Plots of the peak current against square root of scan rate (B), the peak potential against ln(scan rate) (C) and the peak potential against the scan rate (D).

Diffusion coefficient of CLP for the electrochemical oxidation at AgChit-CNT/GCE is determined using chronoamperometry (Figure 4.10) by adopting the Cottrell's equation[25] (See Chapter 2, Eq. 2.3), and its value is determined to be 6.12 × 10^{-6} cm^2 s^{-1}.

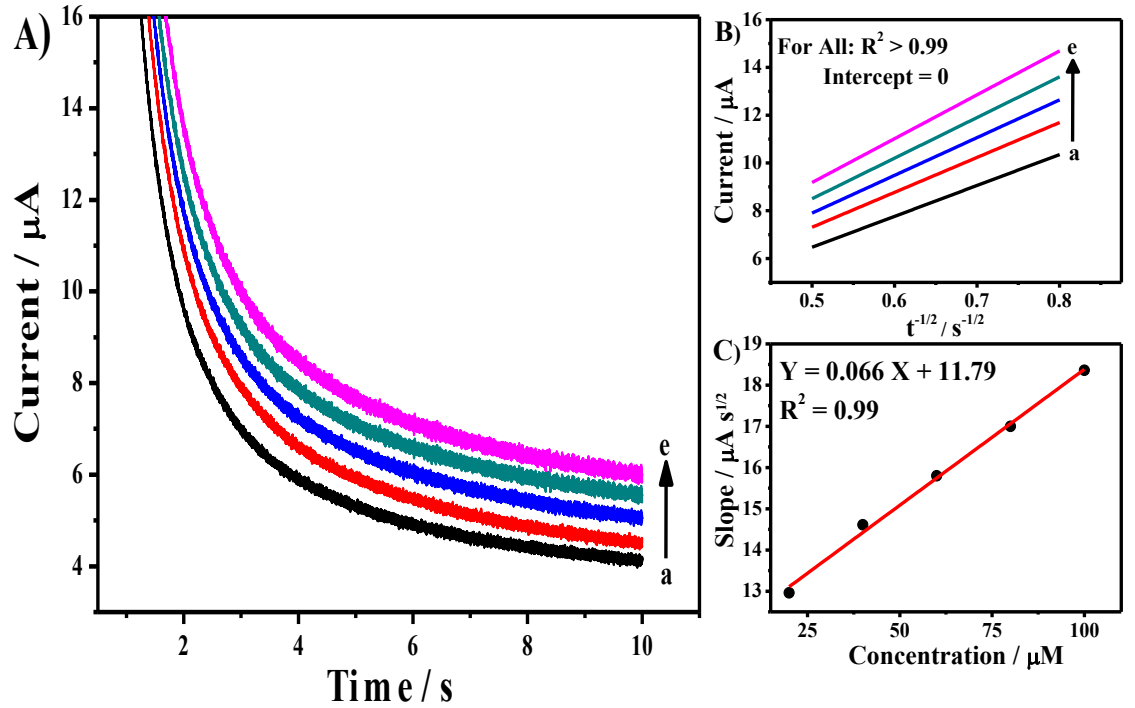

Fig. 4.10. *(A) CA plots of CLP at different concentrations (a=20, b=40, c=60, d=80, e=100 µM) in B-R buffer (pH 3.5) at AgChit-CNT/GCE. (B) i vs. $t^{-1/2}$ plot and (C) plot of the slope of (i vs. $t^{-1/2}$) against the concentration of CLP.*

4.3.4. Electrochemical impedance spectroscopy (EIS)

Electrochemical impedance spectra of bare GCE, CNT/GCE, AgChit-CNT/GCE in aq. 1 mM $K_3[Fe(CN)_6]$ + 0.1 M KCl were examined at the open circuit potential over the frequency range of 100 kHz to 10 mHz. The resulting Nyquist and Bode plots are shown in Fig. 4.11. The obtained data were analyzed with various equivalent circuit models, and the observed results were found to best fit with Randles equivalent circuit (Fig. 4.11). The Nyquist plot of bare GCE shows a semi-circular pattern followed by a linear plot, and the charge-transfer resistance (R_{ct}) for electron-transfer at bare GCE is determined to be 2.3 kohm. However, the Nyquist plots of both CNT/GCE and AgChit-CNT/GCE (Fig. 4.11(A)) exhibit only a linear plot relevant to a mere diffusion behaviour alone, indicating the very good conductivity of the nanocomposite modified electrode with negligible charge transfer resistance. The Bode plots (Fig. 4.11(B)) clearly show that the diffusion behaviour of redox species towards the AgChit-CNT/GCE was higher compared to CNT/GCE and that the active surface area was increased by making composite with SNP embedded chitosan.

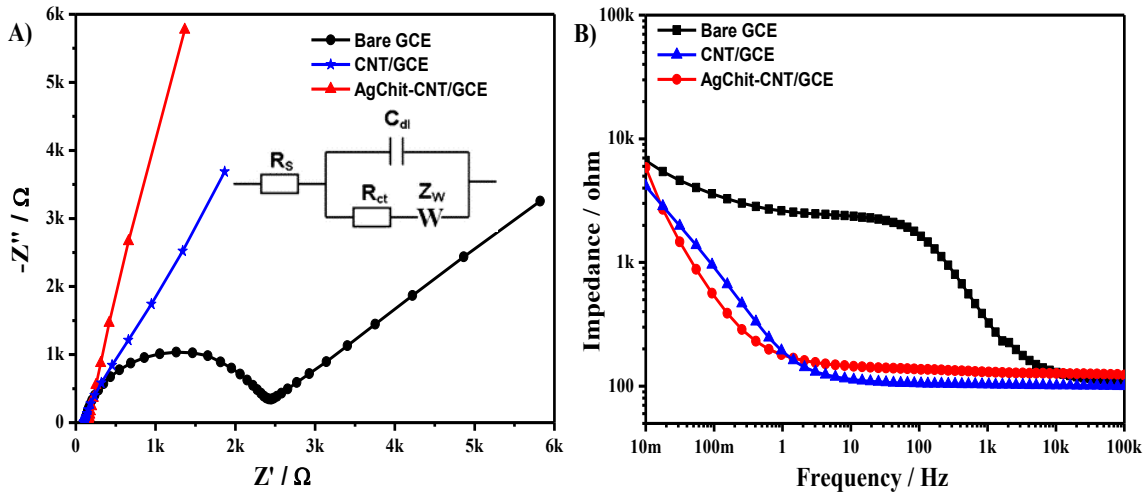

Fig. 4.11. *EIS measurements (A) Nyquist and (B) Bode plots of EIS analysis at bare GCE, CNT/GCE, SNP-CNT/GCE in 1 mM $K_3[Fe(CN)_6]$ + 0.1 M KCl. Inset: Randles circuit.*

From the cyclic voltammetry and EIS analysis results it can be inferred that the AgChit-CNT nanocomposite film providing a facile electron transfer to catalyze the electrochemical oxidation of CLP. This is to say that the AgChit-CNT-Chit composite comprising SNP implanted chitosan layered CNTs has provided a good linkage and the fine dispersion of nanotubes in the chitosan matrix enhanced the electrochemical activity

of electrodic system. The fabricated AgChit-CNT/GCE is further investigated for quantitative analysis of CLP.

4.3.5. Differential pulse voltammetry (DPV) and Amperometry

Differential pulse voltammetric and amperometric (i vs. t analysis) analysis of CLP at the SNP implanted chitosan and CNT hybrid nanocomposite electrode was carried out for quantitative analysis of CLP. Optimum experimental parameters for a good voltammetric profile with high peak current and minimal background current are established to be 100 mV pulse amplitude, 100 ms pulse width and 10 mV step increment. Differential pulse voltammograms of CLP at AgChit-CNT/GCE electrode were recorded in B-R buffer (pH 3.5) over the concentration range of 0 – 12 µM, and the results are shown in Fig. 4.12(A). A well-defined anodic peak was observed at +0.92 V. The peak current increased gradually with the increase in the concentration of CLP. The peak current was plotted against the concentration of CLP. A linear plot with a regression coefficient of 0.99 was obtained, as shown in Fig. 4.12(B). Low-detection-limit of the sensor system is defined as the change in peak current by three relative standard deviations, and it is determined from the plot to be 30 nM. The linear determination range is 5×10^{-8} – 10×10^{-6} M.

The sensitivity of the AgChit-CNT/GCE towards CLP detection also examined by amperometric i–t curve analysis. Figure 4.12(C) shows the amperometric i–t curve obtained for CLP at AgChit-CNT modified electrode in a mildly and uniformly stirred 50 mM PBS by applying a potential of +1.15 V. The modified electrode showed the initial current response due to 50 nM CLP and further addition of various concentrations of CLP in each step with a sample interval of ~50 s. The current response increases and a steady state current response was attained within 3 s. The dependence of amperometric current with respect to the concentration of CLP was linear from 50 nM to 8300 nM with a correlation coefficient of 0.99 (Fig. 4.12(D)). Even an addition of 10 nM concentration of CLP has given a good current response with an acceptable signal to noise ratio (Inset of Fig. 4.12(D)). Hence, the detection limit of CLP at AgChit-CNT/GCE was determined to be 10 nM (S/N=3).

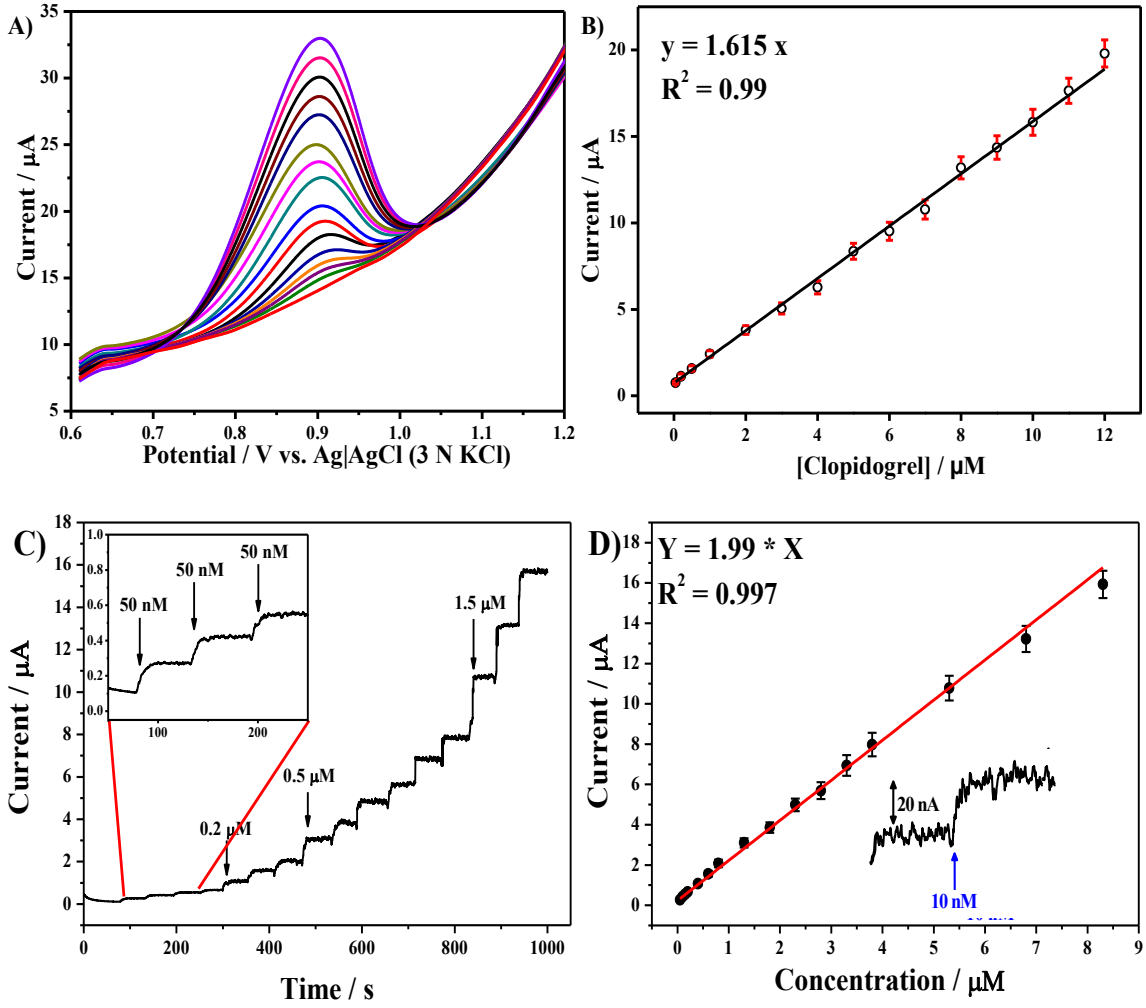

Fig. 4.12. *(A) DPVs of different concentrations of clopidogrel (0.0, 0.05 – 12.0 µM) in B-R buffer (pH 3.5) at AgChit-CNT/GCE. (B) Plot of the peak current against the concentration of clopidogrel. (C) Amperometric i–t curve at AgChit-CNT/GCE in B-R buffer (pH 3.5). Each addition increases the concentration of CLP at regular interval of ~60 s. Eapp = +1.15 V. (D) The plot for anodic peak current vs. concentrations of CLP; Inset: current response of AgChit-CNT/GCE with addition of 10 nM CLP.*

4.3.6. Interference studies

Electrochemical response of CLP in the presence of possible electroactive biological compounds such as ascorbic acid (AA), uric acid (UA), dopamine (DA) and 5-hydroxytryptamine (5-HT) has been investigated at the SNP embedded chitosan layered CNT nanocomposite electrode by DPV method. Figure 4.13 shows the DPVs at the AgChit-CNT/GCE in the mixture of AA, UA, DA and 5-HT 5 µM each and different concentrations of CLP at micromolar concentration levels (1, 2 and 3 µM) in B-R buffer (pH 3.5). At the present electrode system, distinct peaks for AA, DA, UA, 5-HT and CLP each were observed (Fig. 4.13). The peak currents for CLP increased as its concentration increases in the presence of these interferences. Even higher

concentrations of AA, DA, UA and 5-HT together could not affect the current response of CLP in B-R buffer. From the experimental results, it is inferred that the proposed electrochemical sensor could be used for the selective detection of CLP even in the presence of major electroactive biological interferents.

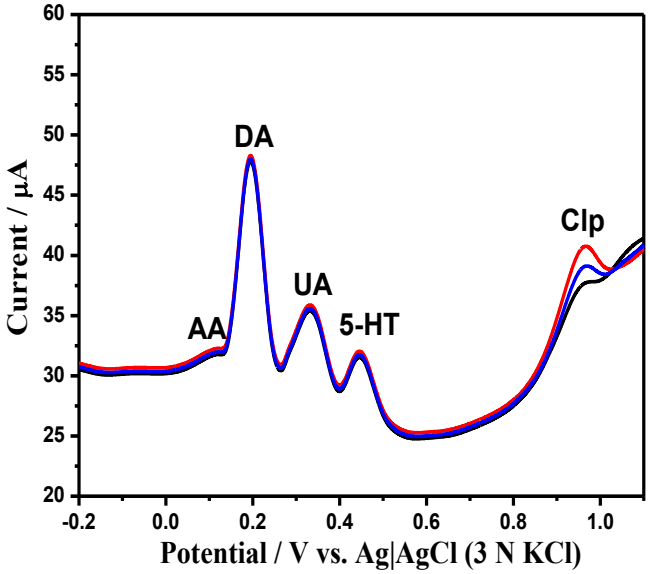

Fig. 4.13. *DPVs recorded at AgChit-CNT/GCE in presence of CLP at different concentrations (1.0, 2.0 and 3.0 µM) in the presence of AA, DA, UA and 5-HT 5.0 µM each in B-R buffer (pH 3.5).*

4.3.7. Reproducibility and Reusability

The stability, reusability and reproducibility of the present sensor system for the detection of CLP was investigated by DPV analysis. DPVs of 10 µM CLP were recorded at a same AgChit-CNT/GCE over a week time period. The peak currents of the recorded DPVs decreased merely by 2.6% in about 15 measurements, and this observation clearly indicates the quite good stability and reusability of the fabricated nanocomposite modified electrode even on storing at ambient laboratory conditions. Further, reproducibility of the modified electrode was examined by recording DPVs of CLP in repeated measurements with the use of six AgChit-CNT/GCE electrodes fabricated individually. The peak currents of the DPVs of 10 µM CLP recorded at these electrodes varied to an extent of only 2.8%. It obviously infers that the SNP implanted chitosan and MWCNT nanocomposite electrode shows impressive reproducibility for the analysis of CLP. In overall, all the observations conclude that the reusability and reproducibility of the present sensor system are quite acceptable.

4.3.8. Determination of CLP in pharmaceutical and artificial urine samples

Finally the developed sensor has been examined for practical applicability. Pharmaceutical samples of CLP (Lotclop 75 mg tablet) were analyzed by using the fabricated nanocomposite sensor with the standard addition method. In Fig. 4.14, the curves "a and b" show the DPVs of the analytical samples containing 0.5 µM of pure CLP together with different concentrations (0.5, 1.5 µM) of CLP from the pharmaceutical injection at AgChit-CNT/GCE. Recovery of CLP from artificial urine was examined by the addition of CLP into undiluted artificial urine of pH 3.5 without any buffer. In Fig. 4.14, curves "c and d" show the DPVs recorded at AgChit-CNT/GCE electrode in artificial urine sample in the presence of 1.0 and 2.0 µM CLP, respectively. The obtained recovery results of CLP from pharmaceutical and urine samples with the developed sensor have been tabulated below (Table 4.1), and the recovery values are quite satisfactory. The linear determination range of the developed sensor (0.03 – 10 µM) along with the very good recovery limits from physiological urine and pharmaceutical samples clearly confirms that the developed nanocomposite sensor would be of biomedical interest.

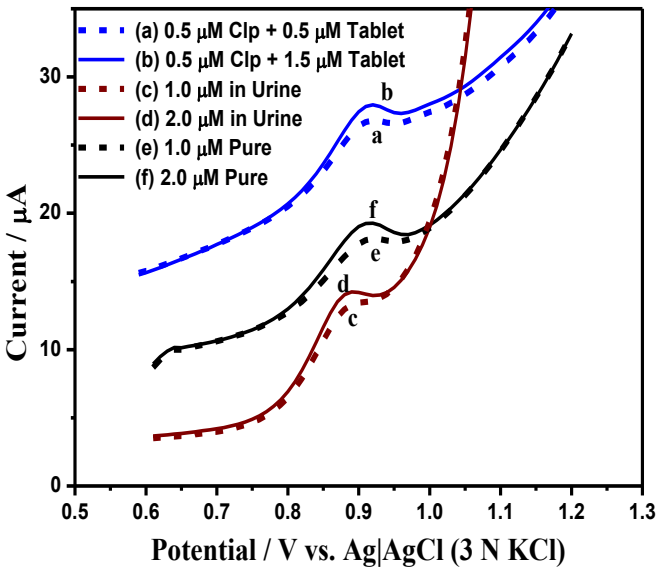

Fig. 4.14. *DPVs recorded at AgChit-CNT/GCE in the presence of a mixture of 0.5 µM pure CLP and different concentrations of CLP (a = 0.5 µM and b = 1.5 µM) .from a pharmaceutical formulation in B–R buffer (pH 3.5). Graphs c-f represents the DPVs of pure CLP in B-R buffer (pH 3.5; e, f) and in artificial urine (pH 3.5; c, d) with the concentrations of CLP at 1.0 µM (c, e) and 2.0 µM (d, f) concentrations.*

***Table 4.1**: Determination of CLP in pharmaceutical tablets and in artificial urine samples using the AgChit-CNT/GCE.*

Sample	Clp added (µM)	Tablet added (µM)	[a]Found (µM)	Average Recovery (%)	[a]RSD (%)
Tablet (Lotclop 75 mg)	0.5	0.5	0.95	95.2	1.2
	0.5	1.5	2.06	102.6	1.8
	0.5	2.5	2.96	98.3	1.4
Artificial Urine	0.5	--	0.49	98.9	0.9
	1	--	0.99	97.6	0.7
	2	--	1.95	99.2	1.2

[a] Mean value of six measurements.

4.4. Conclusions

In this work, we have developed a sensor system utilizing the SNP embedded chitosan layered MWCNT nanocomposite for sensitive determination of CLP by simple drop-cast method. The synthesised AgChit-CNT hybrid nanocomposite film extraordinarily enhanced the electrochemical oxidation current of CLP. The synthesized hybrid nanocomposite provided a continuous network of finite sized SNPs embedded chitosan layer on the surface of MWCNT, and this constructive linkage helped for a facile electron-transfer across the film and for a good electrocatalytic activity. The present electrochemical biosensor was efficient for the detection of nanogram levels of CLP despite the presence of major electroactive biological interferents together and had shown good recovery limits for direct determination from biological fluids and pharmaceutical formulations. The fabricated biosensor exhibited good stability, high sensitivity and simple fabrication procedure. All the advantages obtained with the present biosensor system confirm that the nanocomposite coupling CNT, inexpensive silver nanoparticle and a biocompatible biopolymer chitosan could be explored and extended for selective determination of various pharmaceutical drugs.

4.5. References

[1] B. F. Myasoedov, *Bull. Russ. Acad. Sci. Div. Chem. Sci.* **1992**, *41*, 383–387.

[2] P. D. Patel, *TrAC - Trends Anal. Chem.* **2002**, *21*, 96–115.

[3] G. A. Urban, F.-G. Banica, in *Chem. Sensors Biosens. Fundam. Appl.*, **2013**, pp. 5365–5366.

[4] G. A. Rivas, M. D. Rubianes, M. C. Rodríguez, N. F. Ferreyra, G. L. Luque, M. L. Pedano, S. A. Miscoria, C. Parrado, *Talanta* **2007**, *74*, 291–307.

[5] L. Agüí, P. Yáñez-Sedeño, J. M. Pingarrón, *Anal. Chim. Acta* **2008**, *622*, 11–47.

[6] M. Satyanarayana, K. Y. Goud, K. K. Reddy, K. V. Gobi, *Electrochim. Acta* **2015**, *178*, 608–616.

[7] R. Rawal, S. Chawla, T. Dahiya, C. S. Pundir, *Anal. Bioanal. Chem.* **2011**, *401*, 2599–608.

[8] H. Heli, F. Faramarzi, N. Sattarahmady, *J. Solid State Electrochem.* **2012**, *16*, 45–52.

[9] K. E. Moore, B. S. Flavel, J. Yu, A. D. Abell, J. G. Shapter, *Electrochim. Acta* **2013**, *89*, 206–211.

[10] M. Satyanarayana, K. K. Reddy, K. V. Gobi, *Anal. Methods* **2014**, *6*, 3772–3778.

[11] M. E. Ghica, R. Pauliukaite, O. Fatibello-Filho, C. M. A. Brett, *Sensors Actuators B Chem.* **2009**, *142*, 308–315.

[12] S. Murugesan, K. Myers, V. Ravi Subramanian, *Appl. Catal. B Environ.* **2011**, *103*, 266–274.

[13] P. K. Rastogi, V. Ganesan, S. Krishnamoorthi, *J. Mater. Chem. A* **2014**, *2*, 933–943.

[14] M. Forough, K. Farhadi, *Turkish J. Eng. Env. Sci* **2010**, *34*, 281–287.

[15] Y. Sun, Y. Xia, *Science* **2002**, *298*, 2176–2179.

[16] E. Filippo, A. Serra, A. Buccolieri, D. Manno, *Colloids Surfaces A Physicochem. Eng. Asp.* **2013**, *417*, 10–17.

[17] W. Wang, X. Chen, S. Efrima, *J. Phys. Chem. B* **1999**, *103*, 7238–7246.

[18] N. Samoilova, E. Kurskaya, M. Krayukhina, A. Askadsky, I. Yamskov, *J. Phys. Chem. B* **2009**, *113*, 3395–3403.

[19] J. Xu, X. Han, H. Liu, Y. Hu, *Colloids Surfaces A Physicochem. Eng. Asp.* **2006**, *273*, 179–183.

[20] T. Brooks, C. W. Keevil, *Lett. Appl. Microbiol.* **1997**, *24*, 203–206.

[21] H. Huang, Q. Yuan, X. Yang, *Colloids Surfaces B Biointerfaces* **2004**, *39*, 31–37.

[22] S. Agnihotri, S. Mukherji, S. Mukherji, *RSC Adv.* **2014**, *4*, 3974–3983.

[23] S. Hrapovic, E. Majid, Y. Liu, K. Male, J. H. T. Luong, *Anal. Chem.* **2006**, *78*, 5504–12.

[24] E. Laviron, *J. Electroanal. Chem.* **1979**, *101*, 19–28.

[25] A. J. Bard, L. R. Faulkner, *Electrochemical Methods: Fundamentals and Applications, 2nd Ed.*, John Wiley & Sons, New York, **2001**.

CHAPTER 5

Conducting Polymer Coated Carbon Nanotube Paste Electrode for Electrochemical Detection of Dacarbazine *in-vitro*

5.1. Introduction

Dacarbazine [5-(3,3-dimethy-1-triazenyl)imidazole-4-carboxamide, DTIC] is a commonly used anticancer drug to treat some malignant diseases. The drug is normally administered to the patient via veins with the dosage of 250 mg per day. The half-life of DTIC in human plasma is ca. 35 min, and 43% of the DTIC injected dosage excreted from urine within a period of 6 h. The major side effects are nausea and vomiting. Thus, periodical monitoring/determination of physiological concentrations of DTIC is immensely essential. Various analytical methods such as UV-Visible spectroscopy and HPLC have been employed to determine DTIC from pharmaceutical formulations and physiological liquids. On the other hand, there are only a few reports available for the detection of DTIC using simple and rapid direct in-vitro analytical methods like electrochemical technique. Most of the electrochemical studies of DTIC have focused on the binding interaction of DTIC with DNA [1–3]. Rodriguez et al. [4] reported the detection of DTIC at micromolar concentrations. Blanco et al. [5] reported good detection limits with a complex analytical system containing HPLC integrated with amperometric methods, and Temerk et al. [6] reported an indirect method to the detection of DTIC via Cu^{2+} complex. Here, we have investigated completely a direct electrochemical analysis and detection of DTIC, which is applicable as reagentless in-vitro analysis for the quality control and clinical applications.

Carbon paste-based electrodes (CPE) have been widely employed in fields of electroanalysis of pharmaceutical formulations, drugs, environmental pollutants, as well as other biologically active organic compounds. In CPE, the graphite powder is used as the electrocatalytic material. In fact, a major reason for developing carbon paste electrodes was the ease of surface renewal and reproducibility. From the past decade, a tremendous interest received among this paste electrodes by replacing and/or mixing nanostructured carbon materials such as mesoporous carbons [7,8], carbon nanoparticle [9], carbon nanofibers [10] and carbon nanotubes [11,12] with the graphite powder to increase the electrocatalytic activity. Among this, carbon nanotube has unique properties such as high mechanical strength, nanotubes of few hundred micrometer long tubular geometry and chemically inert nature with high electrical conductivity. Carbon nanotubes provide highly nanostructured surfaces and enhanced electron transfer rate to improve the electrode kinetics which leads to low detection limits, high sensitivities and fast responses [13,14].

Conducting polymer is considered as one of the emerging material in the field of electrochemical sensors/biosensors due to its compatibility with biological molecules in physiological fluids [15–17]. Conducting polymers are mainly organic compounds with an extended p-orbital system through which electrons can move from one end of the polymer to the other, which improves the electrocatalytic properties of the sensor system. A thin layer of a conducting polymer deposited onto the electrode surface is able to enhance the kinetics of electrodic processes. The thickness of the conducting polymer over the electrode surface controls the efficiency and biocompatibility of the sensor/biosensor. The electrochemical polymerization technique is a best and simple method for the formation of conducting polymers with a desirable thickness compared to all other chemical methods [18]. Combining the advantages of the both carbon nanotubes and conducting polymer, we fabricated an electrochemical sensor for the important anti-cancer drug, dacarbazine, using a composite of carbon nanotube and conducting polymer as electrode material.

In this present work, we have fabricated a sensitive and biocompatible electrochemical sensor system for DTIC using the binary system with the combination of the conducting polymer and carbon nanotubes. Low-detection-limit, stability, reproducibility and applicability for physiological and pharmaceutical samples are investigated.

5.2. Experimental

5.2.1. Chemicals and materials

Dacarbazine, ascorbic acid, uric acid, dopamine and serotonin were obtained from Tokyo chemical industry, Japan. 2-amino-1,3,4-thiadiazole was purchased from Sigma Aldrich, USA. MWCNTs (95%, 20–30 nm OD and 10–30 μm length) were purchased from Sisco research laboratories, India. Other chemicals used in this investigation were analytical grade reagents (minimum 99% purity). Britton-Robinson buffer (B-R buffer) was prepared by mixing boric acid, phosphoric acid and acetic acid 40 mM each, followed by the addition of 0.1 M NaOH to adjust the pH (pH 3.0 to 10.0). Artificial urine solution was prepared following a procedure reported in the literature [19]. It consists urea (170 mM), citric acid (2.0 mM), lactic acid (1.1 mM), sodium chloride (90 mM), ammonium chloride (25 mM), sodium sulphate (10 mM), sodium bicarbonate (25 mM), calcium chloride (2.5 mM), potassium dihydrogen phosphate (7.0 mM) and

dipotassium hydrogen phosphate (7.0 mM), and the solution pH was adjusted to pH 8.0 by the addition of 1.0 M NaOH. Double distilled water filtered finally through a 0.2 µm Millipore filter was used to prepare aqueous solutions throughout the investigation.

5.2.2. Fabrication of electrode system

At first, functionalization of MWCNT with carboxyl groups was carried out by treating with hot nitric acid, as discussed in chapter 2. Then, the CNPE electrode was fabricated as follows. A 50 mg of MWCNT and 100 µL of paraffin oil were mixed to get a homogeneous paste. Then, the paste was filled into a Teflon tube of diameter 4 mm and inserted a copper rod from the top of the tube for electrical contact, and finally it is denoted as CNPE. The active surface area of the electrode is polished with a butter paper before the experiment. The fabricated CNPE is then coated with *poly*-ATD by applying the potentiodynamic polarization technique. In this technique, the CNPE electrode was treated with multiple cycles over the potential window of -0.2 to 1.7 V in the solution of 2 mM ATD in 0.1 M H_2SO_4 with the scan rate of 50 mV s^{-1}. The resultant electrodes were dried under RT for 12 h and denoted hereafter as *poly*-ATD/CNPE.

5.2.3. Characterization

FT-IR spectroscopy studies were carried out on Perkin-Elmer FT-IR spectrometer using KBr pellet method for powder samples of ATD and attenuated total reflection (ATR) method using HRATR setup for *poly*-ATD/CNPE electrode. The formed layer of *poly*-ATD film on CNPE was separated by cutting the electrode surface by nearly 2 mm of thickness, and it was used for the FTIR analysis using ATR setup. Similar process was followed for the surface morphological studies of CNPE and *poly*-ATD/CNPE electrodes by scanning electron microscopy. Here, the separated layer was fixed on a conducting carbon tape and sputtered with a thin layer of gold to avoid charging during the analysis. Surface morphological studies were carried out on TESCAN VEGA 3 scanning electron microscope (SEM) operating at 10 - 20 kV.

5.2.4. Electrochemical analysis

Cyclic voltammetry, chronoamperometry, differential pulse voltammetry and i-t curve experiments were carried out using an Electrochemical Potentiostat/Galvanostat (Model 6132e, CH Instruments, USA). Electrochemical impedance measurements were carried out using an electrochemical workstation (Model: IM6e, Zahner, Germany) equipped with Thales software. A conventional two-compartment three-electrode cell of

20 mL volume was used with bare or modified CNPE as working electrodes, spiral Pt wire as counter electrode and Ag|AgCl (3 N KCl) as reference electrode. Electrode potentials were referred against Ag|AgCl (3 N KCl) throughout the chapter. B-R buffer (pH 3.0 – 10.0) was used as the electrolyte for electrochemical experiments. For electrochemical analysis, the experimental solutions were purged with nitrogen gas for 10 min prior to the start of the experiment.

5.3. Results and Discussion

5.3.1. Electropolymerization of ATD on CNPE

A thin film of *poly*-ATD was coated on the surface of CNPE by applying potentiodynamic polymerization method. Figure 5.1 shows the typical cyclic voltammograms (CV) during the potentiodynamic polymerization of ATD in 5 mM ATD + 0.1 M H_2SO_4 by applying 15 cycles in the potential window of -0.20 to +1.70 V. In the first cycle, the oxidation peaks of ATD appeared at +1.52 V. In the next cycle, the oxidation peak current decreased considerably and its potential was slightly shifted to ~+1.48 V. From the third cycle onwards, an increase in the oxidation peak current of ATD was observed in each cycle, which indicates that the oxidative ATD monomer undergoes polymerization on the electrode surface with each additional potential cycle and that the amount of the electroactive polymer increases on the electrode surface with each new cycle. During the oxidation of ATD at +1.52 V, it will generate the radical cation at the amine functional group. The amine radical cations forms the dimers and these dimers are more easily oxidizable than the monomer, resulting in polymerization. The layered conducting polymer of ATD exhibits a redox peak and a quasi-reversible redox peak of weak current intensity nearly at 0.32 V and 0.70 V, respectively, which were not observed in the first segment (Fig. 5.1, inset). The capacitance current increased as the number of cycles increases, indicating that the polymer film grows on the electrode surface. The redox characteristics of the polymer film could enhance the electrocatalytic activity of the sensor system. The formed *poly*-ATD is strongly linked with the carboxyl functional groups of CNTs (Scheme 5.1) and it is confirmed by FTIR analysis *vide-infra.* This linkage could be helpful for a facile electron transfer between the electroactive species and electrode surface, which could lead to an increase in the sensitivity of sensor system

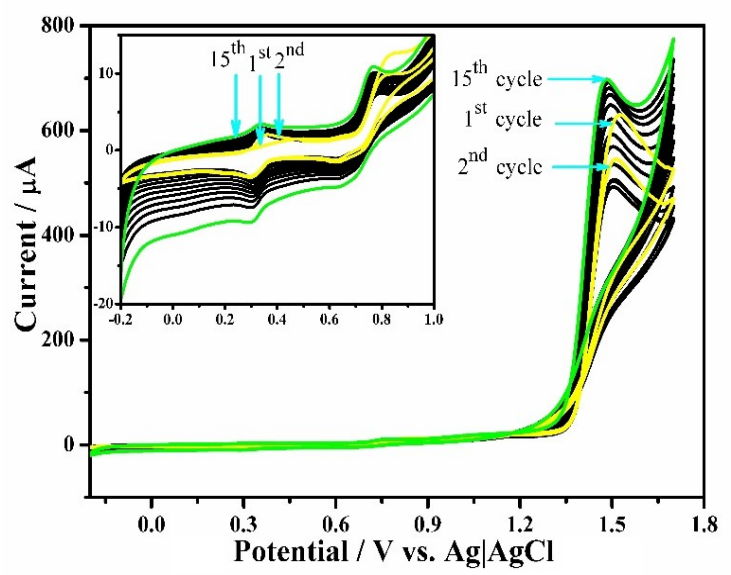

Fig. 5.1. *Potentiodynamic polymerization of ATD (15 cycles) on a CNPE in 5 mM ATD + 0.1 M H_2SO_4 at a scan rate of 50 mV s^{-1}.*

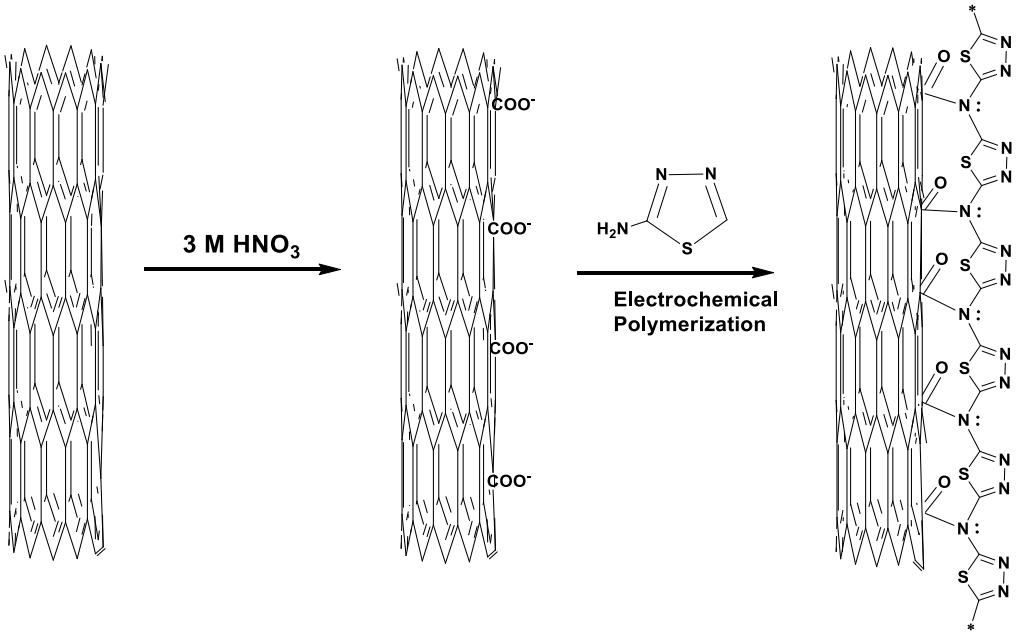

Scheme 5.1. *Mechanism of functionalization of MWCNT and electropolymerization of ATD over CNPE.*

5.3.2. FTIR spectral studies and SEM analysis of poly-ATD/CNPE

The formation of *poly*-ATD on CNPE examined by FTIR spectroscopy. Figure 2 shows the FT-IR spectra of pure ATD (Fig. 5.2a), *poly*-ATD/CNPE (Fig. 5.2b) and CNPE (Fig. 5.2c). ATD shows a weak stretching doublet band at 3090 and 3110 cm^{-1} (Fig. 5.2a) attributed to a primary amine group, and these bands were not appeared in the ATR-FTIR spectra of *poly*-ATD/CNPE film, which infers that the amine groups present

in ATD were involved in the electropolymerization. There is a new peak observed at 1661 cm^{-1}, which represents the stretching band of the carbonyl group attached to a tertiary amino group of the polymer link. Furthermore, there is a shift in all FTIR peaks of *poly*-ATD compared to ATD monomer.

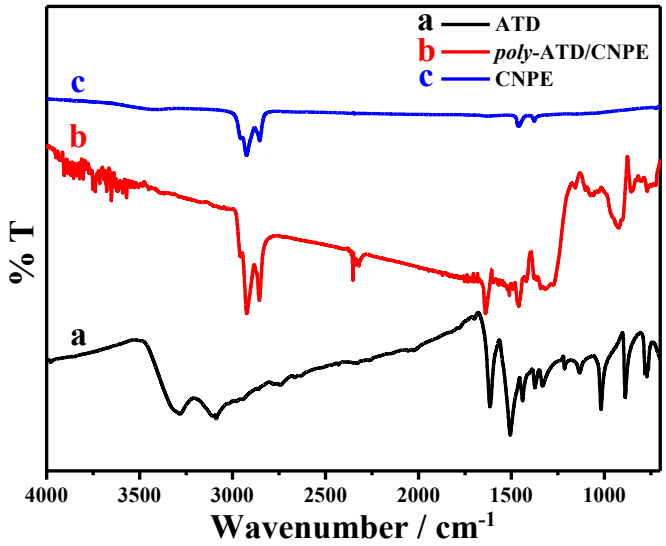

Fig. 5.2. *FTIR spectrum of the ATD in a KBr pellet (a), and ATR-FTIR spectrum of poly-ATD film on CNPE (b) and CNPE (c).*

Surface morphology studies of CNPE and *poly*-ATD/CNPE by SEM have been shown in Fig. 5.3(A and B). In Fig. 5.3(A), a network of well distributed carbon nanotubes was observed over the matrix of CNPE, whereas in Fig. 5.3(B), the CNTs are covered with a polymer layer of ATD evenly all over the surface of CNPE. Due to the reason, we could not see any thread like structures of CNTs in Fig. 5.3(B). From these observations, it is inferred that there is a formation of a thin film of *poly*-ATD all over the CNPE. Figure 5.3(C) represents the EDX analysis of *poly*-ATD/CNPE, and the spectrum clearly shows the peaks of carbon, oxygen, nitrogen and sulphur with the weight ratios of 90.88, 4.61, 3.39 and 1.12, respectively. From these observations, it is confirmed that the formed layer is a polymeric film consisting of ATD. By the results of FTIR and also combining the observations of SEM-EDX, the plausible mechanism for the polymerization process of ATD over CNPE presented in scheme 5.1 is further confirmed.

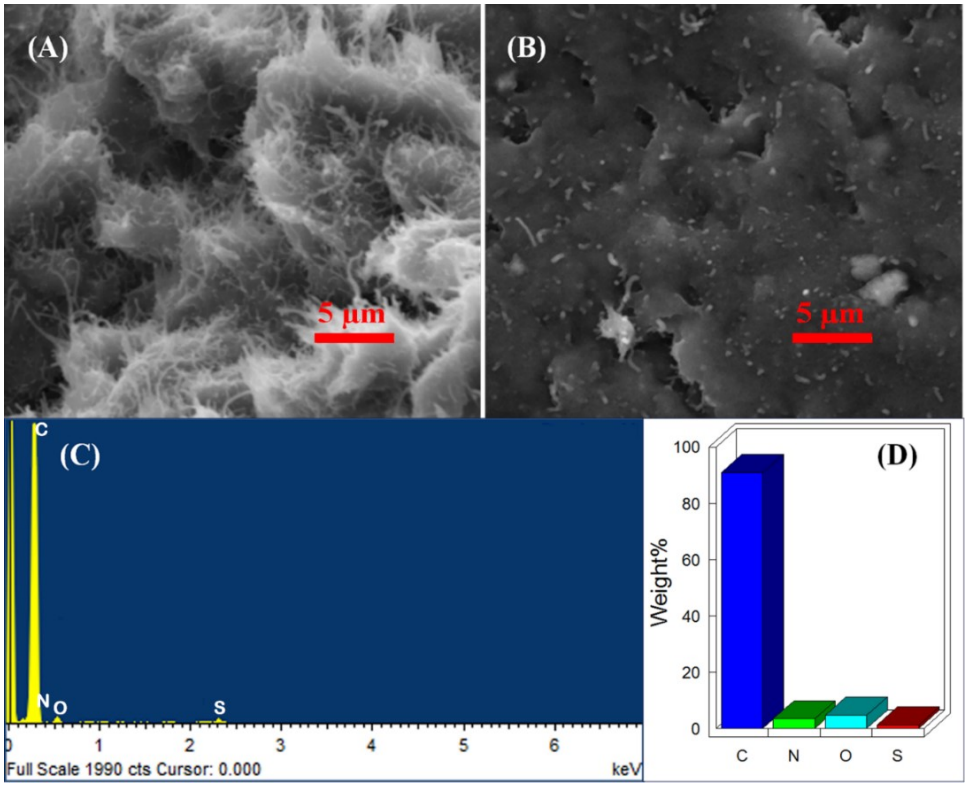

Fig. 5.3. *SEM images of (A) CNPE and (B) poly-ATD/CNPE electrodes. (C) EDX spectra of poly-ATD/CNPE, and (D) Bar representation of weight percentage of major elements (C, N, O and S) present in poly-ATD/CNPE.*

5.3.3. Electrocatalytic oxidation of Dacarbazine

Initially, the amount of polymer coating over the surface of CNPE is optimized. Figure 5.4 shows the electrochemical behavior of *poly*-ATD coated CNT paste electrodes formed by various number of potentiodynamic polymerization cycles (5, 10, 15, 20) towards the electrochemical oxidation of $K_3[Fe(CN)_6]$ in 0.1 M KCl. The *poly*-ATD/CNPE formed by 15 potentiodynamic cycles exhibited a good cyclic voltammogram with high peak current and less peak-to-peak separation values. Hence, the polymer coated electrode formed with 15 potential cycles is selected for the electrochemical detection of DTIC. The electrocatalytic behavior of the fabricated *poly*-ATD/CNPE towards the oxidation of DTIC has been investigated using cyclic voltammetric method. Figure 5.5 shows the electrochemical oxidation of DTIC at CPE, *poly*-ATD/CPE, CNPE, and *poly*-ATD/CNPE in B-R buffer (pH 6.0) containing DTIC at 0.5 mM. In the absence of DTIC, no characteristic peak was observed at any of the electrodes in B-R buffer. In the presence of DTIC, an irreversible anodic peak was observed at all the electrodes. The anodic peak potential for the oxidation of DTIC at CPE, *poly*-ATD/CPE and CNPE is ~ +0.93 V, whereas at *poly*-ATD/CNPE the anodic

peak was observed at a less positive potential, +0.86 V. Further, the oxidation peak current of DTIC at *poly*-ATD/CPE is higher than that at uncoated CPE. Similar phenomena was observed at *poly*-ATD/CNPE compared to CNPE. The thin-film ATD polymer coated carbon paste electrode (*poly*-ATD/CPE) also has not shown an enhancement in the peak current of DTIC compared to bare CNPE, whereas this enhancement is very high at *poly*-ATD coated CNPE. This is due to the well constructive linkage between *poly*-ATD and carboxyl functional groups of carbon nanotubes. The *poly*-ATD/CNPE has shown superior performance compared to all the other electrodes in the form of the increase in peak current and less positive potential for the oxidation of DTIC.

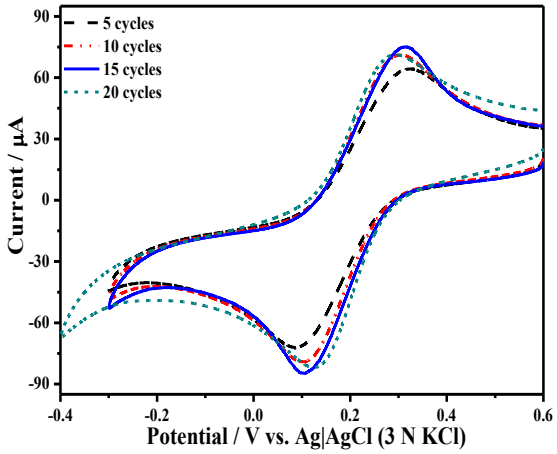

Fig. 5.4. *CVs of 1 mM $K_3[Fe(CN)_6]$ in 0.1 M KCl at poly-ATD-CNPE formed by potentiodynamic polymerization with various number of cycles (5, 10, 15, 20).*

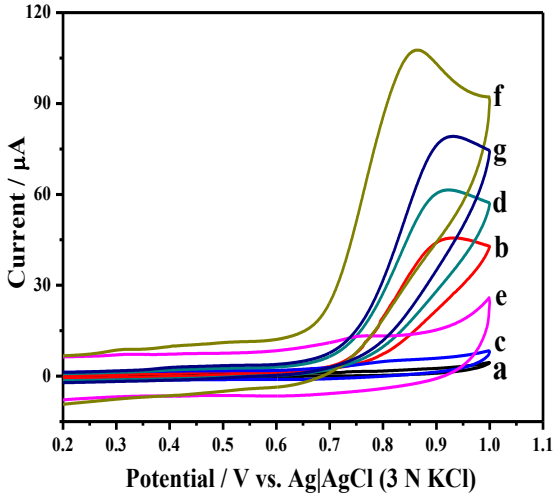

Fig. 5.5*. CVs in the presence (b, d, f, g) and absence (a, c, e) of 0.5 mM DTIC in B-R buffer (pH 6.0) at poly-ATD/CNPE (e, f), CNPE (c, g), poly-ATD/CPE (d), CPE (a, b). Scan rate 100 mV s^{-1}.*

The influence of pH on the oxidation behavior of DTIC at *poly*-ATD/CNPE was examined by varying the pH (pH 3.0 to 10.0) of the B-R buffer solution. The obtained cyclic voltammetric results are shown in Fig. 5.6. The pH of the B-R buffer obviously influenced the oxidation peak of DTIC. The oxidation over potential of DTIC is decreased with the increase in pH, and the plot between Ep and pH (Fig. 5.6(B)) shows that the decrease in Ep is linearly dependent on pH (Fig. 5.6(B)). The slope of the Ep vs. pH plot is 0.032 V, which indicates that the number of protons involved in electrochemical reaction of DTIC are twice the number of electrons transferred in the electrochemical oxidation reaction [20]. The plot of the oxidation peak current on the pH is shown in fig. 5.6(B). The oxidation peak current is nearly equal over the pH range of 3.0 to 6.0, and then it decreases gradually with the increase in pH. By considering the peak current and the peak potential, B-R buffer of pH 6.0 has been considered optimum for all further experiments.

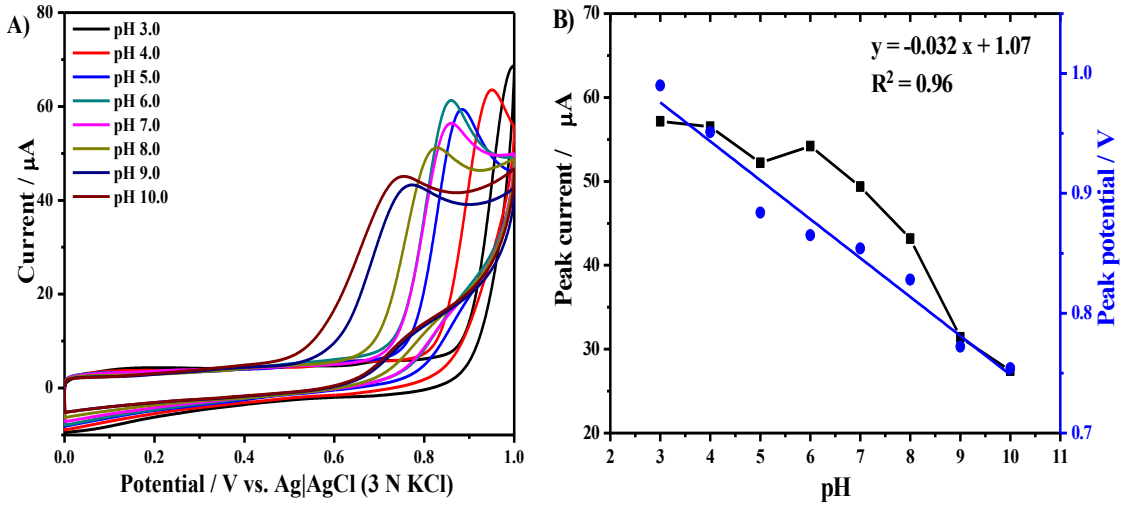

Fig. 5.6. *(A) CVs of 0.2 mM DTIC in B-R buffer with different pH values (3 – 10) at poly-ATD/CNPE. (B) Plots of the peak current vs. pH and peak potential vs. pH.*

Influence of the scan rate on the peak potential of DTIC was studied. Cyclic voltammograms of 0.5 mM DTIC at *poly*-ATD/CNPE were recorded with different scan rates (25 – 300 mV/s) and are shown in Fig. 5.7. The peak currents for oxidation of DTIC gradually increased with the scan rate. The plot between the anodic peak current and the square root of scan rate is linear and is passing through the origin (Fig. 5.7(B)). It clearly indicates that the electrochemical oxidation of DTIC is a diffusion controlled process and also that the permeation of DTIC across the *poly*-ATD film is very facile (*vide infra*).

For an irreversible electrochemical reaction, the relationship between the peak potential Ep and the scan rate ν is expressed in Eq. (5.1) by Laviron [21]:

$$Ep = E° + \frac{RT}{\alpha nF} ln\left[\frac{RTk°}{\alpha nF}\right] + \left[\frac{RT}{\alpha nF}\right] ln(\nu) \qquad (Eq. 5.1)$$

where α is the charge transfer coefficient, k° is the standard rate constant for heterogeneous electron transfer, n is the number of electrons involved in the reaction and E° is the formal potential. According to Eq. (1), the αn value can be determined from the slope of Ep vs. ln(ν) plot (Fig. 5.7(C)), and k° can be calculated from the intercept of the plot, if the value of E° is known. The value of E° can be obtained from the intercept of the Ep vs. ν plot (Fig. 5.7(D)) by extrapolation to the vertical axis at ν = 0, and it is 0.831 V. From the slope of the Ep vs. ln(ν) plot, αn was calculated to be 1.12.

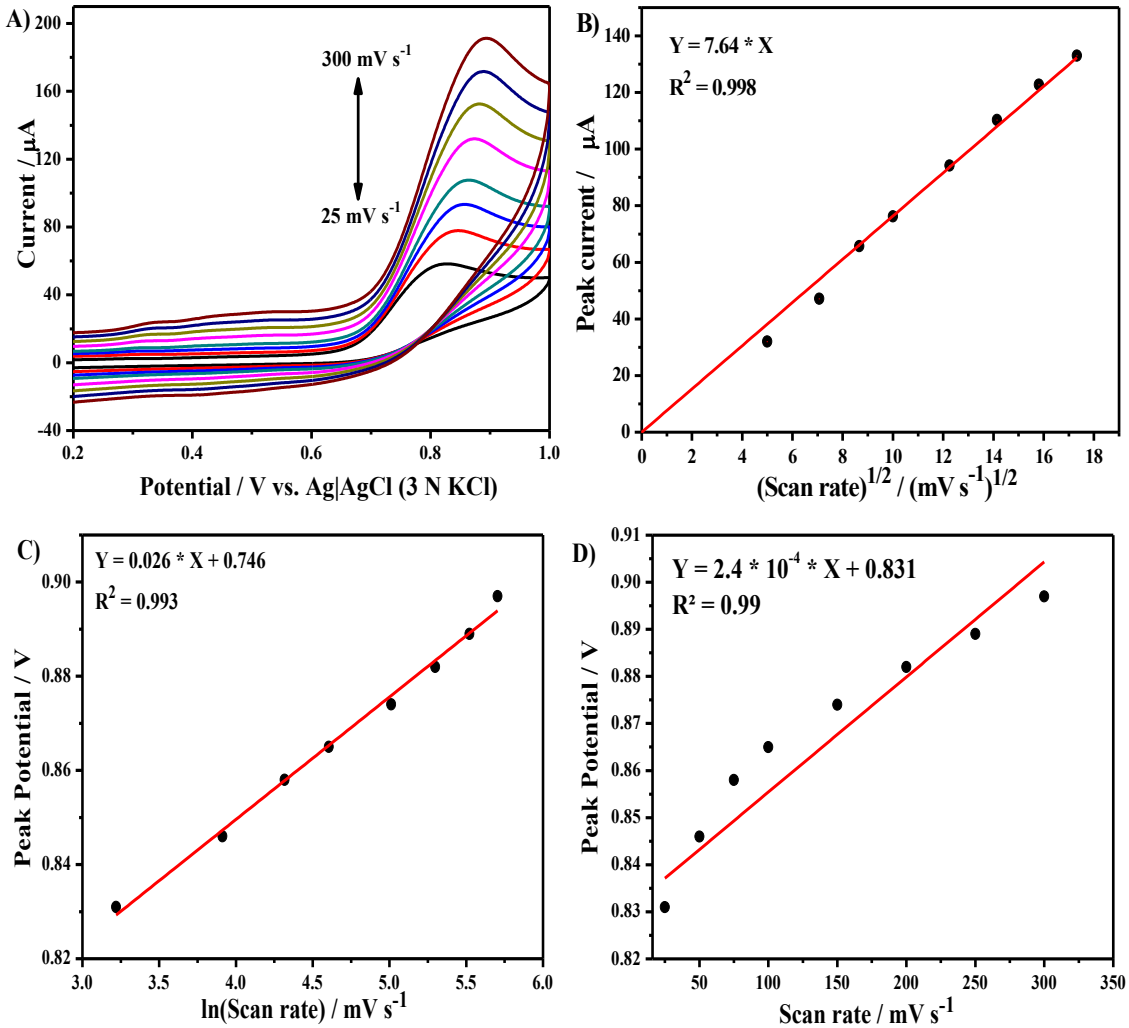

Fig. 5.7. *(A) CVs of 0.5 mM DTIC in B-R buffer (pH 6.0) at poly-ATD/CNPE with different scan rates (25 - 300 mV s^{-1}). (B) Plot of the peak current against the square root of scan rate. (C) Plot of the peak potential against ln(scan rate) and (D) the peak potential against scan rate for the CVs of DTIC at poly-ATD/CNPE.*

Generally, α can be assumed to be 0.5 for an irreversible electrochemical process, and thus the electron transfer number (n) for the oxidation of DTIC becomes 2. Additionally, the k° value is also determined from the intercept of Ep vs. ln(ν). It is found to be 1.44 s^{-1} and the obtained value is comparable with those reported at various other carbon paste and modified electrodes [22–24]. Considering the results of Ep vs. pH and Ep vs. ln(ν) studies together, we could conclude that the electrochemical oxidation of DTIC is a two-electron four-proton transfer process. The plausible electrochemical oxidation mechanism of DTIC is provided by adopting the mechanism reported elsewhere [4] (Scheme 5.2).

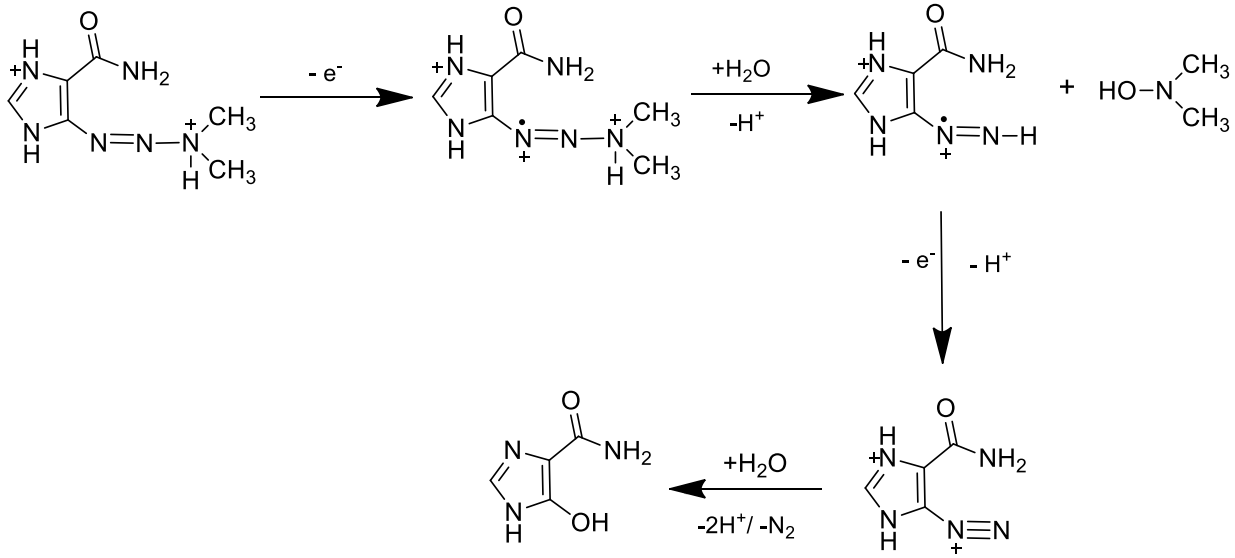

Scheme 5.2. *Electrochemical oxidation mechanism of DTIC*

Diffusion coefficient of DTIC for the electrochemical oxidation at *poly*-ATD/CNPE is determined using chronoamperometry (Figure 5.8) by adopting the Cottrell's equation[25] and its value calculated to be 8.87 × 10^{-6} cm^2 s^{-1}.

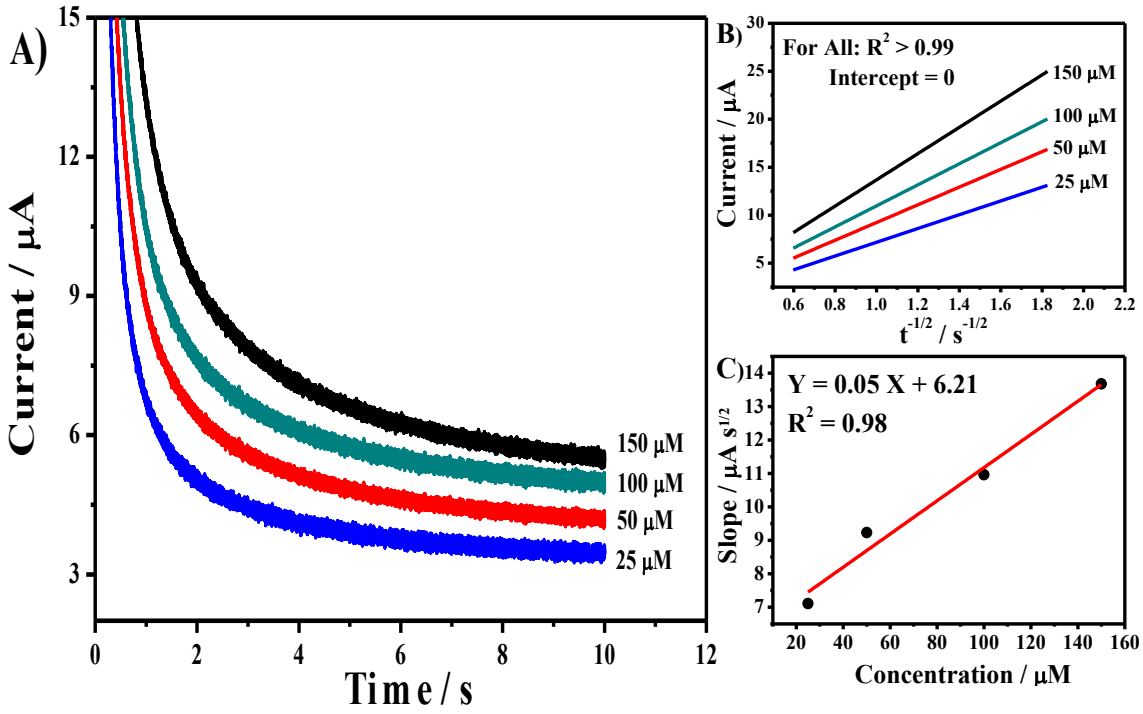

Fig. 5.8. *(A) CA plots of DTIC in B-R buffer (pH 6.0) at different concentrations (25, 50, 100, 150 µM) at ploy-ATD/CNPE. (B) Plot of i vs. $t^{-1/2}$ and (C) plot of the concentration of DTIC against the slope of (i vs. $t^{-1/2}$) plots.*

5.3.4. Electrochemical impedance spectroscopy (EIS)

Electrochemical impedance spectroscopy of the electrode was examined to study the interfacial properties of the electrode and solution. Charge transfer resistance (R_{ct}) determined here is an important characteristic of electron-transfer across the electrode interface [26,27]. Electrochemical impedance spectra of CPE, *poly*-ATD/CPE, CNPE, and *poly*-ATD/CNPE in 2 mM $K_3[Fe(CN)_6]$ + 0.1 M KCl were examined at the open circuit potential over the frequency range of 100 kHz to 100 mHz. The results were best fit with Randles equivalent circuit, and the resulting Nyquist plots are shown in Fig. 5.9. The Nyquist plot of CPE, *poly*-ATD/CPE, and *poly*-ATD/CNPE shows a semi-circular pattern, whereas the Nyquist plot of CNPE exhibits only a linear plot relevant to a mere diffusion behavior alone, indicating the very high conductivity of the carbon nanotube paste electrode with negligible charge transfer impedance. The carbon paste electrode even after thin-film *poly*-ATD coating (*poly*-ATD/CPE) shows less R_{ct} compared to CPE, which infers that the slow electron transfer of CPE has been enhanced after the polymerization. The *poly*-ATD/CNPE electrode shows a semicircular pattern, indicating the existence of charge-transfer resistance at the polymerized electrode, however the R_{ct} of *poly*-ATD/CNPE is quite lower than those of CPE and *poly*-ATD/CPE electrodes.

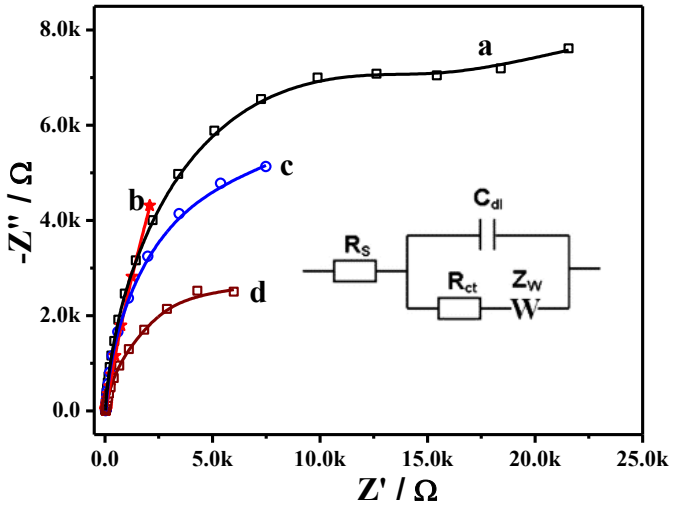

Fig. 5.9. *Nyquist plots of EIS analysis at CPE (a), CNPE (b), poly-ATD/CPE (c) and poly-ATD/CNPE (d) in 2 mM $K_3[Fe(CN)_6]$ + 0.1 M KCl. Inset: Randles circuit.*

5.3.5. Differential pulse voltammetry (DPV) and Amperometry

Differential pulse voltammetric analysis of DTIC at p*oly*-ATD/CNPE was carried out for quantitative analysis of DTIC. Optimum experimental parameters for a good voltammetric profile with high peak current and minimal background current are established to be 100 mV pulse amplitude, 100 ms pulse width and 10 mV step increment. Differential pulse voltammograms of DTIC at *poly*-ATD/CNPE electrode were recorded in B-R buffer (pH 6.0) over the concentration range of 0 – 24 µM DTIC, and the results are shown in Fig. 5.10(A). A well-defined anodic peak was observed at +0.65 V. The peak current increased gradually with the increase in the concentration of DTIC. The DPV measurements were repeated four times with independent electrodes, and the peak current was plotted against the concentration of DTIC. A linear plot with a regression coefficient of 0.99 was obtained, as shown in Fig. 5.10(B). Low-detection-limit of the sensor system is defined as the change in peak current by three relative standard deviations, and it is determined from the plot to be 35 nM. The linear determination range is 5×10^{-8} – 24×10^{-6} M, and the analysis time is as low as 25 s.

The sensitivity of the *poly*-ATD/CPE towards DTIC detection also examined by amperometric i–t curve analysis. Figure 5.10(C) shows the amperometric i–t curve obtained for DTIC at *poly*-ATD/CPE in a in a gently and uniformly stirred 40 mM B-R buffer by applying a potential of +0.9 V. The modified electrode shows the initial current response for 50 nM DTIC and for further addition of various concentrations of DTIC in each step with a sample interval of ~50 s, the current response increases and a steady

state current response was attained within 3 s. The dependence of amperometric current with respect to the concentration of DTIC was linear from 50 nM to 10800 nM with a correlation coefficient of 0.99 (Fig. 5.10(D)). The low-detection-limit of DTIC at *poly*-ATD/CPE was determined to be 20 nM (S/N=3).The performance of the present sensor is further examined for the detection of DTIC in the presence of various potential biological interferents and from complex physiological and pharmaceutical samples.

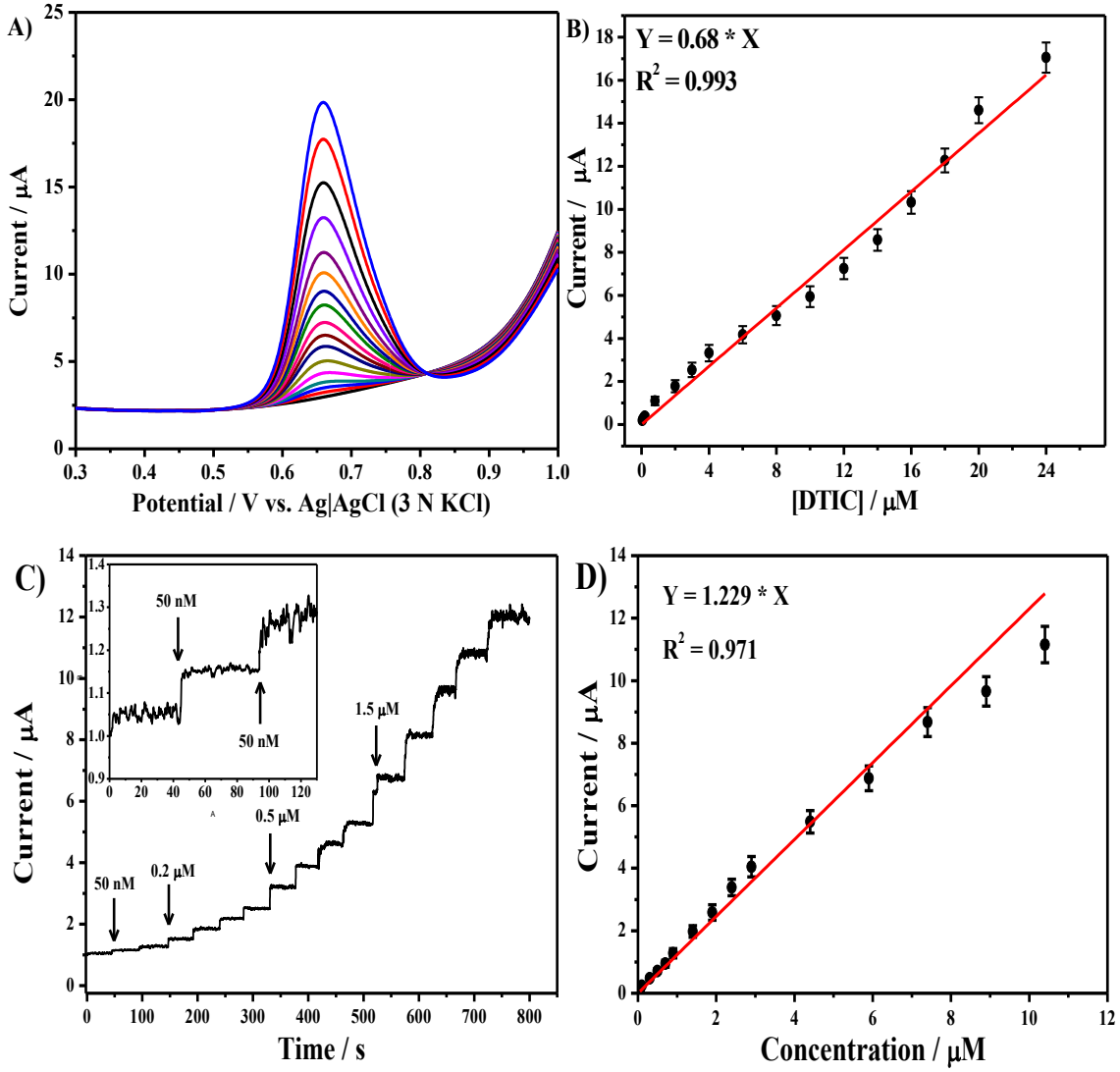

Fig. 5.10*. (A)DPVs recorded at poly-ATD/CNPE of different concentrations of DTIC (0.0, 0.05 – 24 µM). (B) Plot of i_p vs. concentration of DTIC. (C) Amperometric i-t curve at poly-ATD/CNPE in B-R buffer (pH 6.0). Each addition increases the concentration of DTIC at regular intervals of ~50 s. Eapp = +0.9 V. (D) The plot for anodic peak current vs. concentration of DTIC.*

5.3.6. *Interference studies*

Electrochemical response of DTIC in the presence of possible electroactive physiological components such as ascorbic acid (AA), uric acid (UA), dopamine (DA) and 5-hydroxytryptamine (Serotonin or 5-HT) has been investigated at *poly*-ATD/CNPE electrode using DPV method. Figure 5.11 shows the DPVs at *poly*-ATD/CNPE with distinct peaks for DA, 5-HT (each 5 µM) and DTIC (0.0, 2.0, 3.0, 4.0, 5.0 µM). There is no effect of above interferents on the oxidation peak of DTIC and also there is a good peak separation observed between DA, 5-HT and DTIC. The peak currents for DTIC increased as the concentration of DTIC increases in the presence of these interferences. Even higher concentrations of AA, DA and UA together could not affect the current response of DTIC in B-R buffer. From the experimental results, it is clearly evident that the proposed electrochemical sensor can be used effectively for the detection of DTIC even in the presence of various possible electroactive interferents.

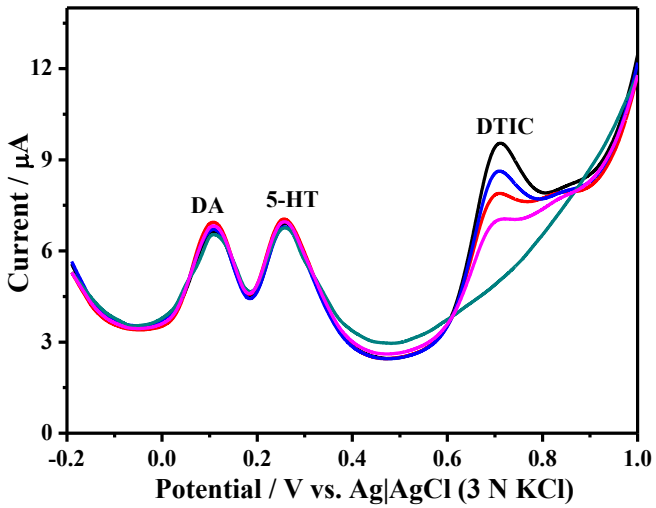

Fig. 5.11. *DPVs recorded at poly-ATD/CNPE in DTIC at different concentrations (0.0, 2.0, 3.0, 4.0, 5.0 µM) in the presence of DA and 5-HT 5 µM each in B-R buffer (pH 6.0).*

5.3.7. *Reproducibility and Reusability*

Performance of the sensor system mainly depends on its reproducibility and repeatability results. The *poly*-ATD/CNPE was examined in 0.02 mM DTIC for multiple analysis by a same electrode to check the reproducibility of the fabricated sensor. During multiple measurements for 20 times in a time period of a week, only a very slight change in the oxidation peak current was observed with a little standard deviation, suggesting that the fabricated sensor system exhibiting excellent stability and repeatability. Further, reproducibility of the modify electrode was examined by recording DPVs of DTIC in multiple measurements with the use of six p*oly*-ATD/CNPE electrodes fabricated

independently. The peak currents of the DPVs of 2 µM DTIC recorded at these electrodes varied to an extent of only 2.6%. It clearly reveals that the nanocomposite electrode is highly reproducible for the analysis of DTIC. In overall, all the observations conclude that the reusability and reproducibility of the *poly*-ATD/CNPE electrode are quite satisfactory.

5.3.8. Determination of DTIC in pharmaceutical and artificial urine samples

Pharmaceutical samples of DTIC (Decarb-200 mg injection) were analyzed by using the fabricated nanocomposite sensor with the standard addition method. Analytical samples containing 0.5 µM of pure DTIC together with different concentrations (0.5, 1 and 1.5 µM) of DTIC of the pharmaceutical injection were examined at *poly*-ATD/CNPE (Fig. 5.12(A)). The recovery values obtained in these experiments varied from 99.3% to 102.6% (Table 5.1) and are quite satisfactory. Recovery of DTIC from artificial urine was examined by the addition of DTIC into undiluted artificial urine sample of pH 6.0 without any buffer (Fig. 5.12(B)). The recovery of DTIC from undiluted artificial urine samples at different concentrations of DTIC (0.5 – 1.5 µM) varied from 98.9% to 101.6% (Table 1). The observed good recovery limits of spiked DTIC concentrations from pharmaceutical formulations and from artificial urine samples demonstrate that the present biosensor is highly promising for determination of DTIC from real samples.

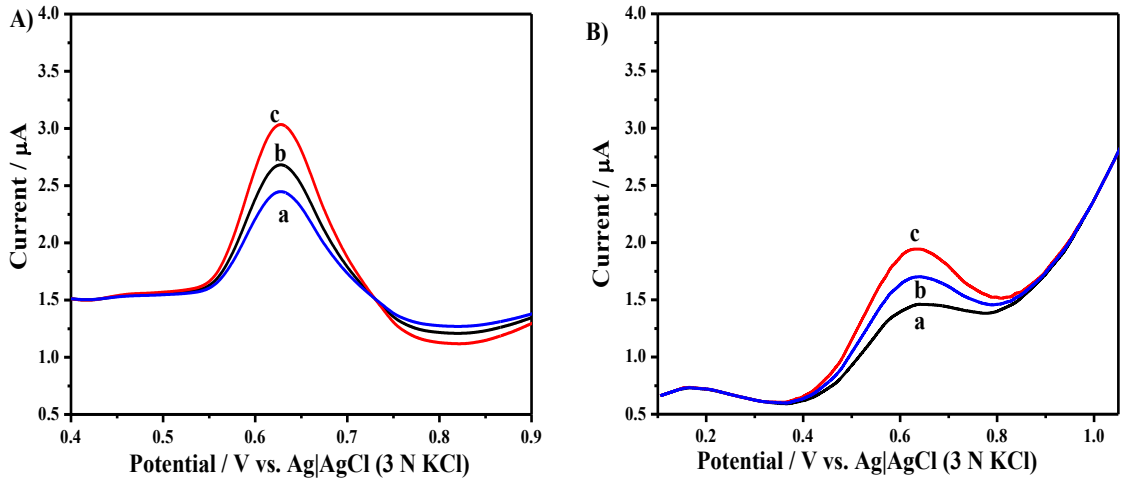

Fig. 5.12. *DPVs recorded at poly-ATD/CNPE (A) in the presence of mixture of 0.5 µM pure DTIC and different concentrations of DTIC (a = 0.5, b = 1.0 and c = 1.5 µM) from pharmaceutical formulation in B–R buffer (pH 6.0) and (B) in the presence of (a = 0.5, b = 1.0 and c = 2.0 µM) DTIC in artificial urine.*

Table 5.1: Determination of DTIC in pharmaceutical injection and in artificial urine samples using the *poly*-ATD/CNPE.

Sample	DTIC ($\times 10^{-6}$ M)	Injection Added ($\times 10^{-6}$M)	[a]Found ($\times 10^{-6}$M)	Average Recovery (%)	[a]RSD (%)
Injection (Decarb 200mg injection)	0.5	0.5	1.01	102.6	1.6
	0.5	1.0	1.51	100.7	1.1
	0.5	1.5	1.99	99.3	1.5
Urine Sample	0.5	-	0.49	98.8	0.9
	1.0	-	1.02	101.6	0.8
	2.0	-	2.02	101.4	1.2

[a] Mean value of six measurements.

5.4. Conclusions

In this work, a conducting polymer (*poly*-ATD) coated carbon nanotube paste electrode has been fabricated by adopting a potentiodynamic polarization method for the electrochemical detection of an important anticancer drug dacarbazine. The formation of *poly*-ATD coating on the surface of carbon nanotube paste electrode was confirmed by FTIR and SEM-EDX analysis. The –NH group of the *poly*-ATD forms a strong linkage with –COOH groups of functional carbon nanotube which promotes the facile electron transfer through it. The *poly*-ATD film further increased the electrocatalytic behavior of the carbon nanotubes by remarkably enhancing the peak current response and decreasing the oxidation overpotential of DTIC. The present electrochemical biosensor was efficient for the nanolevel detection of DTIC. It selectively detects DTIC against potential electroactive biological interferents and had shown good recovery limits for direct determination from biological fluids and pharmaceutical formulations. The fabricated biosensor exhibited good stability, high sensitivity, reusability, and simple fabrication procedure.

5.5. References

[1] A. Radi, A. Eissa, H. M. Nassef, *J. Electroanal. Chem.* **2014**, *717-718*, 24–28.

[2] M. Song, R. Zhang, X. Wang, *Mater. Lett.* **2006**, *60*, 2143–2147.

[3] Q. Shen, X. Wang, D. Fu, *Appl. Surf. Sci.* **2008**, *255*, 577–580.

[4] J. R. B. Rodriguez, A. Costa-García, A. J. M. Ordieres, P. T. Blanco, *Electroanalysis* **1989**, *1*, 529–534.

[5] A. J. M. Ordieres, A. C. Garcia, P. T. Blanco, W. F. Smyth, *Anal. Chim. Acta*

1987, *202*, 141–149.

[6] Y. M. Temerk, M. M. Kamal, M. S. Ibrahim, H. S. M. Ibrahim, W. Schuhmann, *Electroanalysis* **2011**, *23*, 1638–1644.

[7] M. Zhou, J. Guo, L. Guo, J. Bai, *Anal. Chem.* **2008**, *80*, 4642–4650.

[8] X. Bo, J. C. Ndamanisha, J. Bai, L. Guo, *Talanta* **2010**, *82*, 85–91.

[9] B. J. Sanghavi, G. Hirsch, S. P. Karna, A. K. Srivastava, *Anal. Chim. Acta* **2012**, *735*, 37–45.

[10] Y. Liu, H. Teng, H. Hou, T. You, *Biosens. Bioelectron.* **2009**, *24*, 3329–3334.

[11] M. Chicharro, A. Sánchez, E. Bermejo, A. Zapardiel, M. D. Rubianes, G. A. Rivas, *Anal. Chim. Acta* **2005**, *543*, 84–91.

[12] M. L. Pedano, G. A. Rivas, *Electrochem. commun.* **2004**, *6*, 10–16.

[13] M. Satyanarayana, K. K. Reddy, K. V. Gobi, *Anal. Methods* **2014**, *6*, 3772–3778.

[14] M. Satyanarayana, K. Koteshwara Reddy, K. Vengatajalabathy Gobi, *Electroanalysis* **2014**, *26*, 2365–2372.

[15] L. Zhang, L. Wang, *J. Solid State Electrochem.* **2013**, *17*, 691–700.

[16] P. Kalimuthu, S. A. John, *Talanta* **2010**, *80*, 1686–1691.

[17] V. Ratautaite, S. D. Janssens, K. Haenen, M. Nesládek, A. Ramanaviciene, I. Baleviciute, A. Ramanavicius, *Electrochim. Acta* **2014**, *130*, 361–367.

[18] S. B. Revin, S. A. John, *Electrochim. Acta* **2011**, *56*, 8934–8940.

[19] T. Brooks, C. W. Keevil, *Lett. Appl. Microbiol.* **1997**, *24*, 203–206.

[20] G. Yang, F. Zhao, *J. Mater. Chem. C* **2014**, *2*, 10201–10208.

[21] E. Laviron, *J. Electroanal. Chem.* **1979**, *101*, 19–28.

[22] X. Zhang, S. Duan, X. Xu, S. Xu, C. Zhou, *Electrochim. Acta* **2011**, *56*, 1981–1987.

[23] W. Sun, Y. Li, Y. Duan, K. Jiao, *Electrochim. Acta* **2009**, *54*, 4105–4110.

[24] M. Satyanarayana, K. Y. Goud, K. K. Reddy, K. V. Gobi, *Electrochim. Acta* **2015**, *178*, 608–616.

[25] A. J. Bard, L. R. Faulkner, *Electrochemical Methods: Fundamentals and Applications, 2nd Ed.*, John Wiley & Sons, New York, **2001**.

[26] Y. Feng, T. Yang, W. Zhang, C. Jiang, K. Jiao, *Anal. Chim. Acta* **2008**, *616*, 144–151.

[27] R. Pauliukaite, M. E. Ghica, O. Fatibello-Filho, C. M. A. Brett, *Electrochim. Acta* **2010**, *55*, 6239–6247.

CHAPTER 6

SUMMARY and CONCLUSIONS

6.1 Summary

The introduction chapter was focussed on describing the concepts of chemical sensors starting from the principles, latest advances and the state-of-the-art. Various types of chemical sensor were discussed based upon its principle, and applications of chemical sensors towards the monitoring of target molecules have been discussed in detail. A brief discussion on CMEs and literature reports on different types of materials used in chemical modification of electrodes have been given. Various electrochemical strategies for the detection of diverse pharmaceutical drug molecules (Anti-inflammatory, Anti-cancer, Anti-depressant, Gastro-intestinal drugs, Antibiotic drugs, Cardiovascular agents, etc.) were critically reviewed. Necessity for the development of electrochemical sensors for the specific detection of vital drug molecules was realized and the objectives of the present study were defined. Development of electrochemical sensors for selected drugs such as *Isoniazid*, *5-Fluorouracil, Clopidogrel* and *Dacarabazine* was defined as the objective of the present study. Electrochemical techniques have been elucidated as efficient transduction methods towards the development of sensors for the above selected pharmaceutical drugs.

In *Chapter 2*, A reagent-free electrochemical sensor is fabricated for sensitive determination of the important anti-tubercular drug isoniazid (INH). The electrochemical response of the fabricated multiwall carbon nanotube (MWCNT)–chitosan (chit) nanocomposite modified glassy carbon electrode (MWCNT-chit/GCE) towards the detection of INH is investigated by cyclic voltammetry, chronoamperometry (CA), electrochemical impedance spectroscopy (EIS) and differential pulse voltammetry (DPV). The carbon nanotube–chitosan nanocomposite electrode exhibits an excellent electrocatalytic effect towards the oxidation of INH. The overpotential for the electrochemical oxidation is reduced largely by ~ 800 mV to +0.17 V vs. Ag|AgCl at MWCNT-chit/GCE compared to +0.97 V vs. Ag|AgCl at bare GCE, and the electrocatalytic current is enhanced nearly four times of magnitude. Applying DPV method at optimized conditions, a linear calibration plot is achieved over the concentration range of 1.0×10^{-7} M – 1.0×10^{-5} M INH and the biosensor could detect as low as 5.5×10^{-8} M INH in ~ 12 s. The modified electrode shows very good selectivity towards the specific recognition of INH in the presence of important biological interferents. The electrochemical biosensor detects INH *in-vitro* directly from spiked

drug formulations and undiluted urine sample as low as 5×10^{-7} M with recovery limits of 102 % and 101.4 %, respectively.

In Chapter 3, A fast and facile electrochemical sensor for the detection of an important anti-cancer drug, 5-fluorouracil, is fabricated using a gold nanoparticle decorated multiwall carbon nanotube (GNP-MWCNT) composite modified electrode. GNP-MWCNT composite has been prepared by a simple one-pot synthesis in the presence of chitosan, which acts as a reducing as well as stabilizing agent. Synthesized GNP-MWCNT is characterized by UV-Visible spectroscopy, Raman spectroscopy, XRD analysis and FESEM for the structural and chemical properties of nanocomposite, and the size of the gold nanoparticles is determined to be ~30 nm by different methods. The electrochemical capability of the fabricated GNP-MWCNT composite modified electrode for the detection of 5-FU is examined by cyclic voltammetry, chronoamperometry (CA), electrochemical impedance analysis and differential pulse voltammetry. The nanoAu decorated carbon nanotube electrode is found to be efficient for electrocatalytic oxidation of 5-FU. Peak current of the DPVs exhibited a linear relationship against 5-FU over a wide concentration range of 0.03 – 10 μM with a low-detection-limit (3σ/b) of 20 nM, and the analysis time is as low as 25 s. Practical utility of the developed GNP-MWCNT nanocomposite biosensor has been demonstrated for the detection of 5-FU directly from artificial urine and pharmaceutical formulations with good recovery limits.

In Chapter 4, A highly sensitive electrochemical sensor has been fabricated with silver nanoparticles embedded chitosan (AgChit) and carbon nanotube (CNT) hybrid nanocomposite as sensor interface for the detection of the important anti-platelet drug, clopidogrel (CLP). Synthesized AgChit-CNT nanocomposite is characterized by UV-Visible spectrophotometer, X-ray diffraction (XRD), Raman spectroscopy, energy dispersive X-ray analysis (EDXA) and field emission scanning electron microscopy (FE-SEM) for its chemical and structural information. The electrochemical response of the fabricated AgChit and CNT nanocomposite modified glassy carbon electrode (GCE) towards the detection of clopidogrel is investigated by cyclic voltammetry (CV), chronoamperometry and electrochemical impedance spectroscopy (EIS). The silver nanoparticles of about 35 nm are well distributed in the matrix of chitosan and form constructive linkage with CNTs. The Ag nanoparticles patterned carbon nanotube hybrid

nanocomposite electrode exhibits an excellent electron transfer mediation towards the oxidation of clopidogrel. Differential pulse voltammetry (DPV) and amperometric i-t curve analysis was carried out by changing the concentration of clopidogrel, a limit of detection of 30 nM obtained with the linear concentration range of 0.05 μM – 12 μM by DPV and the limit of detection obtained by amperometric i-t curve analysis is about 10 nM. The practical applicability of the fabricated sensor has been demonstrated for the determination of clopidogrel in artificial urine and pharmaceutical formulation with a good recovery.

In Chapter 5, A low-cost and reusable electrochemical sensor ensembling carbon nanotubes and a conducting polymer together is fabricated for the detection of an important anti-cancer drug, dacarbazine (DTIC). A thin film of a conducting polymer, poly(2-amino-1,3,4-thiadiazole) (*poly*-ATD) is formed on the carbon nanotube paste electrode (CNPE) by employing potentiodynamic polymerization technique. The fabricated sensor surface has been characterized by FT-IR spectroscopy, scanning electron microscopy (SEM) for the structural and chemical properties of electrode system. The electrochemical capability of the fabricated *poly*-ATD/CNPE composite modified electrode for the detection of DTIC is examined by cyclic voltammetry (CV), chronoamperometry (CA) and electrochemical impedance spectroscopic analysis (EIS), and the mechanism for the electrochemical oxidation of DTIC derived by CV studies shows that it was a two-electron four-proton transfer diffusion controlled process. Optimization and evaluation of the sensor system is examined by differential pulse voltammetry (DPV) and amperometric i-t curve analysis. A linear relationship of DTIC concentration over the peak current of DPVs is exhibited over a wide concentration range of 0.05 – 24.0 μM with a low-detection-limit (3σ/b) of 35 nM, and by applying amperometric method the limit of detection obtained to be 20 nM. Practical utility of the fabricated *poly*-ATD/CNPE biosensor for the detection of DTIC directly from artificial urine and pharmaceutical formulations has been demonstrated with very good recovery limits.

Electrochemical sensors have been fabricated here successfully for the selected pharmaceutical drugs and the performance of each sensor has been presented in terms of low-detection-limit, linear concentration range of detection and real time analysis. The electrochemical reaction parameters such as number of electrons involved in the

oxidation of analyte (n), heterogeneous electron transfer rate constant (k°) and diffusion coefficient (D) are calculated. Together with this, the plausible reaction mechanism also has been provided. Research findings reported in this thesis were summarized in the form of a table (Table 6.1).

6.2. Conclusions

In this research work, a number of electrochemical sensors have been fabricated with different carbon nanotube based hybrid nanocomposite modified electrodes, and quite excellent low-detection-limits were established. Further, a variety of materials such as gold nanoparticles, silver nanoparticles, proteins, carbon nanotubes and biopolymers were investigated effectively in developing the electrochemical biosensors.

Table 6.1: *Summary of the developed electrochemical sensors for selected drugs and their respective findings.*

Analyte	Sensor Platform	n	D ($cm^2\ s^{-1}$) ($\times 10^{-6}$)	LOD (nM)		Linear Range (µM)	Real Sample Analysis
				DPV	Amperometry		
INH	MWCNT-Chit/GCE	2	3.80	55	--	0.1 – 10	Artificial Urine, Pharmaceutical Tablet
5-FU	GNP-MWCNT-Chit/GCE	1	9.62	20	--	0.03 – 10	Artificial Urine, Pharmaceutical Injection
CLP	AgChit-CNT/GCE	1	6.12	30	10	0.05 – 12	Artificial Urine, Pharmaceutical Tablet
DTIC	*poly*-ATD/CNPE	2	8.87	35	20	0.05 – 24	Artificial Urine, Pharmaceutical Injection

n – No. of electrons involved in the electrochemical oxidation of analyte.
D – Diffusion coefficient of analyte ($cm^2\ s^{-1}$).

All these results clearly establish the versatility, efficiency and applicability of the electrochemical sensors based on various hybrid nanocomposite based CMEs for detection of selected pharmaceutical drugs and further provide confidence for efforts in future to develop electrochemical sensors for the analysis and sensitive detections of diverse target groups such as biomarkers, environmental pollutants and food toxins by employing highly catalytic nanostructured materials based CMEs.

LIST OF PUBLICATIONS & BIO-DATA

LIST OF PUBLICATIONS & BIO-DATA

Publications in Peer-Reviewed/Refereed International Journals

1. *Multiwall carbon nanotube ensembled biopolymer electrode for selective determination of isoniazid in vitro"*
   M. Satyanarayana, K. Koteshwara Reddy and K. Vengatajalabathy Gobi
   Analytical Methods 6 (2014) 3772–3778 (Impact Factor **1.855**)

2. *"Nano-Biocomposite based Electrochemical Sensor for Sensitive Determination of Serotonin in Presence of Dopamine, Ascorbic acid and Uric acid in-vitro"*
   M. Satyanarayana, K. Koteshwara Reddy, K. Vengatajalabathy Gobi*
   Electroanalysis, 26 (2014) 2365–2372 (Impact Factor **2.502**)

3. *"Biopolymer Stabilized Nanogold Particles on Carbon Nanotube Support as Sensing Platform for Electrochemical Detection of 5-Fluorouracil in-vitro"*
   M. Satyanarayana, K. Koteshwara Reddy, K. Yugender Goud, K. Vengatajalabathy Gobi
   ***Electrochimica Acta, 2015,178* , 608–616** (Impact Factor **4.504**)

4. "*Development of Highly Selective Electrochemical Impedance Sensor for Detection of Sub-micromolar Concebtrations of 5-Chloro-2,4-dinitrotoluene*"
   K. Yugender Goud, **M. Satyanarayana,** K. Koteshwara Reddy, K. Vengatajalabathy Gobi
   Journal of Chemical Sciences (Accepted) (Impact Factor **1.191**)

5. *"Biopolymer Protected Silver Nanoparticles on the Support of Carbon Nanotube as Interface for Electrocatalytic Applications"*
   *M. Satyanarayana, V. Sunil Kumar, K. Vengatajalabathy Gobi**
   AIP Conference Proceedings, 1724, 020097 (2016); DOI: 10.1063/1.4945217

6. *"Conducting Polymer Coated Carbon Nanotube Paste Electrode as Sensor Interface for Electrochemical Detection of Dacarbazine"*
   M. Satyanarayana, K. Koteshwara Reddy, K. Yugender Goud, K. Vengatajalabathy Gobi
   Sensors & Actuators B (Under Review) (Impact Factor **4.097**)

7. *"Disposable and portable electrochemical aptasensor for label free detection of aflatoxin B1 in alcoholic beverages"*
   K. Yugender Goud, Gaëlle Catanantea, Akhtar Hayata, **Satyanarayana M,** K. Vengatajalabathy Gobi, Jean Louis Marty
   Sensors & Actuators B (Under Review) (Impact Factor **4.097**)

8. *"Carbon nanotube ensembled hybrid nanocomposite electrode for direct electrochemical detection of epinephrine in pharmaceutical tablets and urine"*

K. Koteshwara Reddy, **M. Satyanarayana,** K. Yugender Goud, K. Vengatajalabathy Gobi

Sensors and Actuators (Communicated) (Impact Factor **4.097**)

9. *"Silver Nanoparticles Implanted Chitosan Layered Carbon Nanotube Hybrid Nanocomposite as a Sensor Interface for Sensitive Detection of Clopidogrel in-vitro"*
M. Satyanarayana, K. Koteshwara Reddy, K. Yugender Goud, K. Vengatajalabathy Gobi
(Manuscript under Preparation)

Publications in Peer-Reviewed/Refereed International Conference Proceedings

1. "*Electrochemical Detection of Isoniazid using Carbon nanotube - Chitosan biocomposite Modified Electrodes*"
Satyanarayana M. & K.V. Gobi
ISEAC-ELAC-2013: PAGE 449-454 **ISBN No: 978-81-901950-5-8**

2. "*Highly sensitive nanocomposite-based electrochemical sensor for determination of serotonin in the presence of dopamine, ascorbic acid and uric acid*"
Satyanarayana M., K. Yugender Goud, K. Vengatajalabathy Gobi
ISEAC-DM-2014: PAGE 97-102 **ISBN No: 978-81-901950-6-5**

3. "*Synthesis and Characterization of Au-Chit-Pd Supported on Carbon Nanotubes for Highly Active Methanol Electro-oxidation in Alkaline Media*"
Sunil Kumar V., **Satyanarayana M.,** Gobi K. V.
MATCON-2016: VOLUME 2, PAGE 441-443 ISBN No: 978-93-80095-738

BIO-DATA

Satyanarayana Moru

Contact Address
S/O. M. Lakshmaiah
Hamaliwada
Mancherial (Mandal)
Adilabad (District) – 504 208
Telangana, India.
E-mail: satyam.moru@nitw.ac.in
satyam.nitw@gmail.com
Mobile: +91-9959704030

Objective: To be professionally associated with an organization, where I can utilize my Doctoral Research experience in solving the practical challenges and achieve the goals of the organization

Academic Qualifications:

July 2009 – Present : **Research Scholar (PhD Student)**
Under the supervision of **Dr. K. V. Gobi**, Associate Professor, Department of Chemistry, National Institute of Technology Warangal, Telangana, India

Research Topic: "*Development of Carbon Nanotube based Hybrid Nanocomposites as Sensing Platform for Electrochemical Detection of Pharmaceutical Drugs of Intensive Care Monitoring*"
Status: To be awarded (Thesis submitted)

July 2007 – June 2009 : **Master of Science in Chemistry**
National Institute of Technology Warangal, Telangana, India
Grade Point Average: **7.57** (First Class)

June 2003 – May 2006 : **Bachelor of Science (Mathematics, Physics, and Chemistry)**
Kakatiya University, Warangal, Telangana, India
Percentage of Marks: **73.0 %** (Distinction)

June 2001 – May 2003 : **Intermediate (Mathematics, Physics and Chemistry)**
Board of Intermediate Education, Andhra Pradesh, India
Percentage of Marks: **68.6 %** (First Division)

June 2000 – April 2001 : **Secondary School Certificate (High School)**
Board of Secondary Education, Andhra Pradesh, India
Percentage of Marks: **81.3 %** (First Division)

Professional Summary:

- **Ph.D. Research Fellow** at National Institute of Technology, Warangal, Telangana, India, from July 2011 to till date.
- **Lecturer** in Physical Chemistry at New Science Degree College, Bhupalapally from August 2010 to April 2011.
- **Industrial training experience** from April 2010 to June 2010 at **MSN Laboratories**, Hyderabad during M. Sc. Program as a part of External Project.

Personal Details:

- Name : Satyanarayana M.
- Father's Name : Lakshmaiah
- Date of Birth : 11-02-1987
- Gender : Male
- Marital Status : Married
- Nationality : Indian
- Languages Known : Telugu, English and Hindi

Achievements:

- Qualified Graduate Aptitude Test in Engineering (**GATE**) 2011.
- Secured 72nd rank in National Institute of Technology Warangal Entrance Test **(NITWET)** 2008 for M. Sc. Admissions.

Technical Skills:

- Expertise in utilizing the software - Microsoft Office, Ngraph, Origin etc., Cemistry Related software - ChemDraw Ultra 12.0, HyperChem Release - 8.0.9, X'Pert HighScore Plus.
- Expertise in MENDELEY Reference Manager.

Expertise in Instrumental Techniques:

- Electrochemical Impedance Analyzer, Zahner-Elektrik (IM6e), GmbH, Germany
- Electrochemical Workstation, Sinsil CHI 619D and CHI6132e.

- UV-Visible Spectrophotometers, Analytik Jena Specord 205 and Shimadzu 1601
- FTIR Spectrophotometer, PerkinElmer
- Raman spectrometer, HR800 LabRAM confocal
- Differential Scanning Calorimeter, Q10 TA instruments, USA
- Scanning Electron Microscope, VEGA3, Tescon, USA
- Other small instruments relevant for materials characterization and analysis

Research Interests:

- Biosensors and Electrochemical Sensors
- Nanostructured Materials
- Nano-composites towards Practical Applications of Electrochemistry.
- Electrochemical Techniques

Memberships:

- Indian Society for Electroanalytical Chemistry (ISEAC – LM161)

Other Capabilities:

- Capable of carrying out both collaborative and independent research
- Motivated strong ethics and providing efficient service
- Very good interpersonal and communication skills along with management skills
- Good experience in writing technical papers, presentations and reports
- Guided many post-graduate students for their projects